School of Chemistry

Thermionic Emission Studies of Surface Functionalized Diamond Semiconductor Materials for the Production of Collectors in Thermionic Energy Converters

Samuel Wills

April 2022

This thesis is submitted in partial fulfilment of the requirements for the Honours degree of MSci at the University of Bristol

Supervisor: Dr Neil Fox

Second Assessor: Paul May

Physical and Theoretical

Abstract

Thermionic energy converters for the most part have been neglected as viable devices for energy production due to their low efficiency, however with recent advances and possible further research their viability as efficient devices becomes more feasible and is certainly a concern for the future of clean energy production. For the most part investigations into this field have been concerned with the construction of strong thermionic emitters, for this project the focus was in the determination of viable semiconductor electron collectors in these devices and in particular investigating the effect that surface functionalisation and therefore the electron affinity of the material can have on the overall efficiency of these systems.

A variety of chemical vapour deposition(CVD) diamond films were used as the experimental collectors used for thermionic testing, as well as a hydrogen terminated nitrogen doped diamond film as the sample emitter. Two types of diamond films were grown using the microwave plasma enhanced CVD technique, namely, nitrogen doped diamond and phosphorous doped diamond films. These materials were used with varying surface terminations of hydrogen, oxygen and tin monoxide. The surfaces were analysed using Raman spectroscopy and SEM in order to determine their quality of growth and differences in growth. For the case of tin monoxide surface termination XPS was used to investigate the quality of the deposition of this layer. The thermionic profiles taken for each material were performed at 25 V and 5 V in order to determine the effect of the surface termination in a case with and without space charge mitigation. The maximum recorded current of 0.408 mA was measured for the hydrogen terminated phosphorous doped diamond collector surface at a bias voltage of 25 V this is due to its low work function and high negative electron affinity. The lowest overall measured current of 0.00139 mA was measured in the hydrogen terminated nitrogen doped diamond sample at a bias voltage of 5V. Similarly the lowest recorded effective work function of the emitter sample was measured for the hydrogen terminated phosphorous doped diamond, the measured effective work function was 2.251±0.002 eV.

The motivation behind this research was to determine, if any, the possible benefits to having a collector in a thermionic energy converter with a positive electron affinity but a low work function as a means of optimising the efficiency of a device, by mitigating the back emission that is possible in thermionic energy collectors. This research is with a view to producing a viable thermionic energy converter which can operate with low space charge mitigation effects within.

Acknowledgments:

I would first like to thank Ed Smith, Gary Wan, Hugo Dominguez-Andrade and Ramiz Zulkharnay for their continued help and guidance during the process of the project, particularly given that they themselves had many projects of their own to focus on. Most importantly I would like to thank them for their support during the difficult and uncertain portions of this endeavour.

I would also like to thank my supervisor Neil Fox for his continued guidance, enthusiasm and assistance with the direction of the project. Additionally, I would also like to thank my second assessor Paul May for offering problem solving ideas. Moreover, I would also like to extend my thanks to Jude Laverock and Sami Ullah for their help with performing XPS, UPS and deposition on my samples. My thanks also goes to Adrian crimp in the physics mechanical workshop.

Finally I would like to thank all the members of the University of Bristol diamond group for their support and encouragement which empowered me to complete this report.

Table of Contents:

1.0 Introduction

1.1 Diamond

Since their discovery and use as decorative status symbols or engagement articles, diamonds have transformed from the glamorous to the useful such as in the use of diamond coated tools. Recently, however, they have taken a different form as possible alternatives for energy production. Their usefulness in this endeavour is derived from their strong thermal resistance and from the discovery of a method to synthetically produce diamond. Despite the sizable bandgap of 5.47 eV[21] of natural diamond the possibility of doping synthetically grown diamonds allows for them to become a viable energy source by reducing this.

In this way as the sophistication of the synthesis process was furthered it became possible to grow diamond films allowing for different shapes and sizes to be formed, for instance diamond nanotubes. This allows for a myriad of uses for diamond to be investigated such as in the fields of energy production or in bactericidal surfaces[24]. Most importantly for the field of energy production it allows for the possibility of the creation of solid state devices[54] which can be used to generate power via thermal or photovoltaic conversion.

Initially the first reported and verified creation of a synthetic diamond was performed by General Electric in 1955 using a technique which would come to be known as the high pressure high temperature technique(HPHT). In short, this technique operates by using a very high temperature and pressure system with a metal solvent capable of dissolving graphite which then forces the crystallization of diamond to occur due to its insolubility in a metal solvent[1]. This technique, though ground breaking was cumbersome and inefficient providing synthetic diamond of low quality. In this way a new method of diamond synthesis was created, namely, chemical vapour deposition (CVD) synthesis, whereby a diamond film is formed via the deposition of an activated hydrocarbon gas onto a substrate. This was initially achieved by the Soviet group in 1969 and further improved upon via the addition of hydrogen to the gas mixture in the 1970's[2]. The addition of hydrogen improved the purity of the diamond formed by removing graphite during the formation process. Following this the techniques for synthetic diamond formation became more and more complex with the use of hot filament CVD in 1982 by S. Matsumoto et al[3]. In this technique the premise is to use a hydrocarbon gas environment heated to a high enough temperature to produce hydrocarbon radicals which attach to the surface of a substrate forming a diamond layer with subsequent hydrocarbon radicals. However a problem with this technique is the filament material can itself be incorporated into the film at high enough temperatures, producing less pure diamond. In this way a second technique was developed in 1983 by M. Kamo et al using a microwave plasma to heat the gas environment so as not to unintendedly dope the sample with elements of the reactor[4]. The

importance of the CVD method is not only relevant to the purity of the diamond, but also to the fact that it allows for the doping of diamond to occur, allowing for the possibility of conducting diamond.

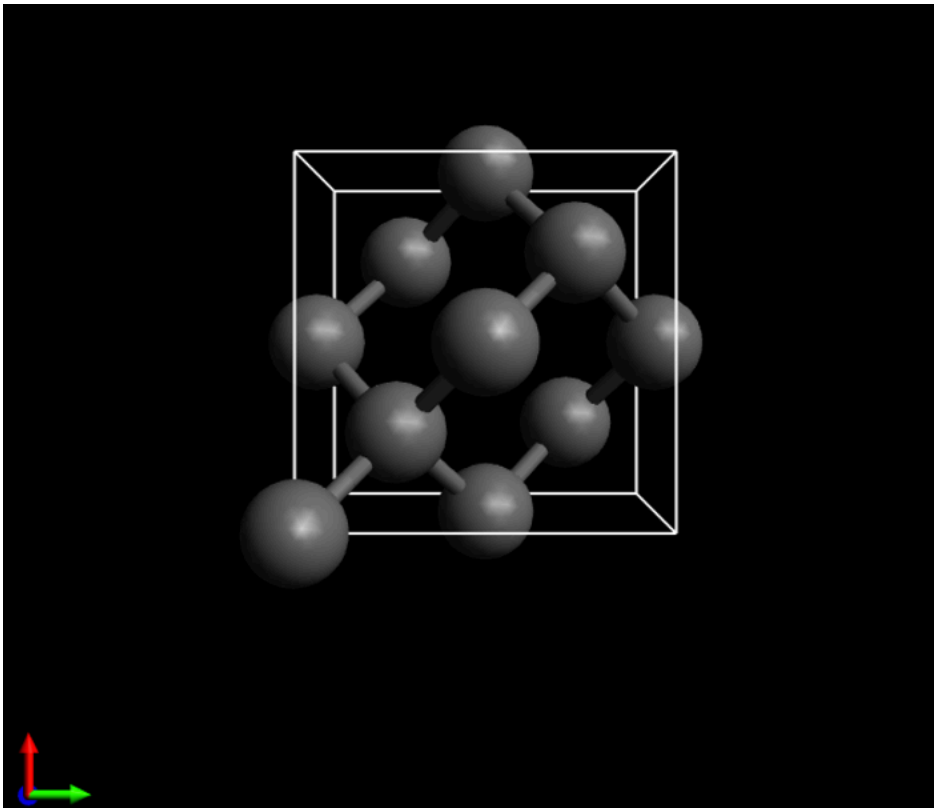

Figure 1: A schematic showing the primitive unit cell of diamond. (Built using Avogadro).

Diamond itself is a material of incredible use, be that for its hardness and therefore its use as a coating for tools or for its strength and resistance to chemical degradation. In its bulk, diamond consists of carbon with sp^3 hybridised covalent bonds formed in a tetrahedral shape which forms a face centred cubic lattice. The primitive unit cell of diamond may be seen in figure 1. The covalent bond strength in diamond is 347kJ/mol which accounts for this large thermal resistance and hardness[2]. Due to the nature of its bonding diamond exhibits a high band gap in its undoped state as there are no free electrons for the carbon in bulk to donate and nor are there holes to accept them. In comparison graphite, another allotrope of carbon, forms layered hexagonal sheets of sp^2 hybridised covalently bonded carbon, see figure 2, which are conducting due to the extra electron remaining from only covalently bonding 3 times. Additionally, this allotrope of carbon in contrast to diamond has a low hardness as the hexagonal layers easily slide over each other due to weak Van der Waals forces in between the layers[55].

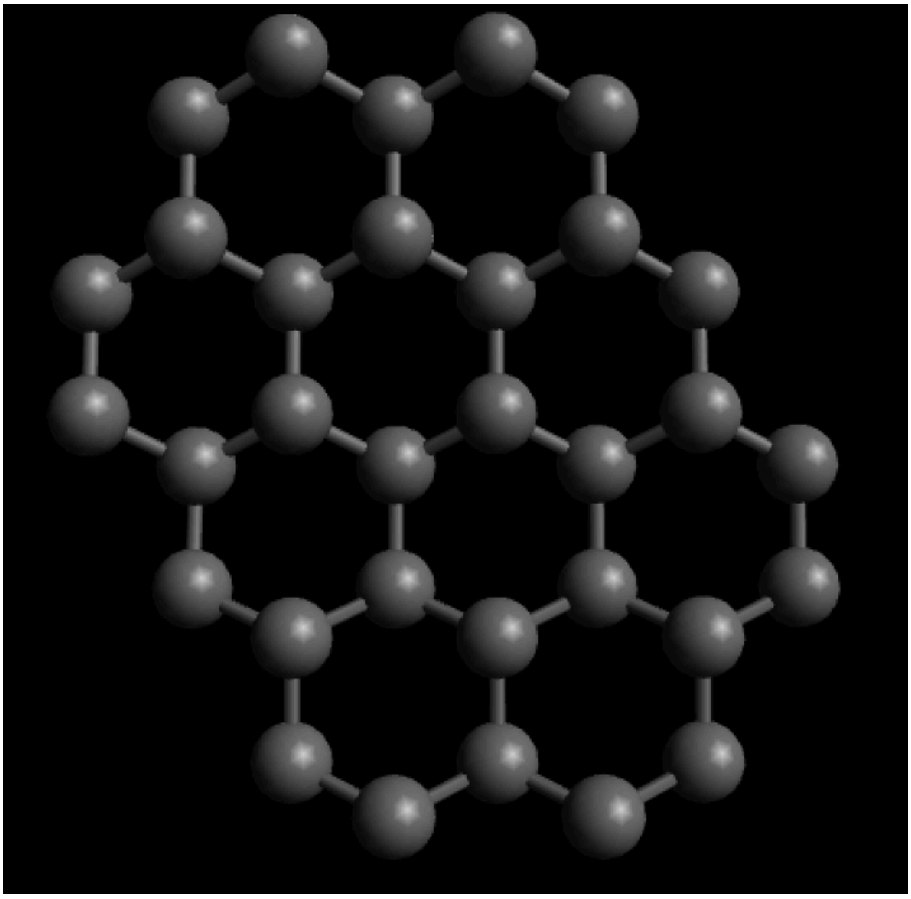

Figure 2: A schematic of the structure of graphite.(Built using Avogadro).

1.1.1 Diamond Film Synthesis

The synthesis of diamond films operates principally by forming a diamond film on a seeded substrate via a homoepitaxial or heteroepitaxial growth method, the substrate is seeded to ensure there are nucleation sites to expedite the growth process. There are many methods for seeding the substrate for instance via abrasion of the surface with nano diamond which roughens the surface to allow for faster nucleation. Another method of seeding is known as electrostatic spray deposition whereby nano diamond particles are deposited on the surface of a substrate via a vapourised solution. It is important to use seeding techniques in order to lower the time taken for growth and in some cases this is a more important factor as the substrate may not form a good enough interfacial carbide layer to allow for diamond growth or in others it may form only a carbide layer, so a substrate that is reactive and yet not too reactive with CH_4 is important for diamond film growth. Additionally, the thermal expansion coefficient and melting temperature of the material must be taken into account when choosing a substrate due to the high operating temperatures of the synthesis and low thermal expansion coefficient of diamond(0.7×10^{-6} K^{-1}[25]). If a material with a high thermal expansion coefficient, relative to diamond, is chosen this will result in difficult synthesis with a high chance of delamination at the end of the growth process. Furthermore, and in particular for this project, a substrate is required also to improve the heating characteristics of the diamond material as the main pathway for heating

diamond is via phononic energy transfer, thus a material which can be radiatively heated efficiently is required.

In general the growth process of a synthetic diamond involves temperatures and pressures of around 1000-1400K and 100-140 Torr respectively, as well as a gas environment of methane and hydrogen in a ratio of 1 percent to 99 percent respectively[5], in some cases oxygen can be used as well. The synthesis of diamond films is an extremely particular process which is dependent on the proportions of hydrogen, oxygen and carbon as well as the temperature and pressure of the system. As such there is an extremely particular ratio of these three elements that allows for diamond growth this can be described by a Bachmann diagram as seen in figure 3. This figure indicates the specific region that allows for diamond growth it can be seen that there is a region which requires only carbon and hydrogen for growth.

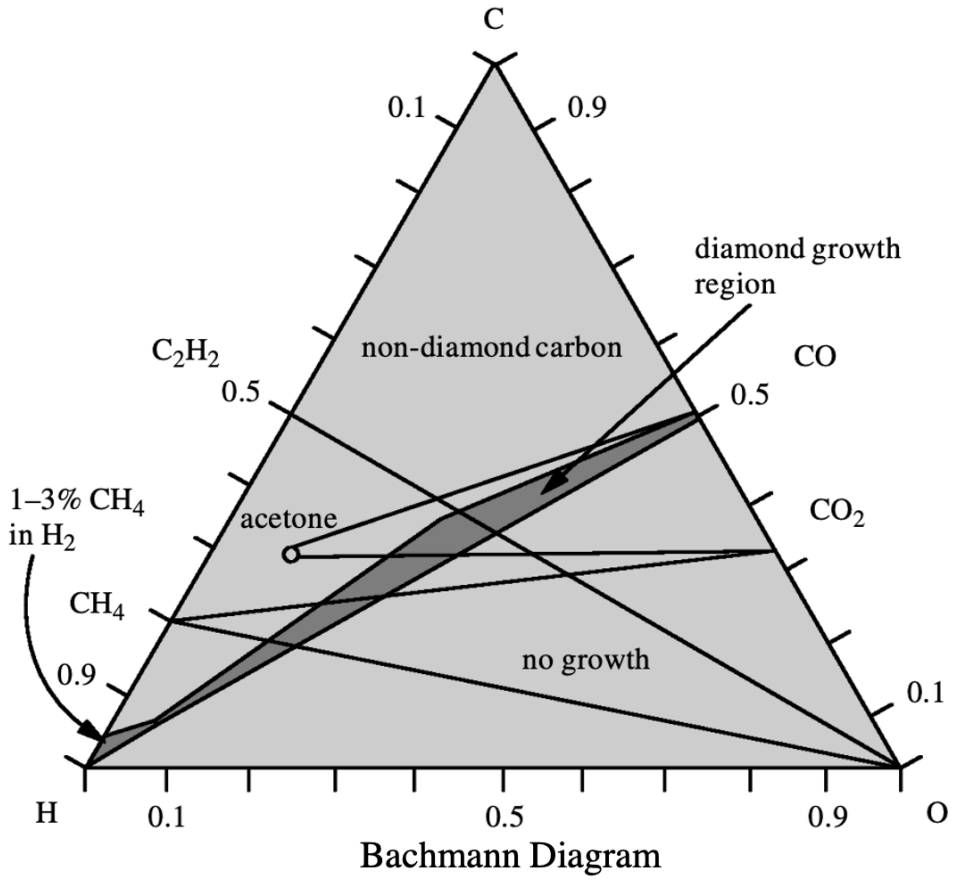

Figure 3: A Bachmann diagram detailing the composition of C,H and O that allows for diamond growth, adapted from [63].

This gas mixture is paramount to the quality of the growth as a higher ratio of methane would result in a considerable quantity of graphitic carbon forming in the diamond film despite a quicker growth as the rate of graphite etching relative to growth of the graphite would be lower. Similarly hydrogen is used in the gas environment to ensure the quality of the film for a multitude of reasons:

1. For etching away unwanted graphite from the surface faster than that of the formed diamond due to the lower density of the sp^2 configuration[57,62].
2. To activate surface C-H to C* by removing the excess hydrogen bonded at the surface.
3. Creating methyl radicals necessary for deposition on the surface itself[56].
4. Surface terminating with dangling bonds at the surface of the material to ensure no cross linkage and subsequent formation of graphite during the growth process[63].

The currently proposed mechanism for the formation of diamond on the surface of a substrate involves the formation of CH_3 and C_2H_2 from CH_4 and C_2H_6 respectively which is then deposited on the surface and then has the subsequent leftover hydrogens removed[61]. A proposed mechanism for the deposition of diamond to a surface may be seen in figure 4.

The two most widely used methods of growth are the hot filament and microwave plasma enhanced CVD (MPECVD) methods, in this study the MPECVD method is used. This method is generally used due to the high quality (lack of graphitic carbon) of the diamond film produced as well as the shorter growth time in comparison to hot filament growth.

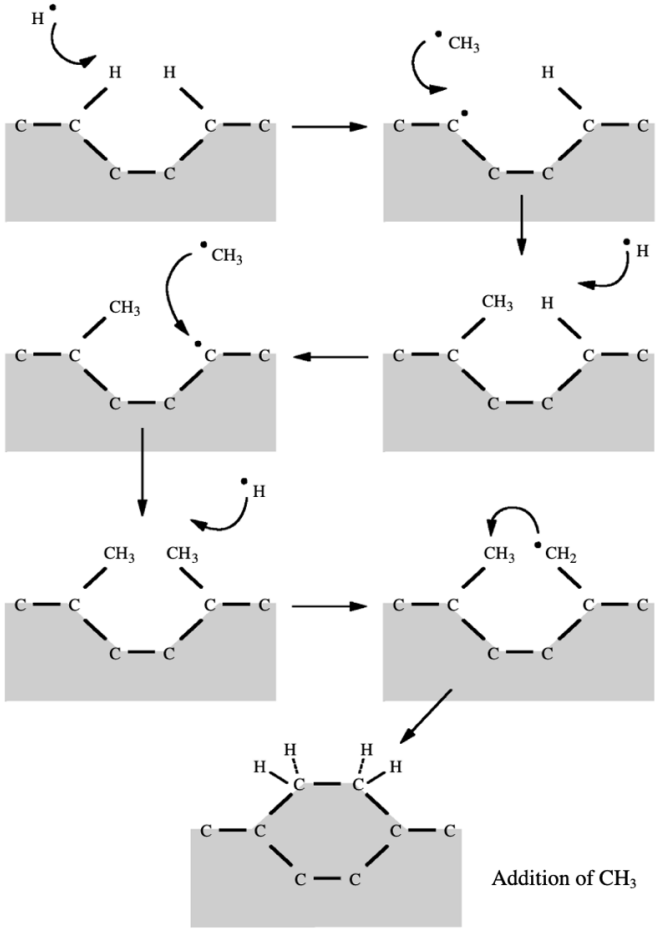

Figure 4: A proposed mechanism for the growth mechanism of diamond films by the addition of CH_3, adapted from[63].

1.1.2 Microwave Plasma Enhanced Chemical Vapour Deposition

The MPECVD method operates by the production of a plasma in the reactor environment which is created using microwaves produced by a magnetron. This plasma is then controlled by the pressure in the reactor and the power output of the magnetron to create a sphere of plasma which lies over the surface of the substrate heating it to temperatures upwards of 1000K, allowing for deposition onto the surface[50,51]. A schematic of this reactor may be seen in figure 5. An advantage of this technique is that there is no possibility of contamination to the diamond film as a function of the reactor materials itself unlike in a hot filament deposition reactor where the material of the filament can be incorporated into the growth.

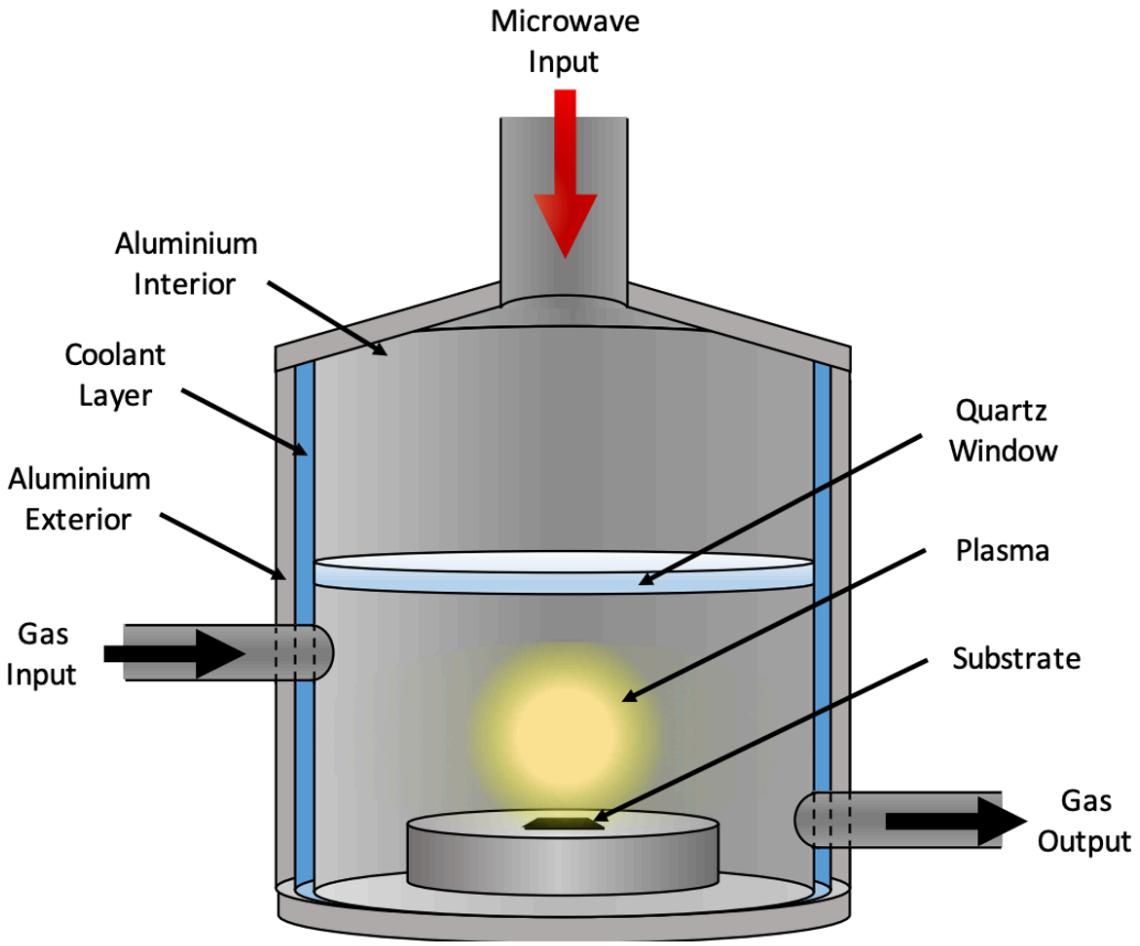

Figure 5: A schematic showing the basic structure of an MPCVD reactor, Taken from [20].

1.2 Conductivity

Though as previously described in its base form diamond is an insulator due to its large band gap and fully bonded carbon atoms, it can be made to conduct via the process of doping. For instance it can be doped with boron or nitrogen to produce p-type and n-type semiconductor behaviour respectively. Furthermore, though the bulk sp^3 hybridised diamond is non conductive, at the grain boundaries of each diamond crystal carbon takes the sp^2 hybridised form i.e. graphite which is conductive. In this way the less pure the diamond film is the more conductive it is due to the increase in graphitic content

due to smaller grain sizes resulting in more grain boundaries. Furthermore due to surface defects such as kinks the charge distribution along the surface will not be homogenous and as such charge will exchange between the surface and the bulk causing the bands to bend at the surface.

1.3 Diamond Doping

Diamond, alongside other materials, can be impregnated with impurities to alter the electrical properties, this process is called doping. When diamond is doped the band gap between the unoccupied conduction band and the occupied valence band is reduced which can produce semiconductor behaviour. The most common dopants used are nitrogen and boron and in some cases phosphorous[58] can be used, however the process is difficult due to a larger difference in atomic radii between carbon and phosphorous. In each case depending on the number of valence electrons relative to that of carbon the material will exhibit n or p type doping[59]. In short, these refer to a situation where a dopant can donate or accept electrons respectively. Furthermore doping can affect the position of the Fermi level due to the conservation of charge neutrality and concentration of free carriers[60]. In the case of an n-doped system the Fermi level moves closer to the conduction band whereas for a p-doped system the Fermi level can be found closer to the valence band, this may be seen in figure 6 and table 1. The doping of a system allows for greater conductivity by lowering the gap between bands to the Fermi level. For example in the case of n-type doping the gap from the Fermi level to the conduction band is smaller than in the intrinsic case. Additionally, depending on the type of doping the bands will bend at the surface differently, in the case of n-type doping the bands will bend up and for p-type the opposite is true. This effect may be seen in figure 7.

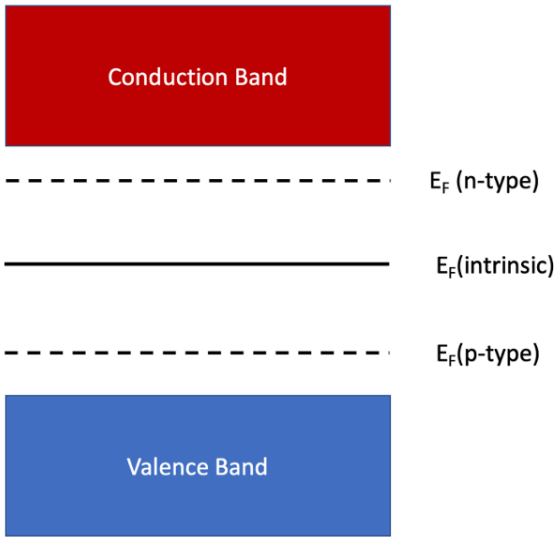

Figure 6: A band diagram showing the structure of bands with the position of the Fermi level relative to the type of doping.

Table 1: A table showing the position of the Fermi level relative to different bands.[11]

Dopant	Phosphorous	Nitrogen	Boron
ΔE of Fermi level to Conduction Band/eV	0.37	1.70	N/A
ΔE of Fermi level to Valence Band/eV	N/A	N/A	0.36

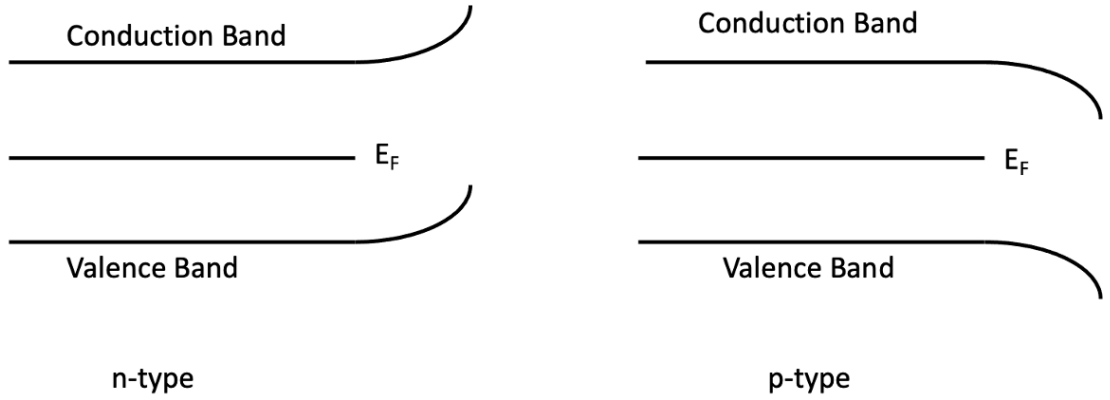

Figure 7: A band diagram outlining the surface band bending exhibited by n-type and p-type semiconductors[11].

1.4 Surface Termination

As previously mentioned the surface of the diamond film is paramount in the production of the film as a whole, the surface atoms of carbon contain one dangling bond necessary to bond with further carbons to form sp^3 hybridised carbon. At the end of the growth cycle these bonds must be terminated with a different atom to ensure no formation of graphite at the surface. These terminations can be achieved with many different atoms and molecules for instance hydrogen, oxygen or even in some cases metal oxides. The addition of these elements can affect the electrical properties of the material depending on the overall electronegativity of these species relative to carbon[54]. This difference in electronegativity produces either what is known as a positive electron affinity(PEA) or a negative electron affinity(NEA). In short, these two outcomes define the position of the vacuum level relative to the conduction band. For a PEA the vacuum level is higher in energy than the conduction band, meaning that in order to allow emission from a surface; an electron excited to the conduction band must have further energy to overcome the vacuum level and leave the surface of the material. Conversely an NEA produces a vacuum level that lies below that of the conduction band allowing for excited electrons to leave the material only with the energy required to excite them to the conduction band. In the NEA case there are two possible forms; a true NEA(tNEA) and an effective NEA (eNEA). A tNEA is a system in which the vacuum level "truly" lies below the conduction band whereas an eNEA is a system where the vacuum level lies at the threshold or under the conduction band and some parts of the conduction band can bend below or upwards of the vacuum level as a result of significant surface treatment[48]. These two regimes for NEA may be seen in figure 8.

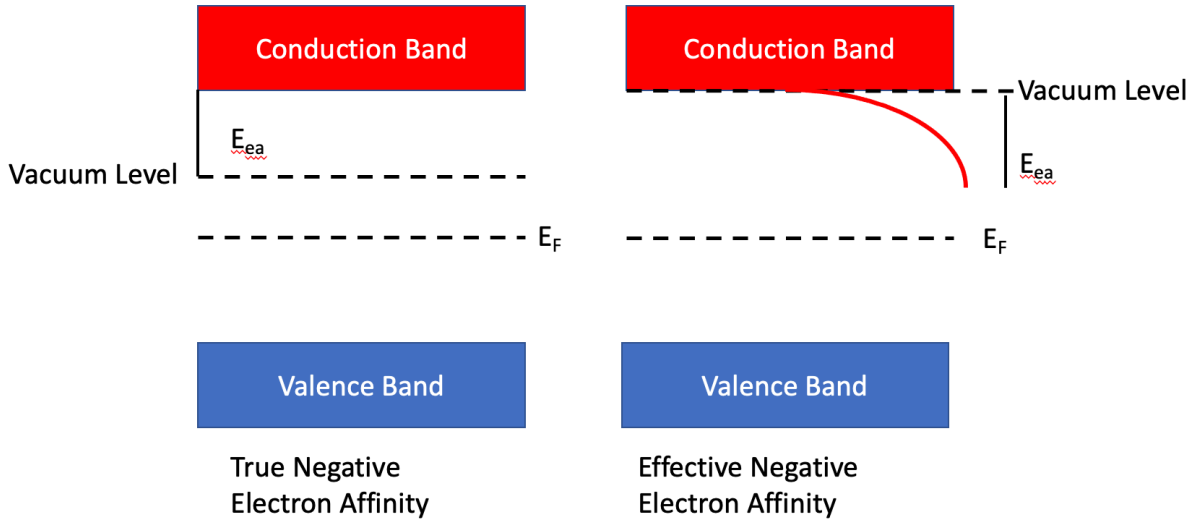

Figure 8: A band diagram exhibiting the difference between true NEA and effective NEA.

1.4.1 Hydrogen Termination

The most general form that a diamond film will be presented in after growth is that of a hydrogen terminated diamond. Due to the abundance of hydrogen in the growth process the 'dangling' carbon bonds on the surface will bond with the reactive hydrogen remaining in the vessel during the cooling process from growth in order to keep the surface diamond structure. The material shows a tNEA due to the more electropositive hydrogen producing a surface dipole with the carbon effectively pulling electrons from the bulk towards the delta positive hydrogen (figure 9). This effect causes a tNEA to form by lowering the energy of the vacuum level[46]. The experimentally achieved values for the electron affinity of these diamond <100> and <111> surfaces are -1.94--2.2eV and -1.98eV respectively[26].

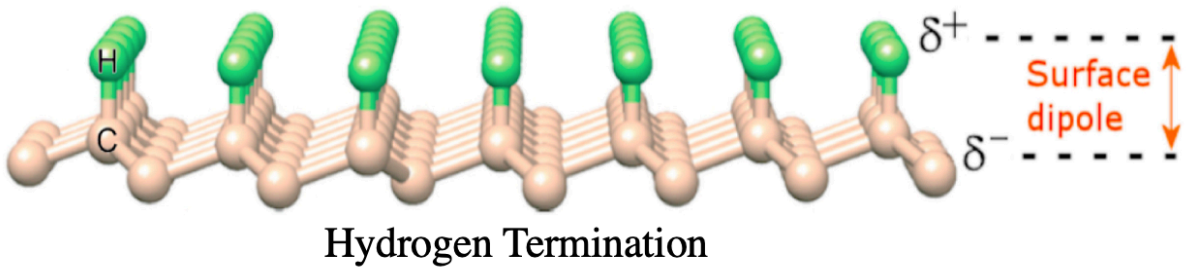

Figure 9: A schematic illustrating the formation of the surface dipole due to hydrogen termination at the diamond surface, adapted from [26].

Despite this useful property of Hydrogen termination there are weaknesses, namely desorption. At temperatures upwards of 750°C termination begins to desorb from the surface and if left at these temperatures will eventually completely desorb from the surface. This is problematic for the construction of a viable thermionic device[15]. Moreover, hydrogen termination is also susceptible to

oxidation via moisture in the air or the oxygen in air itself forming hydroxyl surface terminations which lower the overall effect of the NEA surface which vastly lowers the emission[31]. In this way hydrogen termination is problematic as even if heated at lower temperatures the surface will degrade over time in the wrong environment.

1.4.2 Oxygen Termination

Diamond in its natural state oxygen terminates due to the abundance of oxygen in air in the atmosphere, though there are methods to ensure that the surface is oxygen terminated. This can be achieved via the treatment of the surface in an oxygen-plasma environment or via the cleaning of a the surface via heating and then exposure in an oxygen rich environment using a UV ozone cracker. The oxygen terminated diamond surface also forms a dipole like its hydrogen terminated counterpart however in this case the poles are reversed with the negative charge being on the oxygen atom and not the carbon atom. In effect this causes the electrons in the carbon bulk to be repelled from the surface thus increasing the energy required for emission to occur. This effectively lays the vacuum level above that of the conduction band. This termination can occur in two regimes where the oxygen having 2 possible valence electrons to bond can form either a ketone or ether bond. These regimes can be seen in figure 10. The ketone regime operates via oxygen double bonding to one carbon, whereas the ether regime has a single oxygen atom bonded to two carbon atoms. Both configurations produce a PEA with similar values of around 2.6eV[27]. The advantage of oxygen over hydrogen however is that the threshold temperature of desorption is 1100°C[28]. A further advantage to this form of surface termination is the resistance to chemical attack from H_2O as even though there is a possibility of the formation of hydroxyl termination the surface is more stable in the ketone or ether regimes.

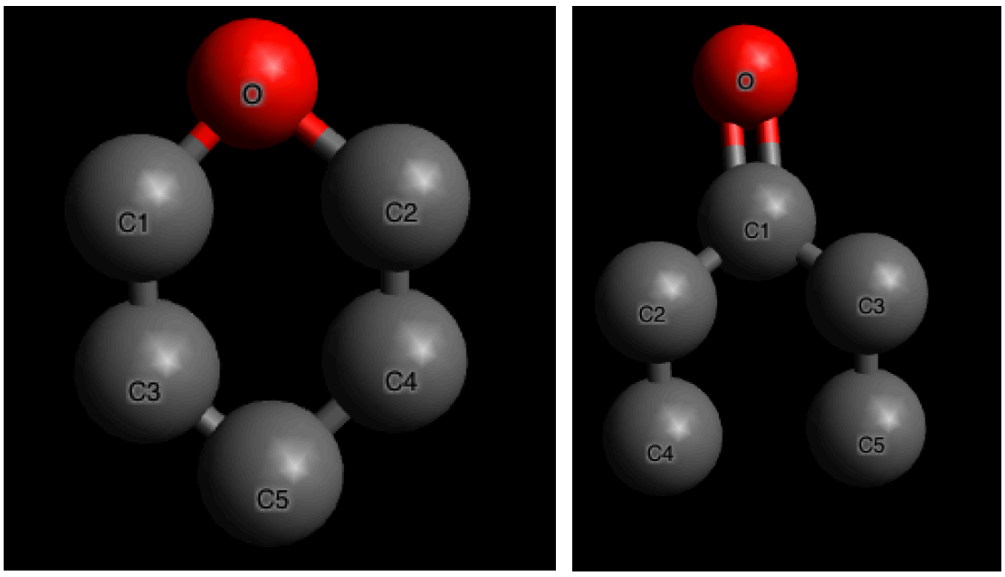

Figure 10: A chemical diagram showing the ether and ketone forms of oxygen surface termination on diamond(Left and Right).(Built in Avogadro)

1.4.3 Metal Oxide Termination

Despite the two main forms of generally occurring termination there are alternatives which pose further benefits. Diamond can be given the state of oxygen termination and then be terminated a second time with a metal to induce a negative electron affinity[28]. The benefits of this are that the resistance to chemical attack from the environment is much greater in metal oxides meaning the overall lifetime of the material is greater. Furthermore the NEA of the material is similar to that of hydrogen termination, for instance tin monoxide terminated diamond has shown a theoretical calculated NEA of around -1.37eV with a half monolayer [32]. Moreover, metal oxide surface terminations have a far greater resistance to temperature than hydrogen terminated surfaces allowing for greater operating temperatures to be utilised and therefore greater emission.

1.4.4 Electron-Beam Physical Evaporation Deposition

Generally materials that are to be metal oxide terminated will be fabricated via the method of Electron-Beam Physical Evaporation Deposition, hereafter referred to as E-Beam Deposition. E-Beam Deposition operates by the bombardment of electrons in a vacuum on a source material causing the sublimation of molecules or atoms on the surface of the source material, leading to the deposition of these sublimated species on the surfaces of the reaction chamber[49]. In most cases a sample stage is prepared with a desired substrate for deposition. Electrons are steered towards the source material using a perpendicular magnetic field. Moreover, some devices also contain a rotating substrate stage to ensure uniform deposition during the process. A typical E-Beam deposition apparatus may be seen in figure 11.

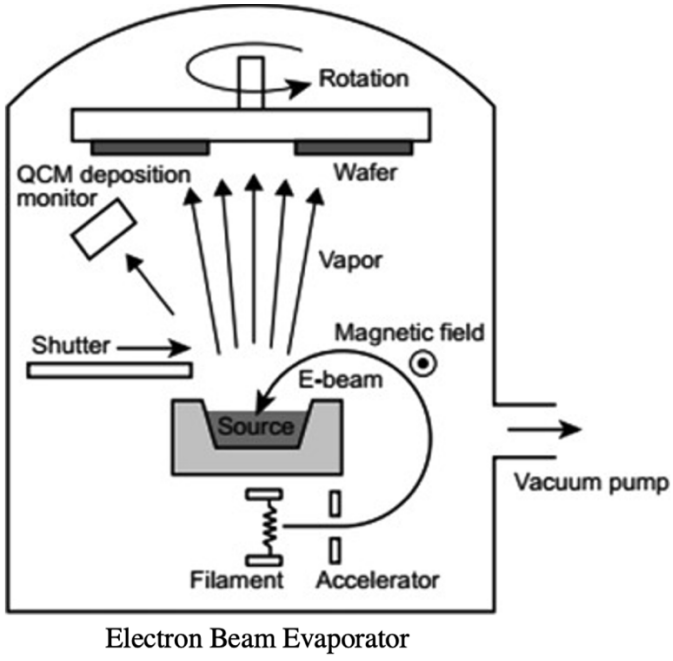

Figure 11: A schematic showing the basic structure of an electron-beam evaporator, adapted from [29].

1.5 Thermionic Emission

Thermionic emission is the emission of electrons from the surface of a material via the transferral of thermal energy to kinetic energy allowing the electrons at the Fermi level to escape past the vacuum level. The most widely accepted relation for this phenomenon is the Richardson equation[45]:

$$J = A_G T^2 e^{\frac{-\phi}{KT}} \quad (1)$$

where J is the current density, A_G is a material specific coefficient, T is the temperature in Kelvin, K is the Boltzmann constant and ϕ is the material specific work function. This equation shows the exponential temperature dependence of thermionic emission as well as the material specific dependence of emission i.e. through the work function.

1.6 Thermionic Emission Devices

The first proposed thermionic energy converter (TEC) device was constructed by Julius Elster and Hans Geitel in 1882 to 1889. The device was simple in its design with two opposing charged electrodes it was noted when heating an electrode that a current would flow through the system. Following this many discoveries were made to improve the understanding of this effect such as the discovery of the electron in 1899 by J.J. Thomson, however, it wasn't until the late 1950's where the progress in device design was made by Joseph Kaye and George Hatsopolous where a parallel plane diode was used to investigate the effect of thermionic emission[7]. Following this the interest in TEC's increased in particular in the realm of space-based applications. Alongside photovoltaics TEC's posed a promising solution to the problem of energy production in spacecraft during the space race, due to the solid state nature of the devices since there are no moving parts which could be disrupted by the low gravity environment or the high acceleration required to escape Earth. Furthermore the lifetime of these devices, being solid state, are large as little maintenance is required.

As well as producing reactors for space craft, the Soviets and the U.S. researched the prospect of nuclear thermionics, whereby a TEC element would be placed in a nuclear reactor instead of a turbine. This research would ,however, be periodically cancelled and then revisited from the 1970's to the late 1980's [9]. The basic operation of a TEC involves the production of electrons at a heated emitter (cathode) which then travel a distance towards a cooled collector (anode) which itself is connected to the emitter allowing for the flow of current and a circuit to form. The basic design of a TEC may be seen in figure 12.

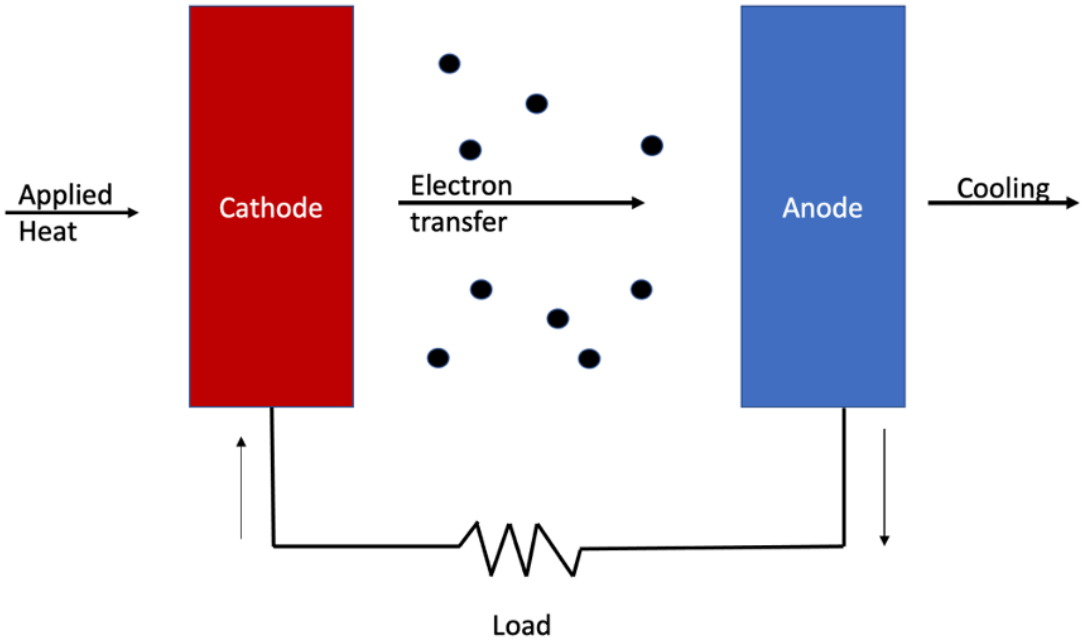

Figure 12: A schematic showing the basic structure of a thermionic energy converter.

With the creation of many different devices over the years came many problems with the viability of them as widely used energy production devices. As well as the above relation many other factors must be accounted for to model the quality of such a device. Firstly the distance of the emitting surface and the collecting surface as though the emitted electrons may be provided with sufficient energy to leave the surface they may not in fact have enough kinetic energy to travel to the collector itself. Therefore, ideally as small a distance as possible is required in devices of this kind, however, one cannot put the two surfaces too close together as either a short circuit will occur or the collector material itself will be heated. This final thought brings us onto the next problem of device construction, namely, emission from the surface of the collector. If the collector is heated to a sufficient temperature for its given work function it too will thermionically emit which will distort the electric field between the emitter and the collector, thus obfuscating the path of electrons from the emitter and lowering the quality of emission. This too is an important consideration and is an effect which adds to what is known as the space charge region, which can also be added to, as discussed previously, by electrons from the emitter with an insufficient amount of energy to cross the emitter-collector distance distorting this electric field. This effect can be mitigated by the application of a potential difference between the emitter and collector as seen in the load in figure 12. This effect of space charge can also be accounted for via the use of Child's Law which relates the voltage of the anode and the distance between the cathode and the anode to the current density of the system[43]:

$$J = \frac{4\varepsilon_0}{9}\sqrt{\frac{2e}{m_e}}\frac{V^{\frac{3}{2}}}{d^2} \quad (2)$$

where J is the current density, ε_0 is the vacuum permittivity, e is the charge of an electron, m_e is the mass of an electron, V is the anode voltage and d is the separation between emitter and collector.

Additionally, the thermodynamic efficiency of the device as a whole must be accounted for using the Carnot relation for a heat engine as the greater the difference in temperature between the collector and the emitter the greater the efficiency the device will have[44],

$$\eta = 1 - \frac{T_C}{T_e} \quad (3)$$

where η is the efficiency of the heat engine, Tc and Te are the temperatures of the collector and emitter respectively in Kelvin. Finally the work functions of both the collector and emitter are important considerations. Both should be as low as possible, for the emitter this is the case in order to ensure maximum emission from the sample and for the collector it is to ensure maximum collection i.e. so the incoming electrons have as minimum of an energy barrier as possible. Given these maxims it is possible to construct a basic thermal energy converter however if taking other surface enhancements into account such as surface termination this becomes a more complicated problem as it is important to consider how the surface termination changes with temperature and over time [15].

1.7 Collector and Emitter Materials

As previously mentioned the work functions of both emitter and collector should be low, ideally with the work function of the collector being lower than that of the emitter. However the two elements of a TEC differ in what is required for construction of an efficient TEC. For an emitter a high thermal conductivity is required to ensure the sample can be heated easily and efficiently. Moreover, the emitter should have a high melting temperature to ensure that there is no instability or damage to the system during thermal excitation. Conversely the collector is required to have a low thermal conductivity to ensure that the temperature difference between the emitter and the collector is as low as possible at all times to increase efficiency of the system. In both cases it is also paramount that both materials be conductive in order for the system, seen in figure 12, to produce current.

1.7.1 Polycrystalline Nitrogen Doped Diamond

Nitrogen doped diamond (NDD) is an n-type semiconducting material which becomes conductive at 300°C, this can be explained by the Fermi-Dirac Distribution[42]:

(6)

$$f(E,T) = \frac{1}{e^{\frac{E-E_F}{K_{BT}}} + 1}$$

where E_F is the Fermi energy and f(E,T) is the probability of a state being occupied by an electron. Clearly it can be seen that as the temperature increases the probability of finding electrons at a higher energy is increased, i.e seeing electrons occupying states beyond the Fermi level, this can be seen in figure 13. The CVD molybdenum grown hydrogen terminated variant has a relatively low work function of a maximum at 4.2eV owing to its use as either an emitter or as a collector[19]. However as previously discussed this hydrogen termination begins to desorb from the surface at temperatures of 600°C. The tin monoxide variant has a reported work function of 4.1eV[12].

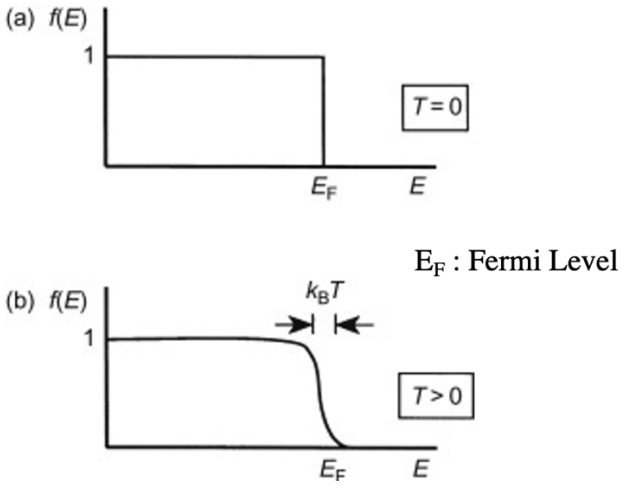

Figure 13: A set of graphs showing the difference in population with relation to temperature and the Fermi-Dirac distribution, adapted from [17].

1.7.2 Polycrystalline Phosphorous Doped Diamond

Similar to NDD, phosphorous doped diamond (PDD) is also an n-type semiconductor with a distance from the conduction band lower than that of nitrogen as seen in table 1. For this reason it can be seen as a viable emitter or collector for thermionic emission. Furthermore the growth process of PDD films is problematic in comparison to that of their nitrogen doped counterparts. This is due to the size of the phosphorous atoms distorting the overall structure of the diamond film disrupting the long range C-C bonding that occurs in the structure and allowing for conductivity[30]. In effect too heavy phosphorous doping can result in the formation of a greater amount of sp^2 carbon bonding which reduces the conductivity of the material and the purity of the diamond film[50]. Therefore it is important to have a low ratio of phosphorous to CH_4 in the reaction chamber. As such the work function is very sensitive to the amount of dopant used in the reaction.

2.0 Experimental

2.1 Aim and Overview

The aim of this thesis is to investigate the possible viable materials that could be used as a collector in a thermionic energy converter, and to investigate the effect that different surface terminations can have on the amount of emission received based on the phenomenon of space charge addition. Specifically, using poly-crystalline diamond films to investigate this effect of space charge. The purpose of this aim is to update the current understanding of TEC construction with a view of moving towards a viable device in the future. The project had 5 major milestones that needed to be met:

1. The acquisition and growth of the base samples for testing and in the case of grown samples the determination of the best seeding technique to use on a molybdenum substrate.
2. The characterisation of the samples to be used in testing via Raman spectroscopy and SEM to determine quality of diamond grown and orientation of the surface.
3. The termination of the samples to be used as collector materials in the thermionic testing as well as the fabrication of a sample loader and the preparation of the emitter sample.
4. The calibration of the sample loader system to ensure the contribution of the current from the loader itself could be subtracted from the overall measured current when testing samples.
5. The full testing of the collector samples in the thermionic system at different voltages to identify the effects of space charge and surface termination.

The materials used in this project are NDD and PDD films with differing surface terminations and are outlined in table 2.

Table 2: A table outlining the samples used for testing.

Collector Samples		
Termination	NDD	PDD
Hydrogen	1	1
Oxygen	1	1
Tin Monoxide	1	N/A

2.2 Seeding

The initial problem of the project involved finding a suitable seeding technique to ensure that the growth of the diamond films was of good quality on a 10x10mm molybdenum substrate. This element of the research was required due to the large difference in thermal expansion coefficient of molybdenum (4.8×10^{-6} K^{-1} [64]) compared to that of diamond, meaning the likelihood of delamination during the growth process was a significant problem to account for. In total, three seeding methods were used to determine the correct method overall to ensure nucleation of the sample, they are: manual abrasion, dip seeding and electrospray. Manual abrasion was performed initially by cleaning the surface of the substrates with methanol and allowing them to dry then using

diamond powder of a size of 2 ± 1μm to produce scratches on the surface of the substrate for nucleation and following this clean once more with methanol to ensure no microdiamond powder remained on the surface. The benchmarked dip seeding method involved cleaning the surface of the substrates with isopropanol and then placing them in a beaker of isopropanol in a sonicator for 3 minutes to ensure maximum cleaning of the surface. Following this the substrates would be placed in a carboxyethylsilanetriol disodium salt for two minutes and then cleaned in two separate beakers of deionised water for 2 minutes to ensure no excess on the surface of the substrates in order to form a monolayer. Immediately after the cleaning process the substrates were then placed in a nano diamond solution (0.018 μm) of water and then cleaned in the same manner as with the silane solution. Finally the substrates were then dried using an air gun to ensure no excess nanodiamond or deionised water was on the surface, once again in an attempt to form a monolayer of nanodiamond on the surface. This method however differed with some samples being cleaned in methanol instead, others being air dried or blow dried and some samples not being cleaned in deionised water after being dipped in the silane solution in order to see if the quality of growth changed. It was observed overall that there were 2 successful growths for the dip seeding technique: one involving the benchmarked technique and another involving a blow dried methanol cleaned technique. Additionally, a further 2 samples showed partial growth on the substrate with the benchmarked technique. The different forms of growth may be seen in figure 14. Finally for the electrospray technique initially substrates were cleaned in isopropanol and then loaded to the spinning stage of the University of Bristol diamond lab electrospray kit and a syringe opposite to the sample was loaded with ten drops of methanol diamond solution (3.3 ± 0.6 μm), a voltage of 37.5 kV was applied to the syringe to vaporise the solution and arc the microdiamond across onto the spinning stage. Overall 14 samples were prepared the success of which may be seen in table 3.

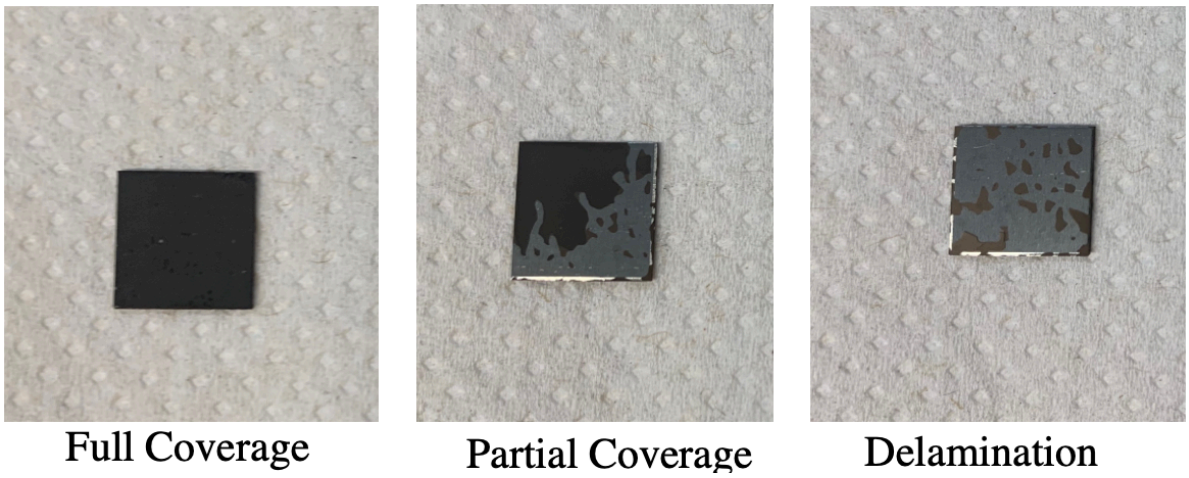

Figure 14: An image showing the difference between full, partial and delaminated deposition.

Table 3: A table outlining seeding techniques and their success.

Seeding Techniques			
Seeding	Abrasion	Dip Coating	Electrospray
Number of samples	3	9	2
Number of successful growths	3	2	0
Number of partial growth	0	2	0

2.3 Growth and Acquisition

The two types of diamond film used in the project, namely, NDD grown on a molybdenum substrate and PDD grown on a <111> n-type silicon substrate were grown using the MPECVD method. Despite the difference in element both substrates are still useful for growth due to their ability to form carbides and withstand high temperatures. The difference in substrate is due to the availability of PDD, ideally it would have been grown on a molybdenum substrate to improve its conduction during the thermionic testing. The PDD was not prepared in the University of Bristol diamond lab but instead grown and acquired from Hasselt University. The films were grown using a plasma of PH_3, CH_4 and H_2 with a 500sccm flow rate of a 10,000ppm PH_3/CH_4 ratio with the PH_3 diluted in 200ppm of H_2 The microwave source used was a 2.45GHz ASTeX PDS17 magnetron and the microwave power set was 2500W with a pressure of 70 Torr and an overall growth time of 3 hours to ensure polycrystalline growth due to the mismatch in size between carbon and phosphorous. Multiple growths were performed with a different percentage of CH_4 used in the gas environment varying from 0.50 - 1.50% thus changing the graphitic content of the material.

The NDD was prepared in the water cooled MPECVD reactor in the University of Bristol diamond lab. The films were deposited at temperatures between 900°C-1100°C and microwave power of approximately 1300W (using an ASTeX 1.5KW magnetron) for a growth time of 1 hour ensure a polycrystalline diamond film growth. The pressure during growth was kept at approximately 130 Torr with a gas mixture of 0.300 SLM of Hydrogen, 12.5 SCCM of CH_4 and 0.30 SCCM of N_2. Additionally, a Raytek Thermalert SX optical pyrometer was used to measure the temperature during growth with an emissivity of 0.17 used. The plasma in the reactor in each case was struck at around 15 Torr using 45 percent microwave power in a solely hydrogen environment then the pressure was set to the desired previously stated value, at around 45 Torr the other gases were fed into the reaction chamber. At the end of the growth cycle the lowering of the temperature of the reactor was performed slowly to ensure the diamond films did not delaminate from the surface of the substrate and the

microwave source was tuned to insure a minimum amount of reflected power so as to not damage the power source.

Of the overall prepared samples 4 were selected for thermionic testing: a 0.75 percent methane growth PDD and 3 abrasion seeded NDD with 1 of the abrasion seeded NDDs to be used as the test emitter and the remaining samples used as sample collectors in the thermionic energy converter.

2.4 Characterisation

2.4.1 Raman Spectroscopy

Raman Spectra were taken using a Renishaw 1000 Raman spectrometer utilising a laser of wavelength 515nm. In each case the measurements were taken centred on the 1332cm^{-1} peak in order to verify the presence of the diamond sp^3 structure in the samples and also determine the quality based on the associated graphite sp^2 peak next to it.

2.4.2 SEM

The surface morphology of the samples were characterised using scanning electron microscopy in the University of Bristol school of chemical imaging facility. Images of the samples were obtained at a top down angle at magnifications of :x20,000, x10,000, x5000, x2000, x1000 and x200. Additionally, images were taken at a 70 degree angle relative to the surface of the sample at magnifications of x5000, x2000, x500. In each case an accelerating voltage of 15kV was used and a working distance of 9mm used for the top down images as well as a working distance of 8.9mm used for the canted images.

2.5 Grating

Due to the refractory nature of molybdenum the material is poor at accepting radiative heat therefore the emitter sample was given a 10.5 μm grating on the back surface to produce a more efficient surface for laser heating via the production of a surface plasmon resonance effect, improving the absorption of the surface infrared photons. This grating was produced using an Oxford Lasers ALPHA 532 system laser cutter and an image of this grating may be seen in figure 15.

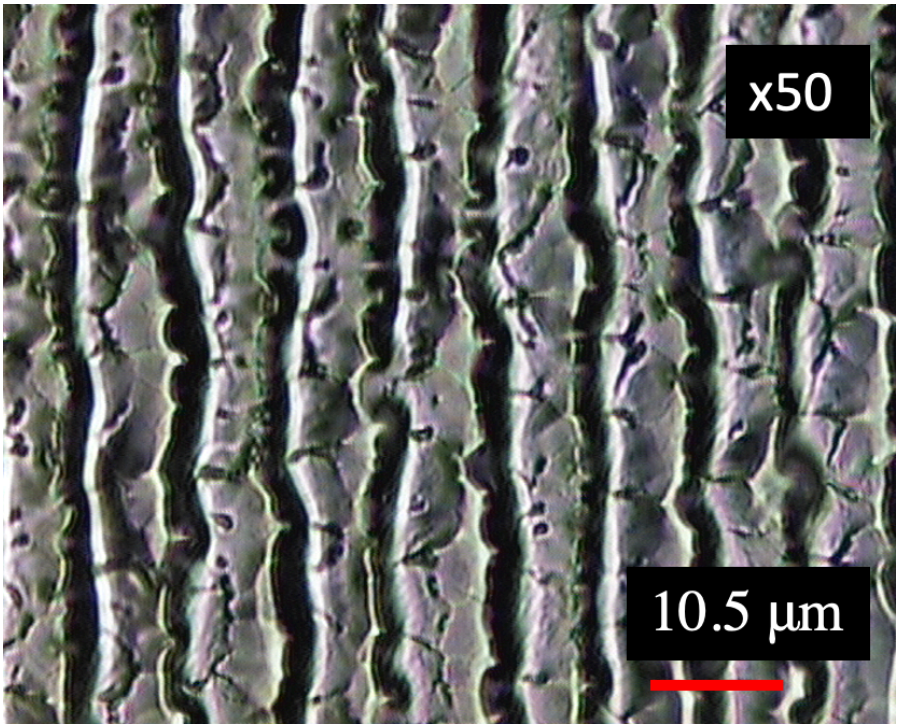

Figure 15: A microscope image taken in the Renishaw 1000 Raman spectrometer of the 10.5 µm grating on the molybdenum backside of the NDD emitter sample.

2.6 Surface Termination

2.6.1 Hydrogen

Hydrogen termination of the samples was performed in order to imbue a negative electron affinity surface to the PDD and the NDD films. This was achieved in the same MPECVD reactor as used for growth utilising a 0.300SLM gas environment solely of hydrogen. The conditions for the hydrogen termination can be seen in table 4.

Table 4: A table outlining the average conditions for hydrogen termination.

Hydrogen Termination Conditions				
Run type	Pressure(Torr)	Power(W)	Temperature(°C)	Time(s)
Heating	90-100	1000W	850-900	2
Termination	45-50	500-560	500	2
Cooling	30	0	N/A	2

For each new thermionic test of a collector sample performed the NDD emitter sample was hydrogen terminated using these conditions. From table 4, the initial heating step is performed in order to clean the surface of the material of any contaminants such as hydroxyl surface terminations, physical contaminants or even hydrocarbon contaminants from the air. The termination step occurs at a lower temperature where the hydrogen in the gas environment is activated forming radicals, allowing for quick surface termination. Finally the cooling step is used to ensure the sample does not delaminate and that any left over vacant sites can be hydrogen terminated. A view of the MPECVD reactor during a hydrogen termination run may be seen in figure 16.

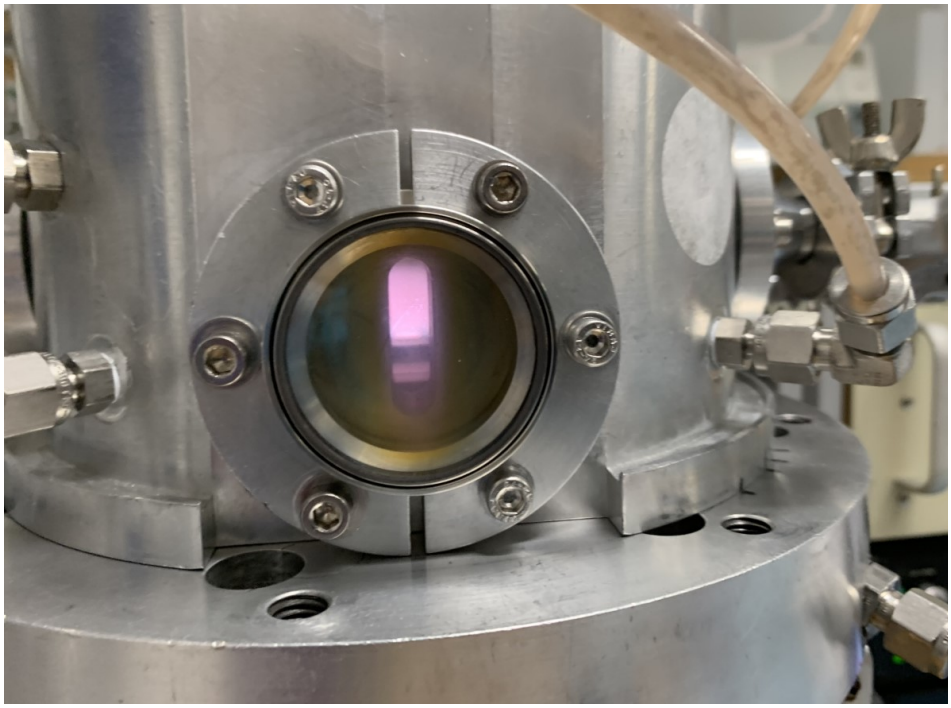

Figure 16: An image showing the interior of the MPECVD reactor during a hydrogen termination cycle of NDD on a molybdenum substrate.

2.6.2 Oxygen

Oxygen termination of the NDD and PDD samples was performed in two steps, firstly by initially hydrogen terminating the sample using the conditions in table 4 in order to clean the surface and prepare it for oxygen termination. Following these steps the samples are then quickly transferred to the UV Ozone cracker in the University of Bristol soft matter at interfaces laboratory. The samples would then be subject to an oxygen environment which is a product of a photolytic reaction with ozone for 30 minutes in the ozone cracker. The UV ozone cracker device may be seen in figure 17.

Figure 17: An image showing the UV ozone cracker used to perform oxygen termination.

2.6.3 Tin Monoxide

The tin monoxide terminated NDD sample was prepared similarly to the oxygen terminated step whereby a hydrogen termination step was performed followed by an exposure to an oxygen environment in the UV Ozone cracker. Upon oxygen termination the material was then transferred to the University of Bristol NanoESCA facility where it underwent E-Beam deposition for 26 seconds at a rate of 7.5 Å/min at 30W, 0.8ML of Sn was used, depositing a 3.2Å layer. Following this the material was annealed at 500°C for 1 hour to improve the surface concentration of the tin monoxide. Following this the quality of the deposition was determined using XPS.

2.7 XPS

X-ray photoelectron spectroscopy (XPS) is a technique used widely in the field of surface and material science as it allows for the identification of a material's elemental and molecular make up. This analytic technique operates principally via the photoexcitation of electrons from a surface of a material using X-ray photons as the excitation source. The emitted photoelectrons then travel and are accelerated by a hemispherical analyser, which is capable of selecting electrons of a particular kinetic energy and then colliding them with a detector which measures the kinetic energy of these photoelectrons.

XPS was performed in the University of Bristol NanoESCA facility on the tin monoxide deposited surface after annealing to analyse the quality and nature of the deposition at an approximate pressure of 10^{-9} Torr. The source was excited using an Al Kα monochromatic excitation source with an energy of 1486.7eV with a dwell time of 0.25s and 2 total sweeps with a scan of kinetic energies between 286.7-1487.7eV with an energy step of 0.5eV. This sweep initially was to determine the location of the peaks relating to carbon, tin and oxygen. Following the general scan individual scans were taken at smaller intervals to investigate the peaks more closely. The intervals are as follows: 1188-1208eV, 971-1011eV and 942-962eV. The initial scan performed in the interval 1188-1208eV is to identify the carbon 1s peak which is used to calibrate the system after the sweeping scan. The binding energies of the peaks are then obtained from the following equation:

$$E_{BE} = E_{PE} - E_{KE} - \phi \qquad (7)$$

where E_{BE} is the binding energy, E_{PE} is the photoexcitation energy , E_{KE} is the electron kinetic energy recorded at the analyser and ϕ is the work function.

2.8 Ultraviolet Photoelectron Spectroscopy (UPS)

UPS analysis was performed in the University of Bristol NanoESCA facility in order to investigate the work function of the surfaces used in this project. Two UV photoelectron excitation sources were

used, namely, a 5.2eV mercury lamp which produces photons of many different wavelengths and a 21.2eV monochromatic helium lamp was used. The two different lamps were used as the helium lamp gives the best results for samples that show insignificant charging whereas the mercury lamp has the opposite function of producing somewhat less accurate results for the work function map of a surface. Additionally, the pressure was kept at approximately 10^{-7} Torr during measurements. The range of energies that were tested were between 1 eV and 5 eV for the work function. 0.75 and 1.25 % PDD samples were initially tested to determine the efficacy of this method as a whole and it was determined that too significant charging effects were observed so the method was not used further in the project instead a work function comparison through thermionic profiles was used.

2.9 Thermionic Testing

2.9.1 Thermionic Test Rig

All thermionic testing was performed on the University of Bristol diamond lab thermionic test rig a schematic of which may be seen in figure 18. The system operates principally by heating a sample using a Synrad firestar 40W IR CO_2 laser which produces a beam of wavelength 10.6 μm and utilises an ametek-land spot r160 optical pyrometer set to the second monochromatic channel with the emissivity set to 0.125 for molybdenum. The uncertainty of the optical pyrometer is ± 0.25% K[41]. Additionally, the system is evacuated using a rotary pump initially to allow for the activation of a turbomolecular pump to achieve vacuum of approximately 10^{-7} mbar for testing. Moreover, the distance between the emitter and collector was set at 200 μm when loading the samples onto the sample stage, this was performed outside of the reactor as initial testing showed that movement of the collector motor was prone to accidental shorting of the collector wires on either the emitter connections or on the reactor wall itself. Additionally, bias's of 25V and 5V were applied across the emitter and collector in order to investigate the effects of back emission on the space charge region in the system.

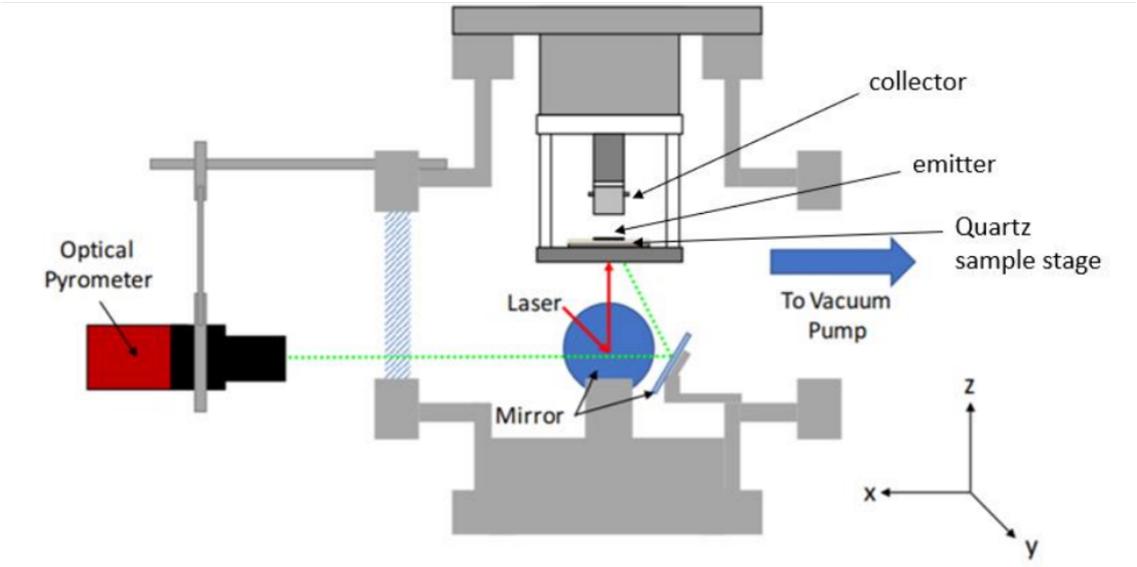

Figure 18: A schematic detailing the elements of the thermionic test rig used to perform thermionic emission, taken from [33].

2.9.2 Sample Loading and Calibration

In order to test the collector materials a sample loader was fabricated in the University of Bristol School of Physics mechanical workshop. Additionally, the collector samples were cut into 5mm diameter discs in order to fit into the sample loader. The sample loader was fabricated from stainless steel and consisted of two moving parts, namely, a 10mm diameter stem which connected to the thermionic test rig containing a 7mm diameter circular recess of approximately 0.5mm to allow the samples to sit as flush as possible with the edge of the stem. The other half of the sample loader consisted of a threaded cap which screws onto the stem which had a 6.5mm inner diameter to allow the samples to be held in place when layed upside-down in the sample loader. These components may be seen in figure 19. Due to the nature of this sample loader it is likely an element of the overall current collected will contain a contribution from the rim of this cap. Therefore in order to account for this contribution initial calibration with the sample loader was performed to determine the overall current without any experimental collector materials. The testing was performed using the NDD hydrogen terminated sample emitter, measuring the overall current across the circuit using just the stem of the collector loader and then using both the stem and the cap components together. The former was then subtracted from the latter allowing for a percentage contribution from the cap to be determined which could then be subtracted from future measurements. This calibration may be seen in figure 20.

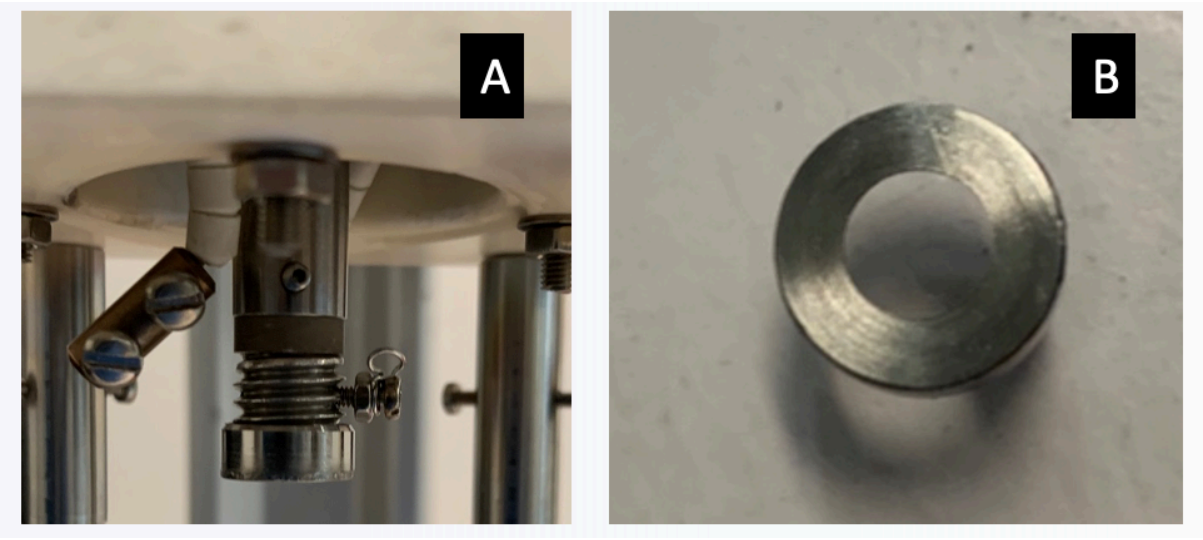

Figure 19: A set of images of the stainless steel collector sample loader where (A) is the combined unit of stem and cap and (B) is a top down view of the cap alone, illustrating the inner diameter.

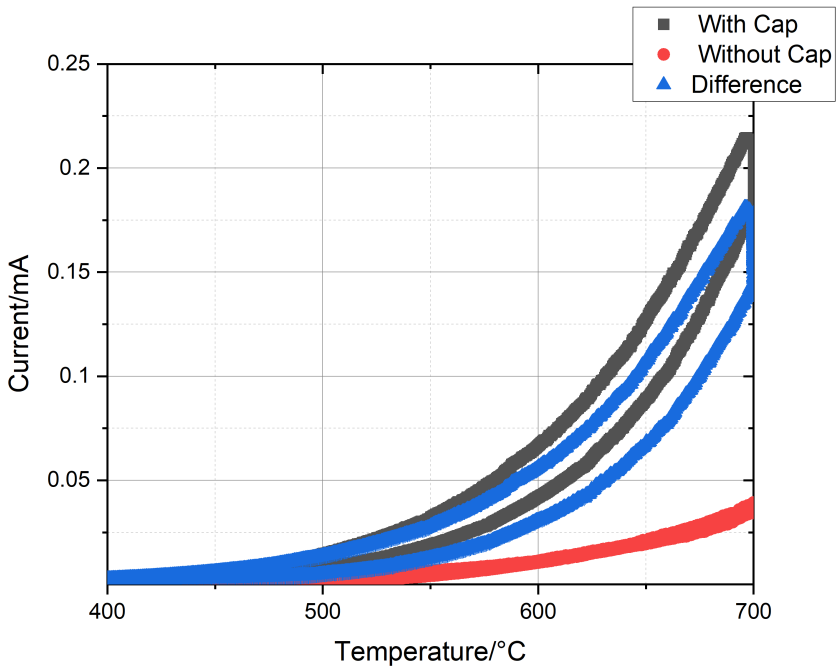

Figure 20: A graph showing the relationship between current and time for the calibration of the stainless steel sample loader.

2.9.3 Thermionic Runs

The thermionic runs to test the output current of the different materials were performed in standardised thermal ramping profiles using a proportional integral derivative controller to adjust the laser power accordingly using a feedback loop to ensure the temperature ramping performed had little uncertainty and was uniform. The standard temperature ramp used in the thermionic tests involved an incremental increase of 1°C/s from a temperature of 400°C-700°C and then back again with the

temperature being held at 700°C for 50 seconds to investigate any surface desorption effects. An average temperature ramping profile may be seen in figure 21. For each sample tested the temperature profile was run six times in total, 3 at a bias voltage of 25V and 3 at a voltage of 5V. The runs would be performed successively starting with a bias of 25V and ending with a bias of 5V. The re-termination of the emitter surface with hydrogen was performed as despite the instability of the surface, the operating temperatures of the runs ensure that the surface termination would not desorb or contaminate significantly between profiles.

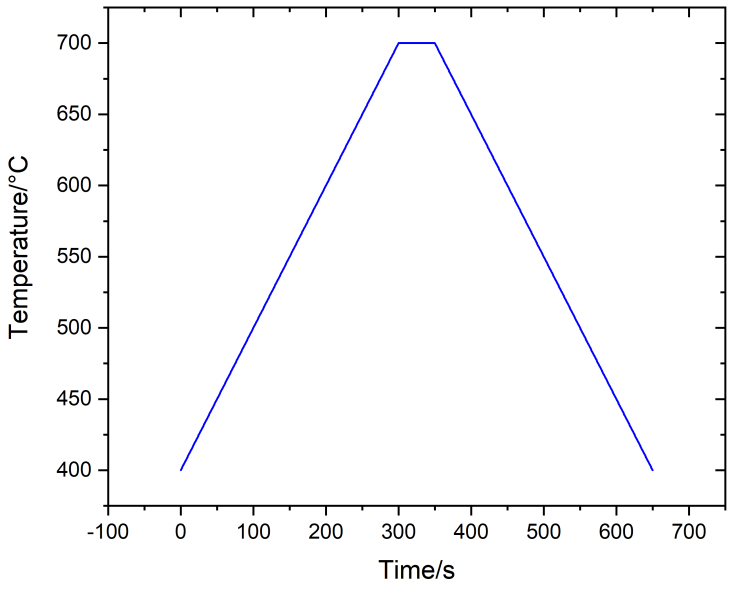

Figure 21: A graph showing the temperature profile used for all thermionic runs.

3.0 Results

3.1 Growth

The growths performed in the MPECVD reactor in total produced 10 successful diamond films with 5 being NDD grown on molybdenum and 5 PDD grown on <111> silicon. Of the growths performed in the University of Bristol diamond lab there were a variety of alterations made to the method of dip seeding to attempt to perform successful nucleation and growth on molybdenum. The initial method tested was abrasion which seeded two successful growths with full surface coverage. Despite this it was clear the growth was not uniform due to one sample exhibiting a darker centre on the surface with lighter edges and the other sample exhibiting the opposite. This may be due to the random nature of the scratches formed on the surface during the seeding technique itself causing some areas to exhibit stronger or deeper nucleation than others or due to the shape of the plasma itself. For the dip seeded

samples there were many samples that were tested with different methods to try and achieve successful nucleation they are as follows:

1. 4 samples were seeded with the bench marked method, previously mentioned, however with 2 of the samples being dried with the air gun at a reduced pressure in order to reduce the possibility of manually removing the seed monolayer. The 2 growths performed with the bench marked seeding produced growth on the surface however with only partial coverage. The growth with a reduced air gun pressure produced one delaminated sample and one successful growth. The delamination could be due to the formation of a multilayered seed meaning the diamond formed on the surface could be forming on top of a seed layer of nanodiamond.
2. 4 samples were seeded without the use of the air gun to dry the substrates, being left instead to air dry. The first sample with this technique was not cleaned in deionised water and resulted in delamination which could similarly be ascribed to the formation of a multi-layered seed. The second and third samples were given the full benchmarked technique without the use of the air gun and equally exhibited considerable delamination, which may in part be due to higher growth conditions used (135 Torr and 1350W) due to a low temperature being recorded in the reactor. The fourth sample was cleaned in methanol and then allowed to air dry and also exhibited delamination which may be in part due to the volatile nature of methanol liberating too much of the seeding nanodiamond such that a monolayer does not form.
3. The final technique attempted for successful dip seeding utilised a methanol cleaning step at the end of the process and blow drying with an air gun which yielded successful growth.

The samples prepared by electrospray exhibited considerable delamination with portions of the substrate showing no growth whatsoever. Alongside the attempts to achieve successful nucleation through the different seeding techniques used, different temperature ramping times were used to investigate the effect of delamination, however they proved inconclusive with both fast and slow cooling times showing some delamination and some successful nucleation. Overall it was observed that the abrasion seeding technique exhibited the best growth on molybdenum substrates which could be due to the mechanical nature of the seeding technique itself meaning that the diamond that does deposit on the surface is better attached to the substrate itself and forms a stronger carbide than those formed solely on a monolayer of a diamond seeding material.

3.2 SEM

There is a clear difference between the NDD and PDD samples, as seen in figures 22, 23 and 24, owing to the substrate used for growth. The phosphorous doped samples exhibit a <111> morphology of “spikey” peaks whereas the nitrogen doped samples show flat plateaus of a <100> nature. This difference is due to the substrate used and the greater microwave power. Despite this generalisation

there are distinct differences in all of the samples. For the NDD tin monoxide terminated sample (figure 25) there is clear <100> type growth at the top of the peaks but the peaks themselves exhibit a form of <111> type morphology in the way that they are more jagged. In comparison the hydrogen terminated NDD sample shows more classically <100> morphology and this can be seen in the top down view images of the samples. Which suggests the tin monoxide samples should show a higher current due to a greater surface area overall and greater number of grain boundaries which should exhibit the sp^2 hybridised graphite form of carbon and therefore be more capable of accepting electrons. Additionally, it is clear to see small clusters attached to the sides of some of the "peaks" in the tin monoxide sample which may be tin or tin oxide nanoclusters. These can be seen further in the bright spots as seen in the top down view from the backscattered SEM image of the surface at low magnification (figure 26).

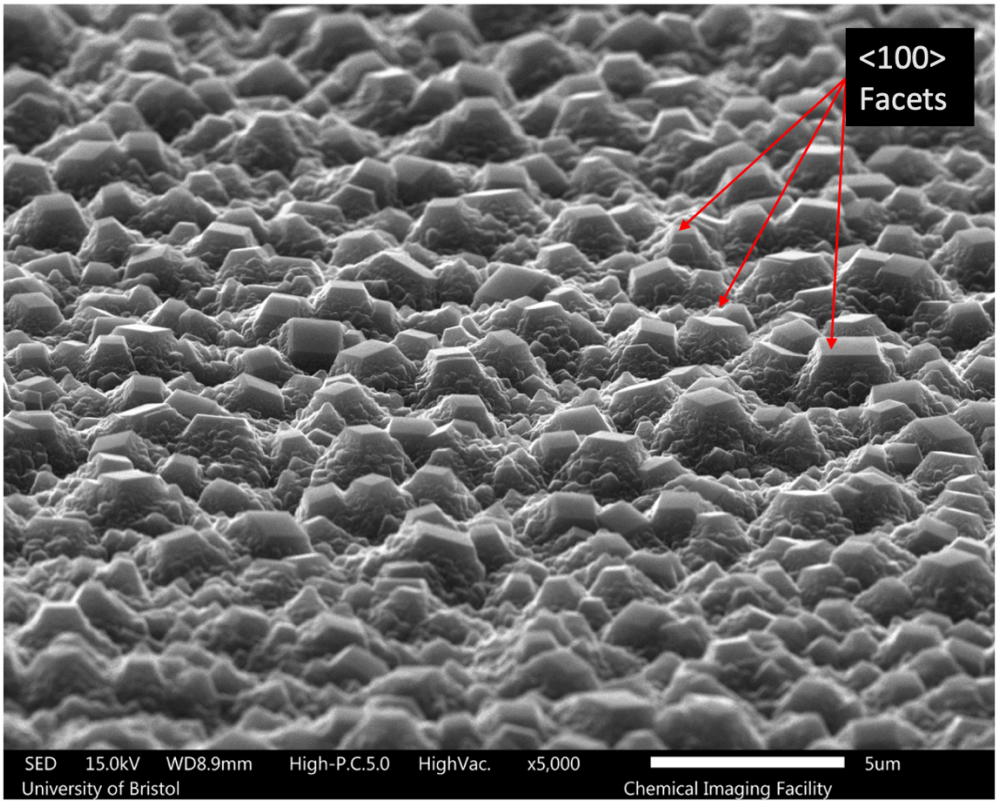

Figure 22: An SEM image taken canted at 70 degrees exhibiting the difference between a NDD surface grown on molybdenum.

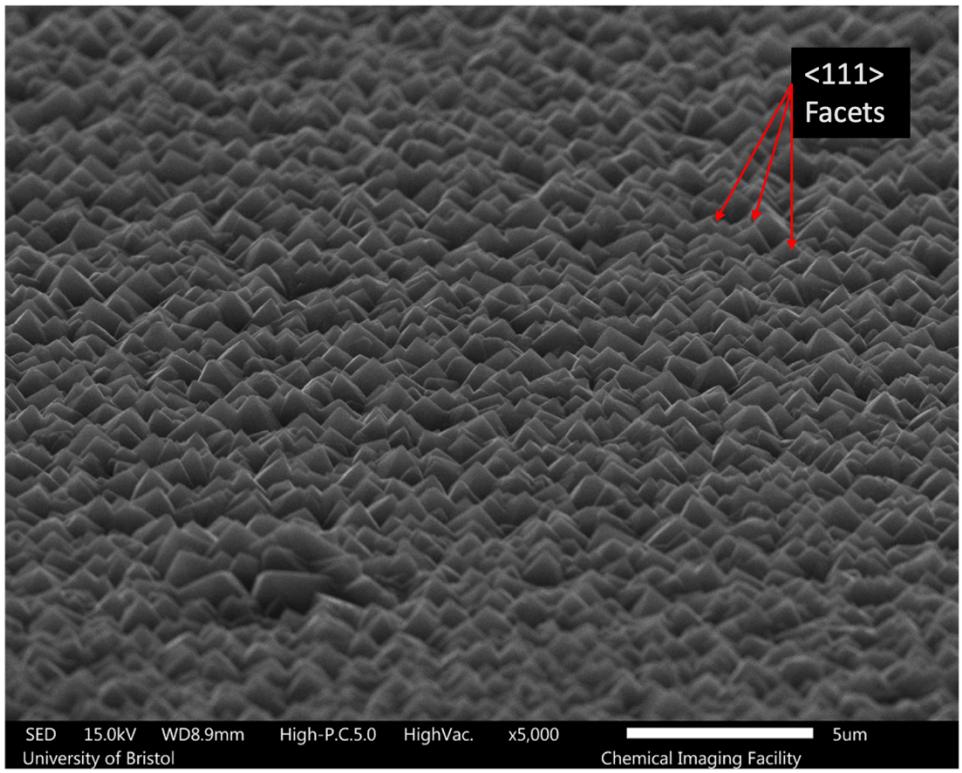

Figure 23: An SEM image taken canted at 70 degrees exhibiting the difference between a PDD surface grown on grown on silicon.

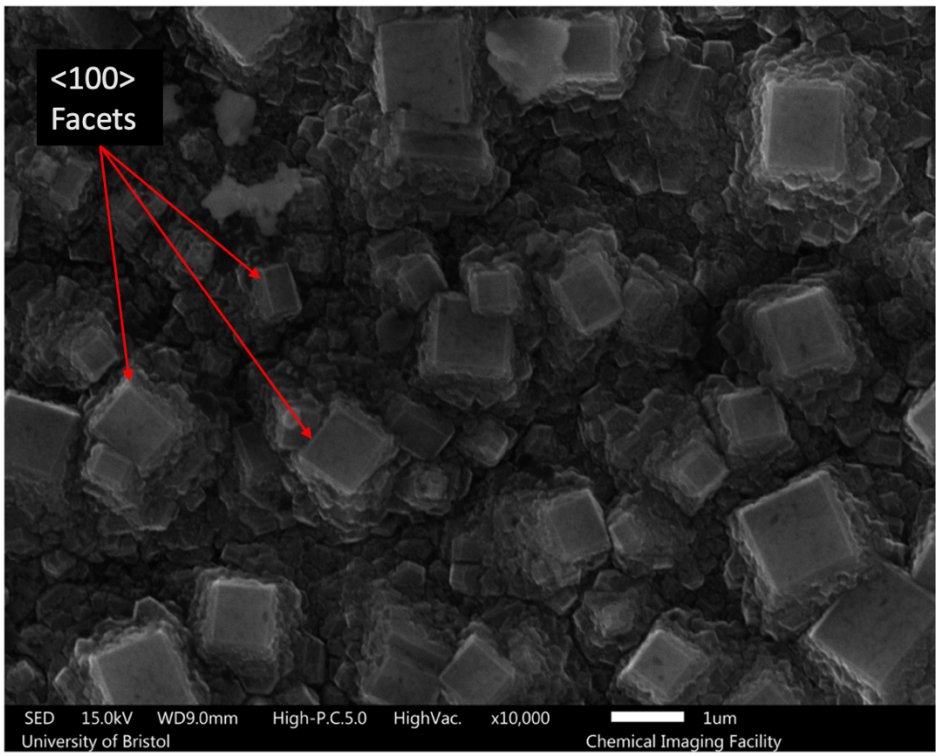

Figure 24: An SEM image taken top down of a NDD surface grown on molybdenum.

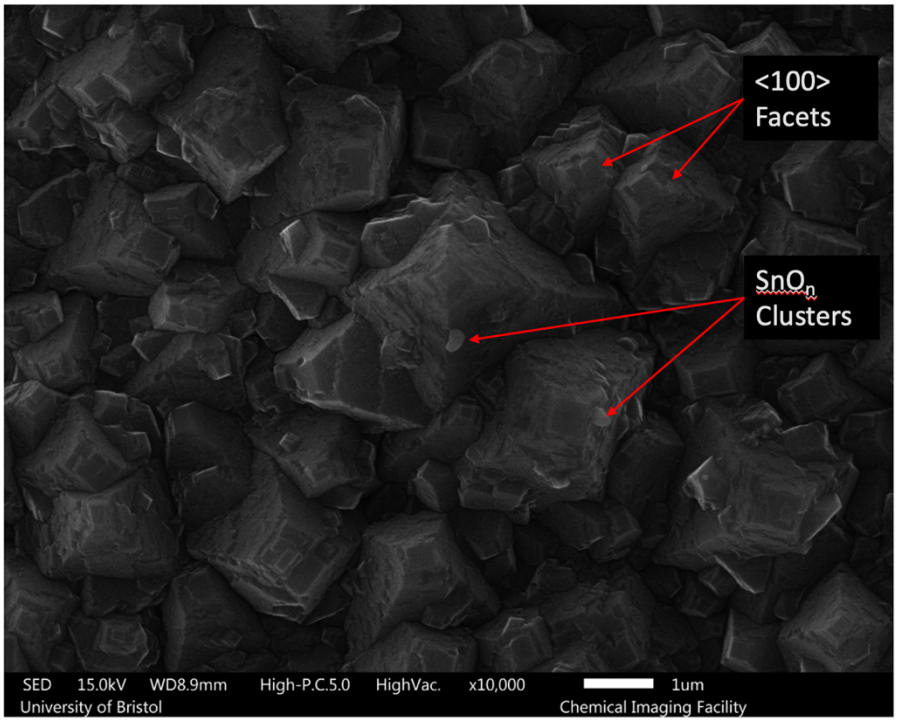

Figure 25: An SEM image taken top down of a tin monoxide terminated NDD surface grown on molybdenum.

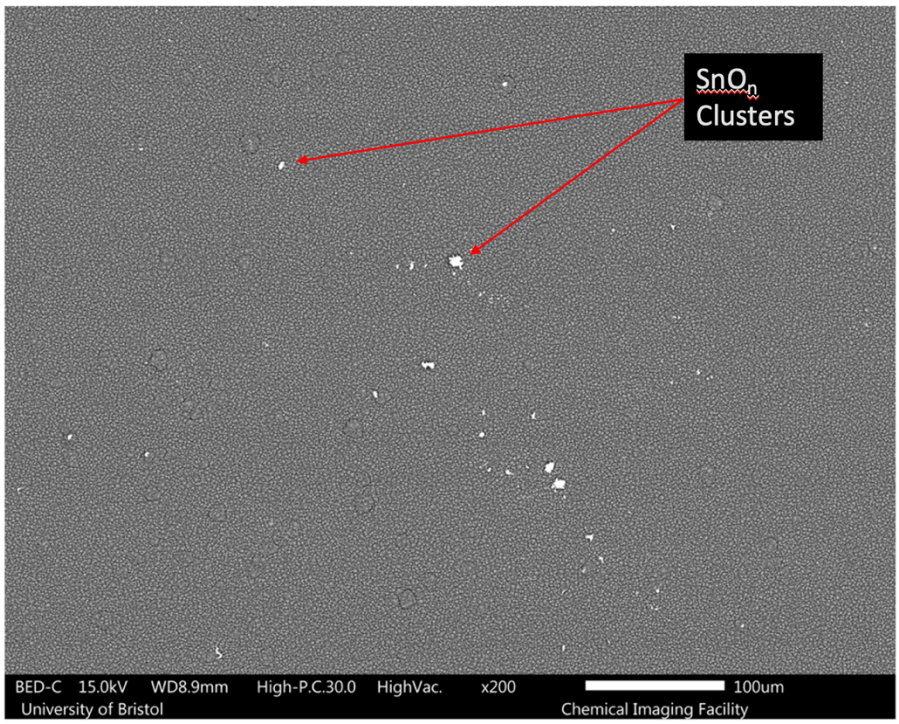

Figure 26: A back scattered SEM image taken top down of a tin oxide terminated NDD surface grown on molybdenum.

3.3 Raman

Raman analysis of NDD and PDD samples was performed in order to determine the difference in growth between the two types of sample by identifying the shift of the sp^3 and sp^2 peaks for carbon respectively(figures 27 and 28). The shift in these peaks is also in part due to the doping itself affecting the bond length in the material. Additionally, the effects of noise in the samples due to their different substrates is investigated with this technique. In the case of the NDD sample the characteristic sp^3 was shifted upwards to a value of 1336cm^{-1} as opposed to the literature value of 1332 cm^{-1} this is most likely due to a bond length shortening caused by the doping in the material[39]. The sp^2 carbon peak was found at a raman shift of 1564 cm^{-1} which differs from the literature value of 1560 cm^{-1} for the same reason as the sp^3 peak[40]. Overall the quality of the diamond film is clear in the spectra with a large relative intensity and there is very little noise in the measurements this can be seen in figure 27. In comparison the PDD sample also exhibited a shift in the sp^3 diamond peak to a value of 1334 cm^{-1} which is also due to the change in bond length of the material. Additionally, a noisy peak was observed between 1478-1540 cm^{-1} corresponding to the sp^2 peak which differs greatly from the literature value and may be in part due to the <111> morphology of the material and also due to the change in bonding of the material, whereby some elements of PDD exhibit bond shortening and others bond lengthening[34]. Moreover, a shallow peak can be seen at 951 cm^{-1} which is due to second-order scattering by the silicon substrate itself[35]. Additionally, the quality of the PDD growth is brought in to question with the far lower intensity for the observed peaks overall in comparison to that of the NDD sample with the PDD spectrum showing intensities one order of magnitude lower than that of the NDD samples suggesting the quality of the diamond growth was lower than that of the NDD diamond film. This, however, we know cannot be true from the SEM images of the diamond samples, it is clear to see that both samples show good quality diamond growth. Equally it is clear that the measurements obtained for the PDD sample exhibit considerable noise which is likely due to the lower overall intensity. Finally measurements of the full width half maximum for the NDD and PDD sp^3 peaks obtained were 10.9 ± 0.4 cm^{-1} and 14.1 ± 0.3 cm^{-1} respectively, suggesting the better quality of the NDD sample.

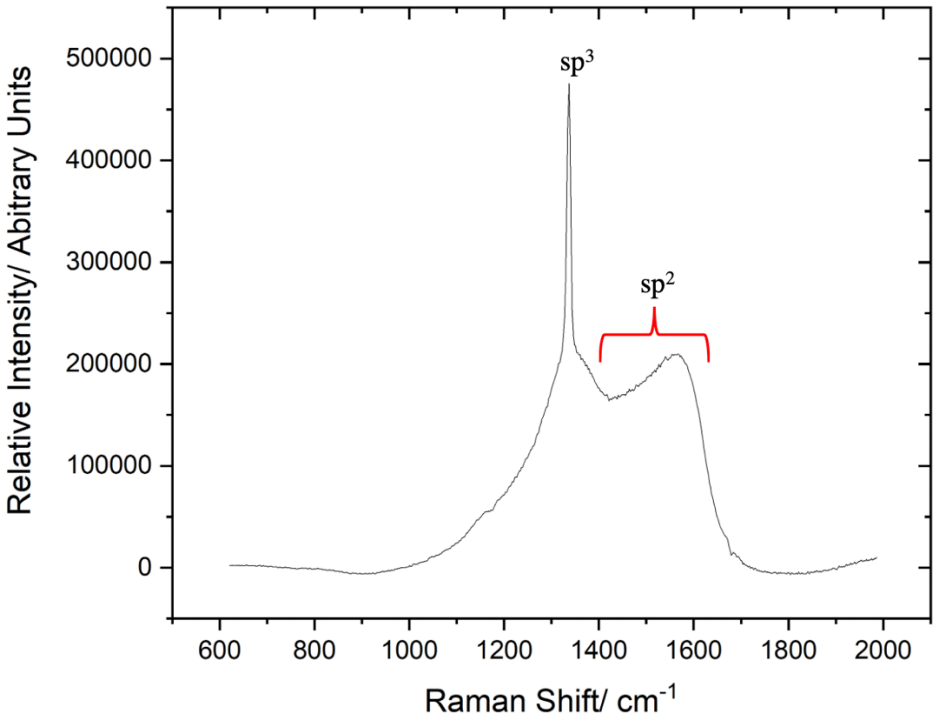

Figure 27: A Raman spectrum taken an NDD sample grown on molybdenum.

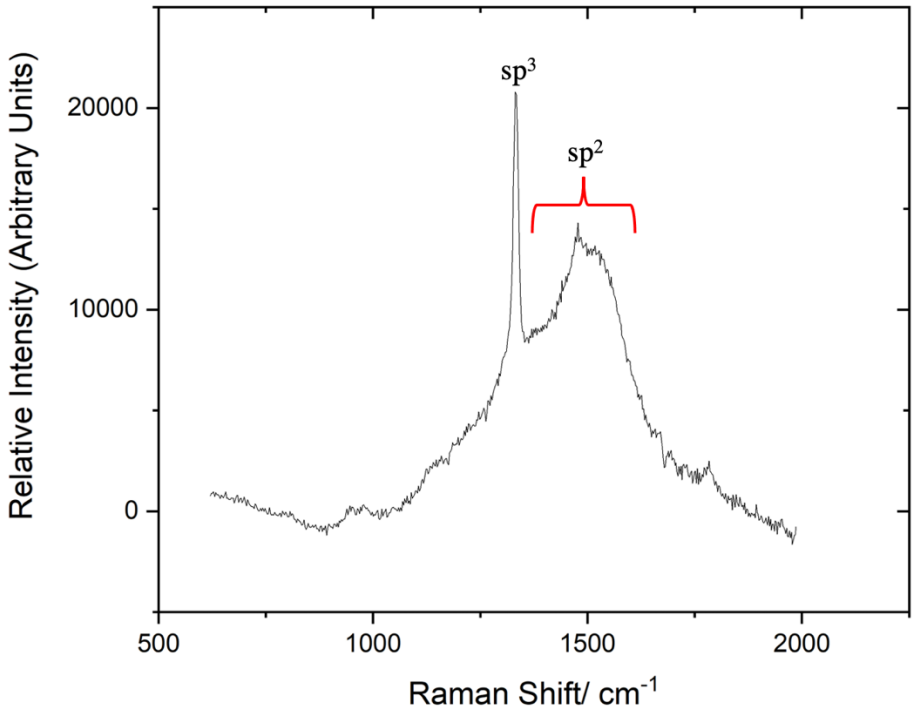

Figure 28: A Raman spectrum taken an PDD sample grown on silicon.

3.4 UPS

The UPS analysis of PDD samples produced surface maps of the work function of the materials. Initially the 1.25% methane growth was tested with both the mercury and helium photon sources and

a work function ranging from 2-2.5eV was observed on the surface. This value is unlikely for the surface of the PDD, therefore it is likely that considerable charging effects led to this low value of work function. The work function map of the surface may be seen in figure 29. This charging may be in part due to a lower purity of the diamond due to the greater quantity of CH_4 used in the growth process leading to a higher proportion of sp^2 graphitic carbon in the material. For the case of the 0.75 percent methane growth sample the initial measurements with the helium lamp yielded very unlikely results for the work function of the surface ranging from 1-2.2eV, suggesting significant charging in the sample. As such the mercury lamp was used instead as a lower excitation energy ensures less charging of the surface in this way a more realistic work function surface was obtained with values ranging from 4-4.4eV across the surface(figure 30). However due to the poor conductivity of the silicon substrate this is believed not to be accurate. As such the method was not used further in the experimentation in order for precise comparison.

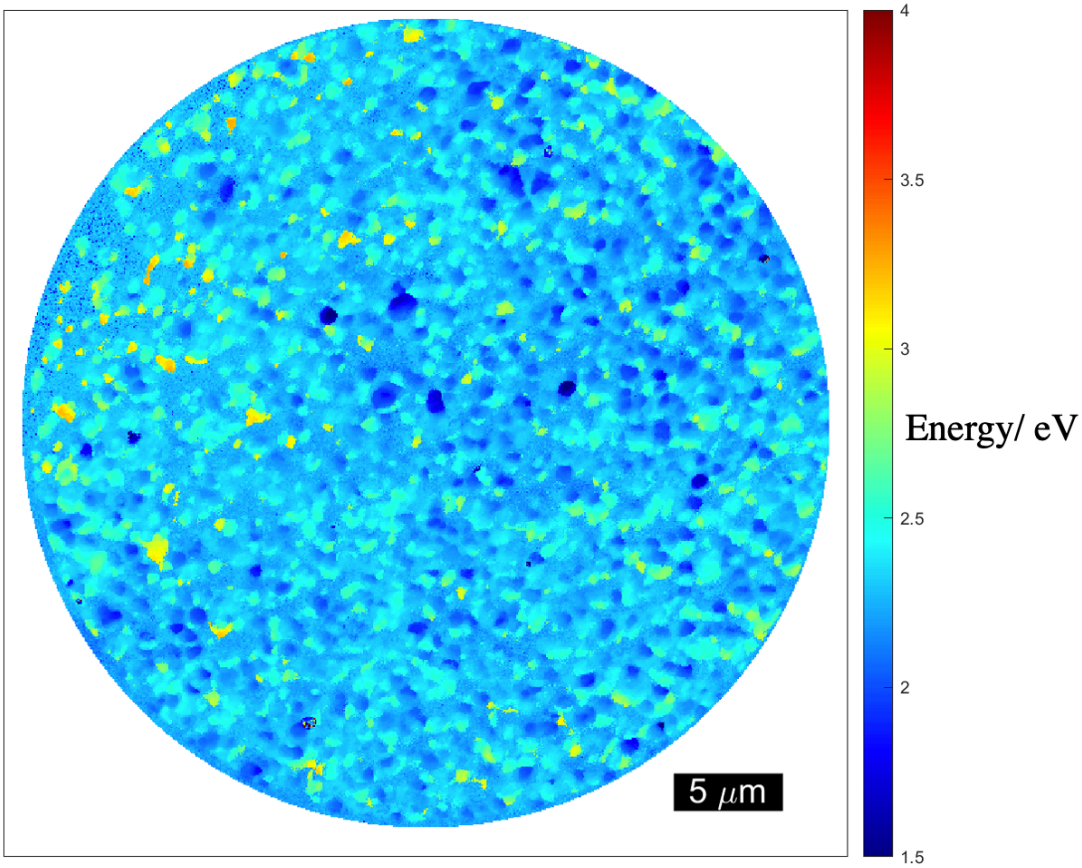

Figure 29: A heat map of the work function of a surface of PDD grown in a gas environment containing 1.25 percent CH_4.

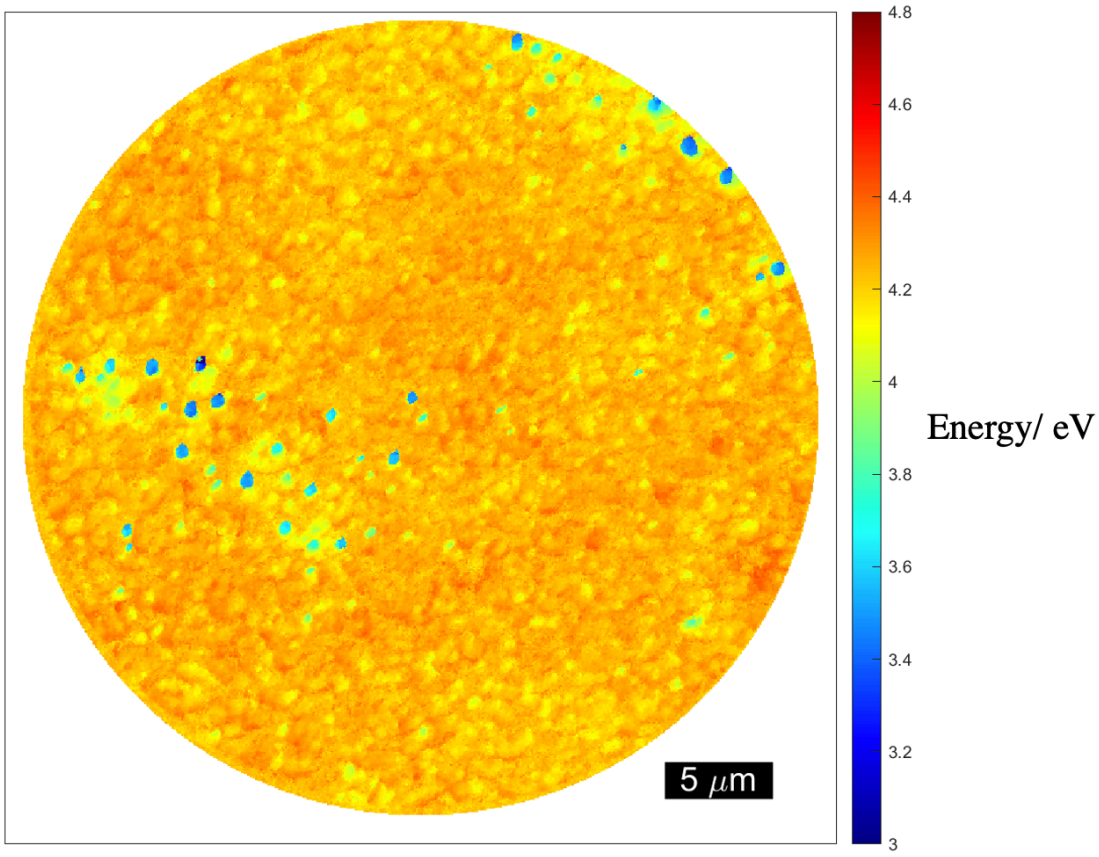

Figure 30: A heat map of the work function of a surface of PDD grown in a gas environment containing 0.75 percent CH_4.

3.5 XPS

The obtained XPS data for the whole scan showed 4 major peaks corresponding to the main elements in the SnO terminated diamond film the data corresponding to this may be seen in table 5 and figure 31. The initial carbon 1s peak used to calibrate the sample appeared at 280.5 eV which is lower than the literature expected 284.8 eV peak[36]. This difference in value will correspond to different expected values overall for the peaks but does not fully explain the difference. The two peaks for the SnO coating obtained were lower from their literature values of 485 eV and 486.5 eV respectively which suggests the formation of nanoclusters of SnO and Sn respectively[37]. Equally, it is possible that the formation of SnO_2 clusters also occurred in the deposition process due to the literature value of the SnO_2 peak of 486.7 eV[37].The difference in obtained to expected value for the peaks is also indicative of the partial oxidation of the tin on the surface or the formation of a sub monolayer of SnO on the surface[12]. It is possible that the formation of nanoclusters is the most likely outcome from the deposition process given this information and the elements that can be seen on the "spikes" in figure 25 and in the charged elements in figure 26 in comparison to the lack of these features in the non terminated NDD film SEM image as seen in figure 22. Additionally, this possibility becomes more apparent with the peak area for the oxygen ketone and ether peak which is also shifted lower than the literature range for these peaks of 531.5-532eV and 533eV[38]. In particular the overall peak

area for this value is far larger than that of the tin oxide peak area suggesting that the full coverage of the surface i.e. the formation of a monolayer is not present, meaning the partial oxidation of tin on the surface or the formation of a sub monolayer or indeed even nanoclusters is feasible.

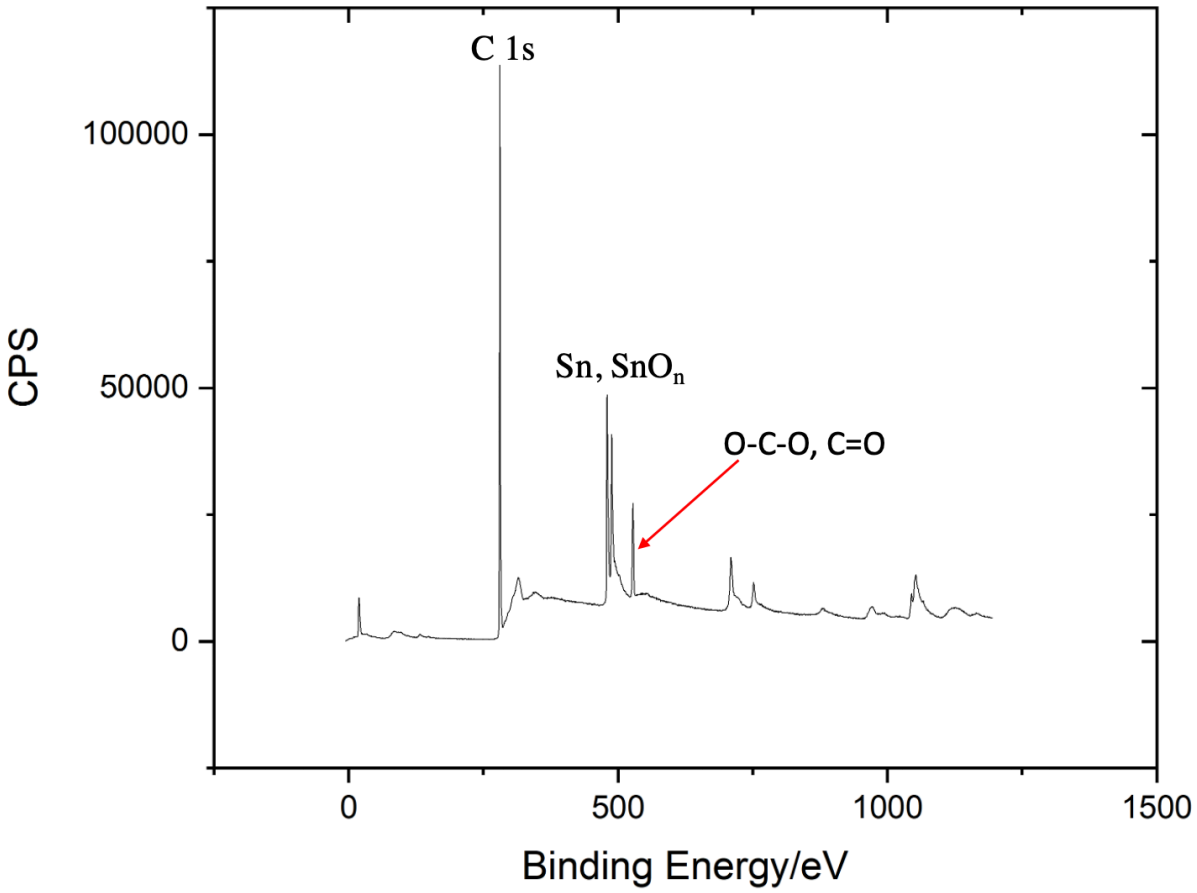

Figure 31: A graph showing the X-ray Photoelectron spectra of an NDD film terminated with tin monoxide after annealing.

Table 5: A table outlining the binding energies and area alongside the associated error of the peaks corresponding to different species present in a sample of tin monoxide terminated nitrogen doped diamond.

XPS Data					
Peak	Binding Energy/eV	Peak Area	Area Error	FWHM	FWHM Error
Carbon 1s	280.5	35000	200	2.40	0.01
Oxygen(Ketone, Ether)	527.5	115000	900	0.992	0.009
Tin $3d\frac{5}{2}$	479.5	53000	2000	1.62	0.07
Tin oxide $3d\frac{5}{2}$	488	36000	1000	1.58	0.06

3.6 Thermionic Profiles

Thermionic profiles were obtained for the PDD oxygen and hydrogen terminated collectors alongside the NDD oxygen, hydrogen and tin monoxide terminated collectors. The thermionic profiles exhibit a

hysteretic shape due to the nature of the temperature profile meaning that in the process of cooling from 700°C the system will be more uniformly heated meaning that the emission and collection will be greater upon cooling due a greater overall temperature on the extremities of the samples.

3.6.1 NDD Profiles

Initially thermionic testing was performed on the NDD samples at a 25 V bias voltage (figure 32) to investigate the effect of space charge mitigation on the collectors tested. It was observed overall that the H-terminated collector exhibited the greatest overall current with a maximum current of 0.286 mA. The second greatest current achieved at this voltage was obtained with the O-terminated surface which is unexpected given its PEA, theoretically the SnO-terminated surface having a NEA should be capable of collecting electrons from the emitter far better than the O-terminated surface. The maximum current obtained for the O-terminated collector measurements was 0.239 mA. Additionally, the initial run for the O-terminated sample showed significant fluctuation in current which may due to random fluctuations in the optical pyrometer causing fluctuations in the PID controller function. Moreover, it is possible that the fluctuations in this measurement may be in part due fluctuations in the voltage across the emitter and collector. Finally the SnO-terminated collector showed the lowest overall emission at this voltage for NDD samples with a maximum current of 0.144 mA which is an unexpected result as previously mentioned. This result may be due to the misalignment of the emitter sample meaning that an inefficient heating occurred allowing for an inefficient thermionic emission from the surface. Additionally, it may be possible that the surface did not have full coverage as suspected given the analysis of the surface using XPS techniques and may in fact have been contaminated with hydroxyl, oxygen or hydrocarbon termination, leading to overall lower collection from the surface. Moreover, it is possible that the formation of solely tin terminated surfaces may have led to the lowering of the overall current as though being more electropositive than carbon and therefore providing a NEA surface the NEA will not be as great as that of a tin monoxide surface. Furthermore the formation of tin clusters over the surface would also lower the overall collection from a surface given the barrier of the work function of 4.5 eV. Additionally, it is clear to see in all three of the profiles that the final run in each case shows the highest overall current which is correspondent with the overall temperature of the system being at its greatest on the third run since the runs are performed successively. This is also a feasible result theoretically as the large bias voltage ensures that the back emitted electrons from the collector materials are mitigated and fall back towards the collector not obfuscating the path of incoming electrons from the emitter.

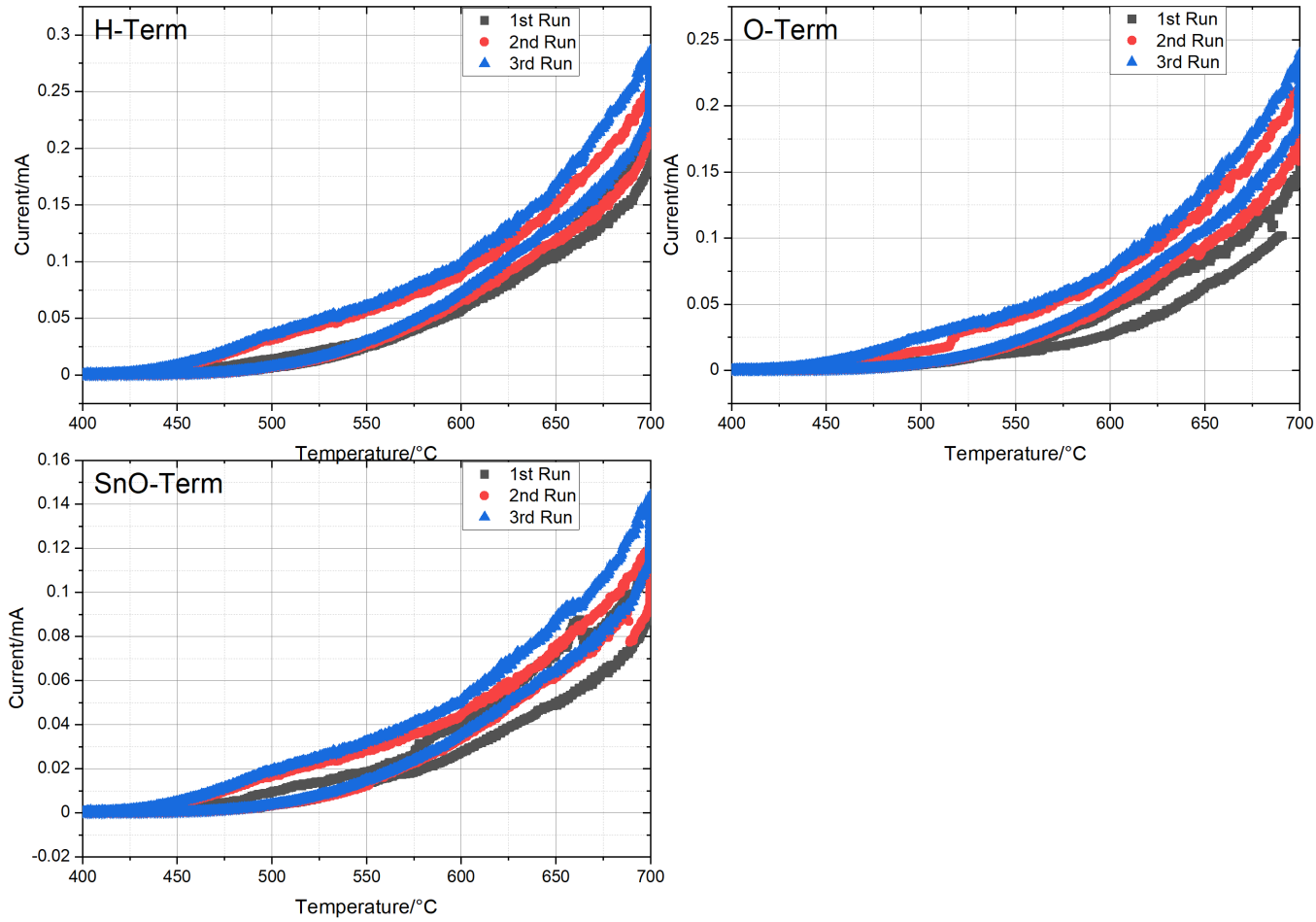

Figure 32: A set of thermionic profiles illustrating the difference in current output between hydrogen, oxygen and tin monoxide terminated NDD with a bias voltage of 25 V.

Following these tests, results were obtained at 5 V bias voltage (figure 33) in order to investigate the effects of space charge and in particular back emission from collector materials. It was observed overall that the O-terminated sample produced the greatest current with a maximum value of 0.00271 mA. This result is expected and feasible theoretically given the low overall bias voltage despite the PEA meaning the overall energy cost of an electron's path from emitter to collector is larger, there is a significant reduction in back emission due to this PEA. This reduction in back emission allows for more electrons overall to cross the distance between the emitter and collector as less electrons are in the space charge region to obfuscate and slow down the path of the incoming electrons. The second highest emission measured, as expected theoretically, was from the SnO terminated sample which having a NEA lower than that of hydrogen should lie in between oxygen and hydrogen termination in terms of overall current. The maximum current measured for this sample was 0.00211 mA. Equally it is clear with this profile that there is some back emission however due to the relatively low NEA it is not substantial. Finally the H-terminated sample exhibited the lowest overall measured current as expected due to its relatively high NEA, meaning a considerable amount of back emission occurs as

the collector sample heats up radiatively from the emitter. The maximum measured current for this sample was 0.00139 mA. Additionally, in each case it is clear to see the difference of the 5 V bias voltage to that of the 25 V bias voltage in that the measured current is far more erratic or noisy as the thickness of the hysteresis curve at each temperature is considerably greater under the 5 V bias. This fluctuation of measured current suggests there are considerable effects from space charge causing the current to change erratically at a given temperature. This was also observed when the material was kept at a steady temperature of 400°C. Moreover, the effects of space charge can be seen in all three profiles in the way that the third and as previously discussed hottest run the lowest current overall is observed, this means that since the third run is the hottest the collectors will be producing back emitted electrons the most, thus populating the space charge region more therefore lowering the overall current.

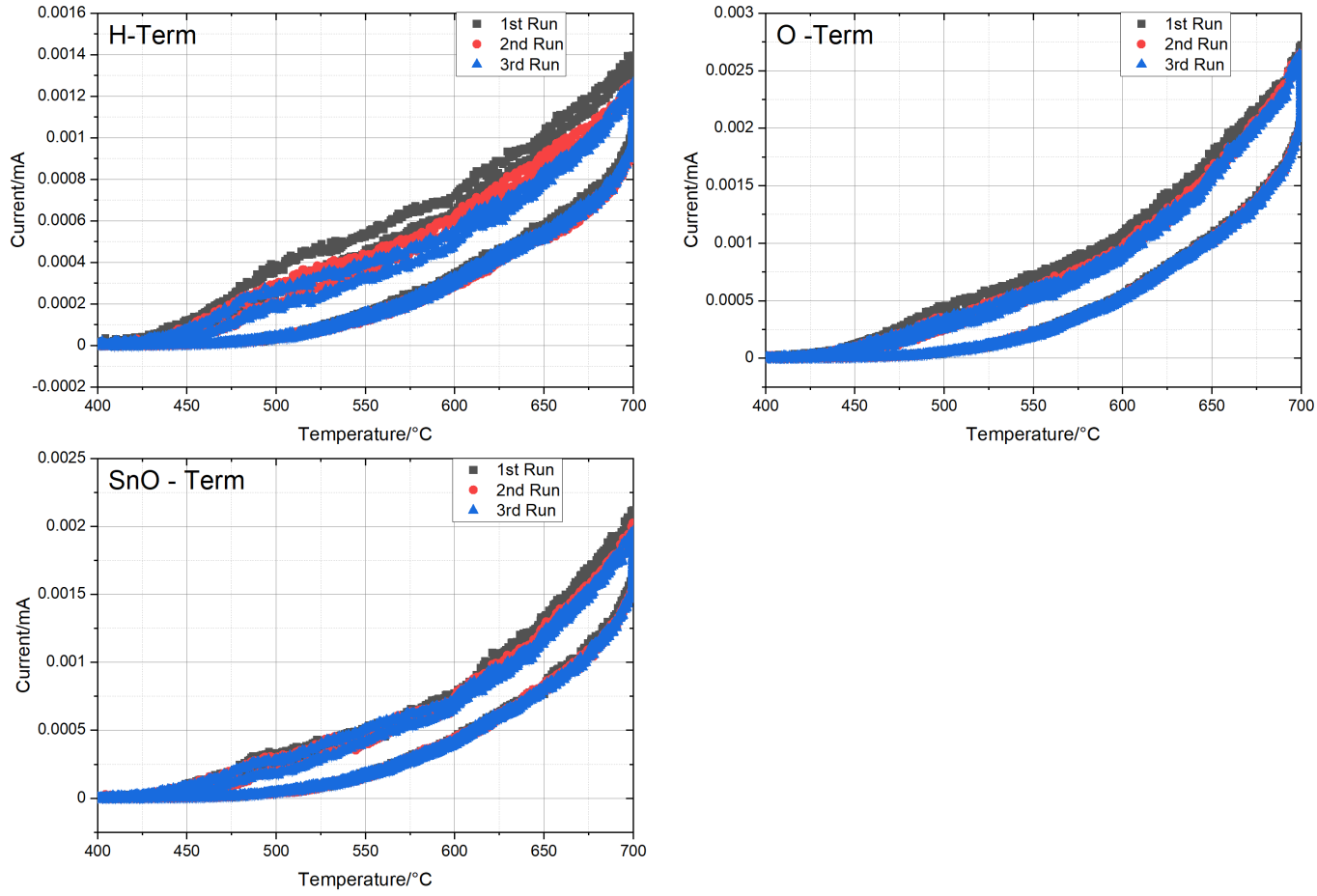

Figure 33: A set of thermionic profiles illustrating the difference in current output between hydrogen, oxygen and tin monoxide terminated NDD with a bias voltage of 5 V.

3.6.2 PDD Profiles

Similarly measurements were initially taken at 25 V for the PDD collector samples (figure 34) and the highest overall current was recorded with the H-terminated sample. This sample also produced the highest overall current out of all the samples tested at 25 V with a maximum recorded current of

0.408 mA. This result agrees with the theory as PDD has a much smaller gap between the donor level and the conduction band than that of NDD as such the energy cost for electrons to move from the emitter to the collector is overall smaller and therefore the amount of electrons that can be accepted overall is larger. On the other hand the O-terminated PDD showed the lowest overall current for all samples tested at 25 V with a maximum current of 0.104 mA which does not agree with the theory. This could be in part due to the alignment of the emitter causing a lower overall heating efficiency. Equally this difference in expected to obtained value could be due to a non uniform oxygen termination of the surface meaning some elements of the surface could be terminated with hydrocarbons which would lower the overall obtained current. Furthermore it is possible that the distance between the emitter and collector could not have been accurate, causing the overall current to be lower than expected. The same trend can be observed as with then NDD samples of the final run exhibiting the greatest current overall.

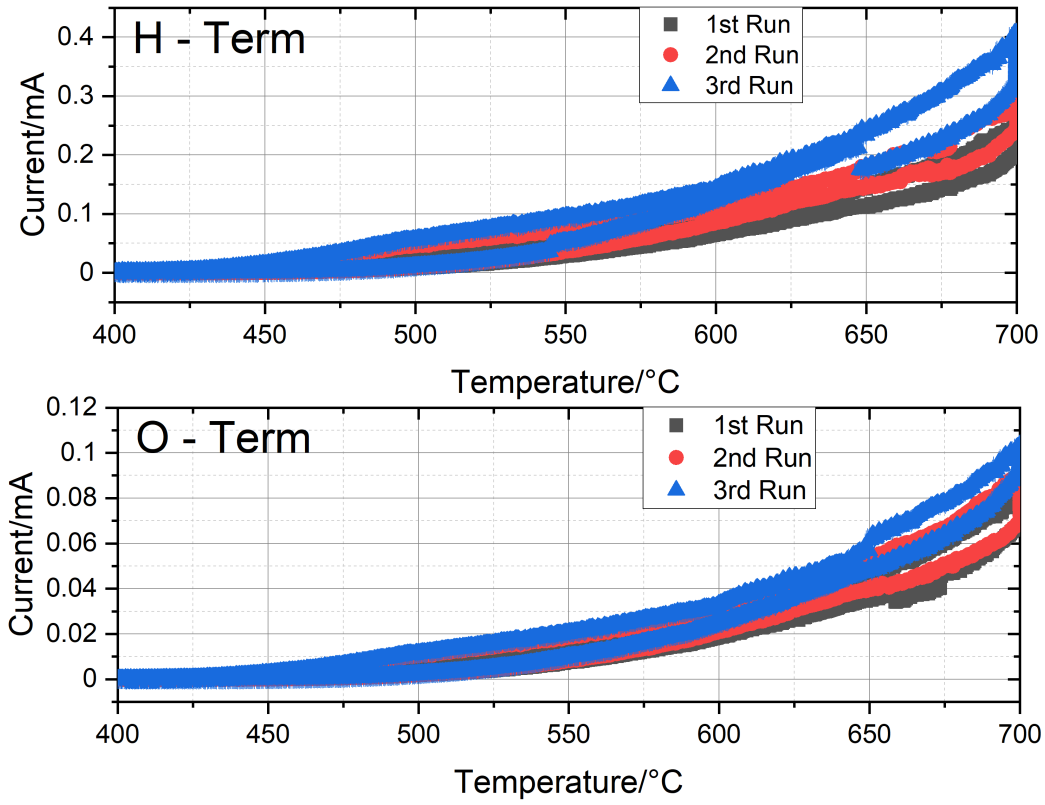

Figure 34: A set of thermionic profiles illustrating the difference in current output between hydrogen and oxygen terminated PDD with a bias voltage of 25 V.

Following the measurements at 25 V measurements were taken at 5 V (figure 35) similarly to investigate the effects of space charge on the overall current produced by the system. It was observed that the H-terminated PDD exhibited the greatest overall current of all the 5 V samples. The measured maximum current for the H-terminated sample was 0.00553 mA. On the other hand the O-terminated sample exhibited the second highest current of all samples with a maximum current of 0.00354 mA

However this value does not correlate with the theory that lower space charge effects would lead to an overall greater current for the system.

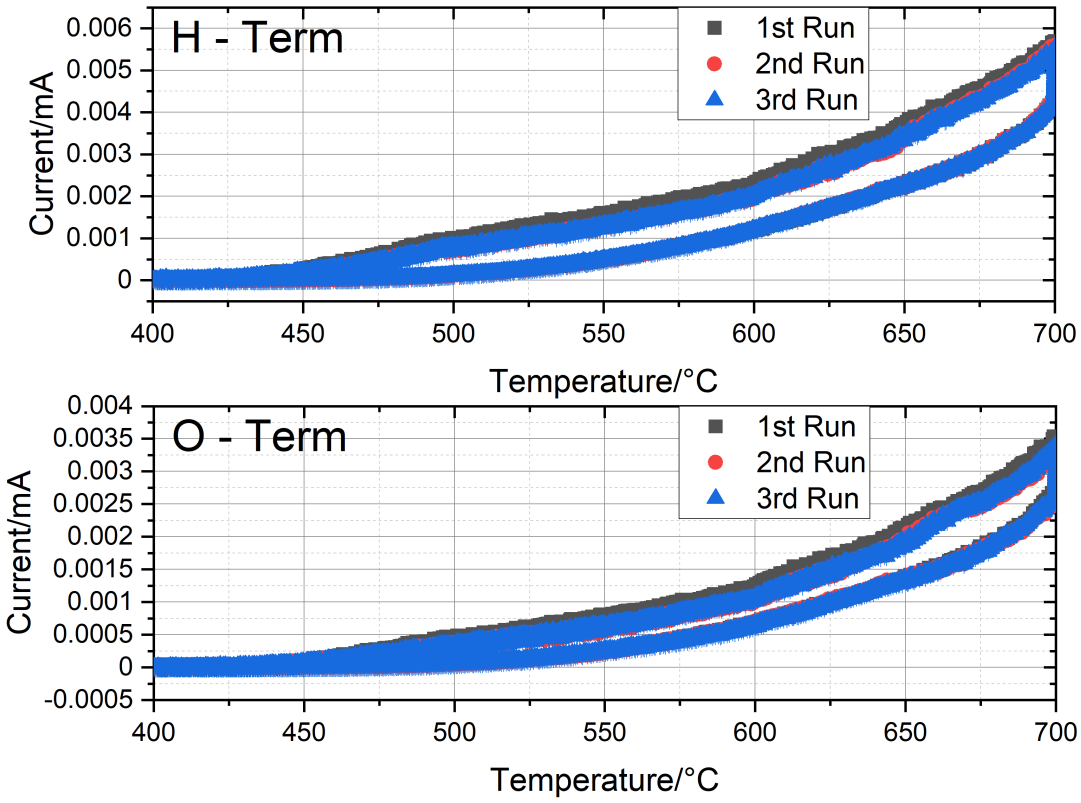

Figure 35: A set of thermionic profiles illustrating the difference in current output between hydrogen and O-terminated PDD with a bias voltage of 5 V.

3.6.3 Effective Work Function comparison

The effective work function of the NDD H-terminated emitter was measured for each different collector tested to investigate the effects of the different materials on the overall current of the system. The values of the effective work function were obtained using the Richardson equation as seen previously with the ideal Richardson constant (1.23×10^6 $Am^{-2}K^{-2}$) used in each case. The effective work function can be seen in table 6 and 7 the error on the work function is obtained by propagating the error on temperature and current via the use of partial derivatives. From table 5 it is clear to see that the lowest overall effective work function under space charge mitigation was exhibited by the PDD H-terminated collector as expected from the temperature profiles. Equally as expected from the thermionic profiles the PDD O-terminated collector exhibited the highest effective work function. Similarly the results for the system with space charge effects shows the PDD H-terminated sample showing the highest effective work function, however the lowest overall work function at 5 V applied bias was the NDD H-terminated sample.

Table 6: A table outlining the effective work function of the NDD H-terminated emitter at a bias voltage of 25 V.

Effective work function of emitter 25V		
Collector sample	Work function/eV	Error/eV
NDD H-Term	2.267	0.002
NDD O-Term	2.283	0.002
NDD SnO-Term	2.329	0.002
PDD H-Term	2.251	0.002
PDD O-Term	2.350	0.002

Table 7: A table outlining the effective work function of the NDD H-terminated emitter at a bias voltage of 5 V.

Work function of emitter 5V		
Collector sample	Work function/eV	Error/eV
NDD H-Term	2.697	0.002
NDD O-Term	2.640	0.002
NDD SnO-Term	2.674	0.002
PDD H-Term	2.575	0.002
PDD O-Term	2.617	0.002

4.0 Conclusion

5 samples of polycrystalline CVD diamond films (3 nitrogen doped and 2 phosphorous doped) were given different surface functionalisations to investigate the effect that electron affinity can have on the overall accepted current in a collector in a thermionic energy converter. Specifically investigating the effects of electron affinity on the emission at low and high applied bias in effect investigating the thermionic emission with and without space charge effects.

For the case without space charge effects it was observed that the H- terminated PDD film grown on silicon exhibited the highest current as a collector. This is theoretically feasible given the overall lower work function that PDD will exhibit over its nitrogen doped counter part due to its smaller donor level to conduction band distance of 0.37 eV. Additionally, this result is feasible to predict given the NEA of hydrogen termination, meaning that the overall cost for an electron to be emitted and cross the distance between the emitter and collector and then overcome the energy barrier to enter the surface is lower. It was observed, however, that the O-terminated PDD exhibited the lowest

overall current out of all the samples at this voltage. This however is an unexpected result as despite the O-termination producing a PEA surface thus increasing the overall cost for electrons to travel from emitter to collector it still has a lower work function than that of the NDD samples. The NDD samples showed the H-terminated surface exhibiting the greatest current followed by the oxygen terminated surface and then the tin monoxide surface. The position of the H-terminated sample at the highest current was theoretically expected however the position of the other two terminations was unexpected as theoretically the oxygen terminated sample, having a PEA should show the lowest current when space charge is mitigated.

For the case with space charge effects it was observed that the material which exhibited the highest overall current was the H-terminated PDD which was not theoretically expected given the high amount of back emission that would be expected from this sample given its large NEA. In theory the highest emission should have been recorded from the O-terminated PDD sample however this was recorded as the second highest emission at this low bias voltage. This difference may be due to problems with the experimental method as the nitrogen doped counterparts showed the theoretically expected results with the O-terminated case showing the greatest current followed by the SnO-terminated sample and then the H-terminated sample showing the lowest overall current as expected given the NEA it exhibits.

5.0 Future Work

Initially work could be performed to confirm the emission of O-terminated PDD in order to verify the above data does not agree with the theoretical expectation of a PEA surface at low bias voltage. Additionally, further testing with lower work function surfaces such as lanthanum hexaboride could be performed to move towards a viable thermionic energy converter device. Additionally, further surface terminations could be investigated in particular high temperature, high chemical resistance and NEA surface terminations which are capable of withstanding repeated thermal cycling. Moreover, current research is being performed at the University of Bristol to move towards a viable thermionic energy converter which utilises visible light as the heat source. In effect this system would operate by patterning the back of a thermionic emitter with a series of horizontal and vertical lines with a 10.6 μm distance between them. This patterning would effect an absorbance of around 90% meaning that a surface could theoretically be heated up to 600°C and thus be well within the threshold for thermionic emission. The results for initial testing of this surface may be seen in figure 36. Furthermore, investigations into the cooling of the collector surface in a thermionic emitter could be performed in order to optimise the efficiency of thermionic energy converters and thus increase the overall current output of these systems. Finally further work could be performed to investigate the process of forming a SnO-terminated surface, in particular to form a true monolayer in order to investigate the effect that

a fully terminated surface has on the electron affinity of the material as a whole. This work would be useful in order to produce a method capable of achieving monolayer metal oxide coverings for future tests with other metals of strong electropositivity.

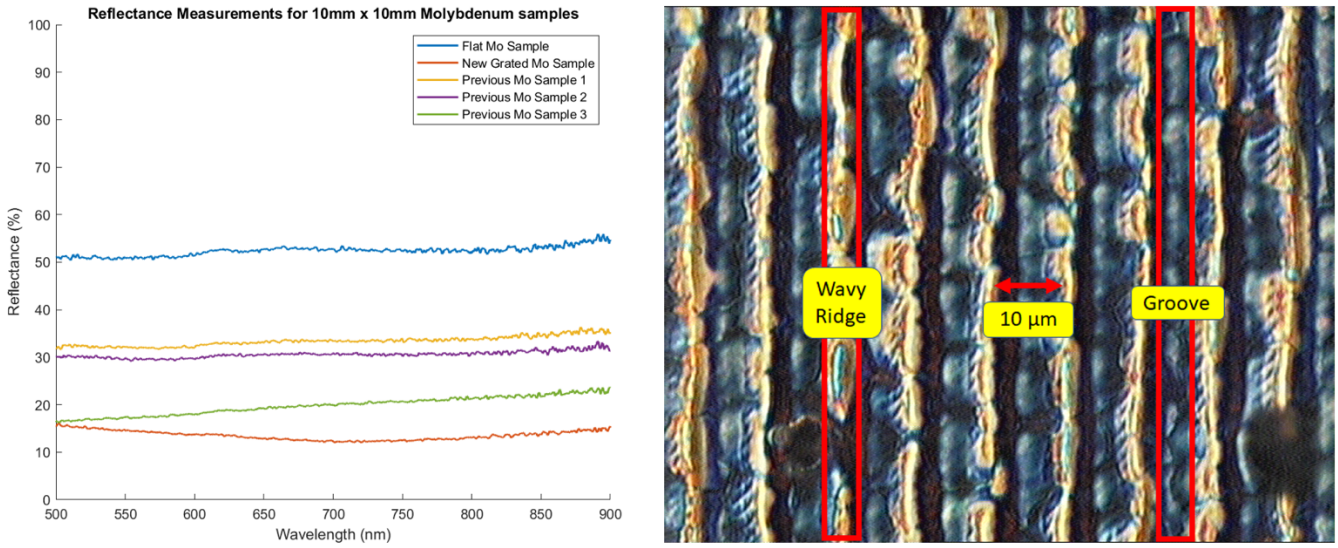

M Cryan,S.Li, S.Wills, E. Smith University of Bristol (2021)

Figure 36: A graph outlining the reflectance measurements for various patterns with the red line exhibiting the reflectance for the horizontal and vertical line patterning which may be seen in the image on the right.

6.0 Bibliography

[1] K. Nassau, J. Nassau "The history and present status of synthetic diamond, Journal of Crystal Growth", Journal of Crystal Growth, Volume 46, Issue 2, 1979, Pages 157-172, ISSN 0022-0248, https://doi.org/10.1016/0022-0248(79)90052-6,

[2] J J Gracio and Q H Fan and J C Madaleno, "Diamond growth by chemical vapour deposition", journal of Physics D: Applied Physics, IOP Publishing,volume 43, number 37, pages 374017, (2010), doi:10.1088/0022-3727/43/37/374017

[3] Seiichiro Matsumoto and Yoichiro Sato and Mutsukazu Kamo and Nobuo Setaka, "Vapor Deposition of Diamond Particles from Methane", Japanese Journal of Applied Physics, IOP Publishing, volume 21, Part 2, no.4, pp. L183 - L185, (1982).

[4] Mutsukazu Kamo, Yoichiro Sato, Seiichiro Matsumoto, Nobuo Setaka, "Diamond synthesis from gas phase in microwave plasma", Journal of Crystal Growth, Volume 62, Issue 3, (1983), Pages 642-644, ISSN 0022-0248, https://doi.org/10.1016/0022-0248(83)90411-6.

[5] Ashfold, M. N. R. and May, P. W. and Rego, C. A. and Everitt, N. M., "Thin film diamond by chemical vapour deposition methods", Chem. Soc. Rev., The Royal Society of Chemistry, (1994), volume 23, issue 1, pages 21-30, doi: 0.1039/CS9942300021

[6] Mehrdad Mehdizadeh, "Microwave/RF Applicators and Probes (Second Edition)", William Andrew Publishing, (2015), Chapter 10 - Plasma applicators at RF and microwave frequencies, Pages 335-363, ISBN 9780323322560, https://doi.org/10.1016/B978-0-323-32256-0.00010-5.

[7] Nottingham,Wayne B. and Hatsopoulos,George N. and Kaye,Joseph , ”Addendum Remarks on a Diode Configuration of a Thermo-Electron Engine”, Journal of Applied Physics, (1959), volume 30, number 3, pages 440-441, doi:10.1063/1.1735183

[8] Strohl, G. Ralph and Sissom, Leighton E., ”thermionic power converter”, Encyclopedia Britannica, 16 Oct. 2015, https://www.britannica.com/technology/thermionic-power-converter. Accessed 21 October 2021

[9] National Research Council , “Thermionics Quo Vadis?: An Assessment of the DTRA's Advanced Thermionics Research and Development Program”, Washington, DC: The National Academies Press(2001), Chapter 3: Overview of the Technology, doi: 10.17226/10254

[10] Staffan Rosander and Olle Wernholm , “Experiences with lanthanum hexaboride cathode guns”, Physica Scripta, IOP Publishing, (January 1997), volume T71, pages 157-160, doi:10.1088/0031-8949/1997/t71/030

[11] M. Lowman, “Thermionic Emission Studies of n-type Semiconducting Diamond”, University of Bristol diamond group, University of Bristol, (2020)

[12] Sami Ullah, Gary Wan, Christos Kouzios, Cameron Woodgate, Mattia Cattelan, Neil Fox, “Structure and electronic properties of tin monoxide (SnO) and lithiated SnO terminated diamond (100) and its comparison with lithium oxide terminated diamond”,Applied Surface Science, Volume 559, (2021), 149962, ISN 0169-4332, https://doi.org/10.1016/j.apsusc.2021.149962.

[13] R. Seddon, “Metal-Oxygen Surface Coatings on Doped Diamond for Thermionic Emission”, University of Bristol Diamond Group, University of Bristol, (April 2018)

[14] Pelletier,J. and Pomot,C., “Work function of sintered lanthanum hexaboride”, Applied Physics Letters, (1979), volume 34, Number 4, pages 249-251, doi:10.1063/1.90769

[15] Dominguez-Andrade, Hugo and Anaya, Julian and Croot, Alex and Cattelan, Mattia and Twitchen, Daniel J. and Kuball, Martin and Fox, Neil A., “Correlating Thermionic Emission with Specific Surface Reconstructions in a <100> Hydrogenated Single-Crystal Diamond”, ACS Applied Materials \& Interfaces, (2020), volume 12, Number 23, pages 26534-26542, doi:10.1021/acsami.0c01677

[16] Kroeger, E. W.(NASA Lewis Research Center Cleveland, OH, United States), Bair, V. L.(NASA Lewis Research Center Cleveland, OH, United States), Morris, J. F.(NASA Lewis Research Center Cleveland, OH, United States), “Diminiode thermionic energy conversion with lanthanum-hexaboride electrodes”, Nasa Technical Reports Server, International Conference on Plasma Science(Monterey, CA), (January 1, 1978),

[17] Voitovich, R. F., and E. A. Pugach, “High-temperature oxidation of lanthanum hexaboride.”, Soviet Powder Metallurgy and Metal Ceramics 12.2 (1973): 145-148.

[18] Lina Bai, Ning Ma, Fengli Liu, ”Structure and chemical bond characteristics of LaB6”, Physica B: Condensed Matter, Volume 404, Issue 21, 2009, Pages 4086-4089, ISSN 0921-4526, https://doi.org/10.1016/j.physb.2009.07.189.

[19] L. Diederich, O.M. Küttel, P. Aebi, L. Schlapbach, “Electron affinity and work function of differently oriented and doped diamond surfaces determined by photoelectron spectroscopy”, Surface Science, Volume 418, Issue 1, 1998, Pages 219-239, ISSN 0039-6028, https://doi.org/10.1016/S0039-6028(98)00718-3.

[20] A. Rowan, “Beta Enhanced Thermionic Emission”,University of Bristol Diamond Group, University of Bristol, (April 2017)

[21] Chris J.H. Wort, Richard S. Balmer, “Diamond as an electronic material”, Materials Today, Volume 11, Issues 1–2, 2008, Pages 22-28, ISSN 1369-7021, https://doi.org/10.1016/S1369-7021(07)70349-8.,

[22] Charles P. Poole, Ruslan Prozorov, Horacio A. Farach, Richard J. Creswick, “1 - Properties of the normal state”, Superconductivity (Third Edition), Elsevier, 2014, Pages 1-31, ISBN 9780124095090, https://doi.org/10.1016/B978-0-12-409509-0.00001-9.

[23] O'Donnell, Kane M. and Martin, Tomas L. and Edmonds, Mark T. and Tadich, Anton and Thomsen, Lars and Ristein, Jürgen and Pakes, Christopher I. and Fox, Neil A. and Ley, Lothar, “Photoelectron emission from lithiated diamond”, physica status solidi (a), Volume 211, Number 10, 2014, Pages 2209-2222, https://doi.org/10.1002/pssa.201431414

[24] P.W. May, M. Clegg, T.A. Silva, H. Zanin, O. Fatibello-Filho, V. Celorrio, D.J. Fermin, C.C. Welch, G. Hazell, L. Fisher, A. Nobbs, B. Su, “Diamond-coated ‘black silicon’ as a promising material for high-surface-area electrochemical electrodes and antibacterial surfaces”, J. Mater. Chem. B. 4 (2016) 5737-5746, doi: 10.1039/c6tb01774f

[25] C. Moelle, S. Klose, F. Szücs, H.J. Fecht, C. Johnston, P.R. Chalker, M. Werner, “Measurement and calculation of the thermal expansion coefficient of diamond”, Diamond and Related Materials,
Volume 6, Issues 5–7, 1997, Pages 839-842, ISSN 0925-9635, https://doi.org/10.1016/S0925-9635(96)00674-7.

[26] Michael C. James, Fabian Fogarty, Ramiz Zulkharnay, Neil A. Fox, Paul W. May, “A review of surface functionalisation of diamond for thermionic emission applications”, Carbon,
Volume 171, 2021, Pages 532-550, ISSN 0008-6223, https://doi.org/10.1016/j.carbon.2020.09.019.

[27] Rutter, M. J. and Robertson, J., “Ab initio calculation of electron affinities of diamond surfaces”,Phys. Rev. B, American Physical Society, Volume 57, Issue 15, April 1998, Pages 9241--9245, doi:10.1103/PhysRevB.57.9241

[28] J. Geldard, “Metal Oxide Diamond Termination as a route to low work function surfaces”,University of Bristol Diamond Group, University of Bristol, (April 2019)

[29] Almas Bashir, Tahir Iqbal Awan, Aqsa Tehseen, Muhammad Bilal Tahir, Mohsin Ijaz, “Chemistry of Nanomaterials”,Chapter 3 - Interfaces and surfaces,Elsevier, 2020, Pages 51-87, ISBN 9780128189085, https://doi.org/10.1016/B978-0-12-818908-5.00003-2.

[30] M-T. Kuo, P.W. May, A. Gunn, M.N.R. Ashfold, R.K. Wild, “Studies of phosphorus doped diamond-like carbon films’,Diamond and Related Materials, Volume 9, Issues 3–6, 2000, Pages 1222-1227, ISSN 0925-9635, https://doi.org/10.1016/S0925-9635(99)00305-2.

[31] Ryo Yoshida, Daisuke Miyata, Toshiharu Makino, Satoshi Yamasaki, Tsubasa Matsumoto, Takao Inokuma, Norio Tokuda,”Formation of atomically flat hydroxyl-terminated diamond (1 1 1) surfaces via water vapor annealing”,Applied Surface Science, Volume 458, 2018, Pages 222-225,
ISSN 0169-4332, https://doi.org/10.1016/j.apsusc.2018.07.094.

[32] Sami Ullah and Neil Fox, “Modification of the Surface Structure and Electronic Properties of Diamond (100) with Tin as a Surface Termination: A Density Functional Theory Study”,The Journal of Physical Chemistry C 2021 125 (45), 25165-25174, DOI: 10.1021/acs.jpcc.1c05973

[33] H. Bolton, “Beta – Enhanced Thermionic Emission Studies of Semiconducting Diamond”, University of Bristol Diamond Group, University of Bristol, (April 2019)

[34] Nie, 思媛 & Shen, Wei & Shen, Shengnan & Li, Hui & Pan, Yuanhui & Sun, Yuechang & Chen, Yinghua & Qi, Haiqin. (2021)., “Effects of Vacancy and Hydrogen on the Growth and Morphology of N-Type Phosphorus-Doped Diamond Surfaces.” Applied Sciences. 11. 1896. 10.3390/app11041896.

[35] J. H. Parker, Jr., D. W. Feldman, and M. Ashkin, "Raman Scattering by Silicon and Germanium", Phys. Rev. 155, 712 – Published 15 March 1967

[36] ThermoFisher Scientific, "Tin, Tin X-ray photoelectron spectra, tin electron configuration, and other elemental information" ThermoFisher Scientific, https://www.thermofisher.com/uk/en/home/materials-science/learning-center/periodic-table/other-metal/tin.html, Retrieved Tuesday 20th march 2021

[37] Surface Science Western, "XPS Reference Pages : Tin" University of West Ontario, http://www.xpsfitting.com/2012/02/tin.html, Retrieved Tuesday 20th march 2021

[38] ThermoScientific, "Oxygen • Non-Metals" ThermoScientific, https://www.jp.xpssimplified.com/elements/oxygen.php, Retrieved Tuesday 20th march 2021

[39] O.A. Williams, "Nanocrystalline diamond", Diamond and Related Materials, Volume 20, Issues 5–6, 2011, Pages 621-640, ISSN 0925-9635,
https://doi.org/10.1016/j.diamond.2011.02.015.

[40] A. Ferrari,J. Robertson, "Raman spectroscopy of amorphous,nanostructured, diamond-likecarbon, and nanodiamond", Philosophical Transactions of the Royal Society of London. Series A: Mathematical, Physical and Engineering Sciences, Volume 362, Number 1824, 2004, Pages 2477-2512, doi:10.1098/rsta.2004.1452

[41] AMETEK-LAND, "Spot-High Precision Pyrometers" Ametek-Land, https://www.ametek-land.com/-/media/ameteklandinstruments/documentation/products/fixedspotnoncontactthermometers/spot/ametek_land_spot_brochure_marcom0355_rev_15.pdf, Retrieved Tuesday 20th march 2021

[42] Hu, Chenming, "Modern semiconductor devices for integrated circuits", Vol. 2, Upper Saddle River, NJ: Prentice Hall, 2010.

[43] Umstattd,R. J. and Carr,C. G. and Frenzen,C. L. and Luginsland,J. W. and Lau,Y. Y., "A simple physical derivation of Child–Langmuir space-charge-limited emission using vacuum capacitance", American Journal of Physics, Volume 73, Number 2, Pages 160-163, 2005 doi:10.1119/1.1781664

[44] Frano Barbir, "Chapter Two - Fuel Cell Basic Chemistry and Thermodynamics", PEM Fuel Cells (Second Edition), Academic Press, 2013, Pages 17-32, ISBN 9780123877109, https://doi.org/10.1016/B978-0-12-387710-9.00002-3.

[45] Karin Potje-Kamloth, "Chapter 11 - CONDUCTING POLYMER-BASED SCHOTTKY BARRIER AND HETEROJUNCTION DIODES AND THEIR SENSOR APPLICATION", PEM Fuel Cells (Second Edition)",Editor(s): Hari Singh Nalwa,
Handbook of Surfaces and Interfaces of Materials, Academic Press, 2001, Pages 445-494, ISBN 9780125139106, https://doi.org/10.1016/B978-012513910-6/50068-2.

[46] Ristein,Jürgen , "The Physics of Hydrogen-Terminated Diamond Surfaces)",AIP Conference Proceedings, Volume 772, Number 1, Pages 377-380, 2005,doi:10.1063/1.1994145

[47] Watts, John F., "X-ray photoelectron spectroscopy." Surface science techniques 45, no. 5 (1994).

[48] Krainsky,I. L. and Asnin,V. M. , "Negative electron affinity mechanism for diamond surfaces", Applied Physics Letters, Volume 72, Number 20, Pages 2574-2576, 1998, doi:10.1063/1.121422

[49] N Maiti, P Karmakar, U D Barve and A V Bapat , "An evaporation system for film deposition using electron beam sources", Journal of Physics: Conference Series, IOP Publishing, Volume 114, Pages 012949, May 2008, doi:10.1088/1742-6596/114/1/012049

[50] Koizumi S, Kamo M, Sato Y, Ozaki H, Inuzuka T., "Growth and characterization of phosphorous doped {111} homoepitaxial diamond thin films.", Applied Physics Letters, 1997 Aug 25;71(8):1065-7.

[51] Liu H, Dandy DS., "Diamond chemical vapor deposition: nucleation and early growth stages.", Elsevier; 1996 Dec 31.

[52] Kobashi K, Nishimura K, Kawate Y, Horiuchi T., "Synthesis of diamonds by use of microwave plasma chemical-vapor deposition: Morphology and growth of diamond films.", Physical review B. 1988 Aug 15;38(6):4067.

[53] Trucchi, Daniele & Cappelli, Emilia & Lisi, Nicola & Ascarelli, P.. (2006). “Feasibility of CVD diamond radiation energy conversion devices.”, Diamond and Related Materials. 15. 1980-1985. 10.1016/j.diamond.2006.08.012.

[54] Shao G., "Work Function and Electron Affinity of Semiconductors: Doping Effect and Complication due to Fermi Level Pinning.", Energy & Environmental Materials. 2021 Jul;4(3):273-6.

[55] Chung DD., "Review graphite.", Journal of materials science. 2002 Apr;37(8):1475-89.

[56] Butler JE, Mankelevich YA, Cheesman A, Ma J, Ashfold MN., "Understanding the chemical vapor deposition of diamond: recent progress.", Journal of Physics: Condensed Matter. 2009 Aug 19;21(36):364201.

[57] Klages CP. , "Chemical vapor deposition of diamond.", Applied Physics A. 1993 Jun;56(6):513-26.

[58] Werner M, Locher R. , "Growth and application of undoped and doped diamond films.", Reports on Progress in Physics. 1998 Dec 1;61(12):1665.

[59] "1. I. P-Type, N-Type Semiconductors" [Internet]. 2021 [cited 2022 Mar 31]. Available from: https://eng.libretexts.org/@go/page/5922

[60] Serge Zhuiykov, "Nanostructured Semiconductor Oxides for the Next Generation of Electronics and Functional Devices: 1 - Electrons and holes in a semiconductor", Woodhead Publishing, 2014, Pages 1-49, ISBN 9781782422204, https://doi.org/10.1533/9781782422242.1.

[61] Dipalo, Michele. (2022). “Nanocrystalline diamond growth and device applications.”

[62] Haubner, R., “Low-pressure diamond: from the unbelievable to technical products.” ChemTexts 7, 10 (2021). https://doi.org/10.1007/s40828-021-00136-z

[63] May Paul W., (2000), “Diamond thin films: a 21st-century material”, Phil. Trans. R. Soc. A.,358473–495, http://doi.org/10.1098/rsta.2000.0542

[64] International Molybdenum Association, “Molybdenum Properties”, IMOA, retrieved from: https://www.imoa.info/molybdenum/molybdenum-properties.php, Accessed 11th April 2022

7.0 Appendix

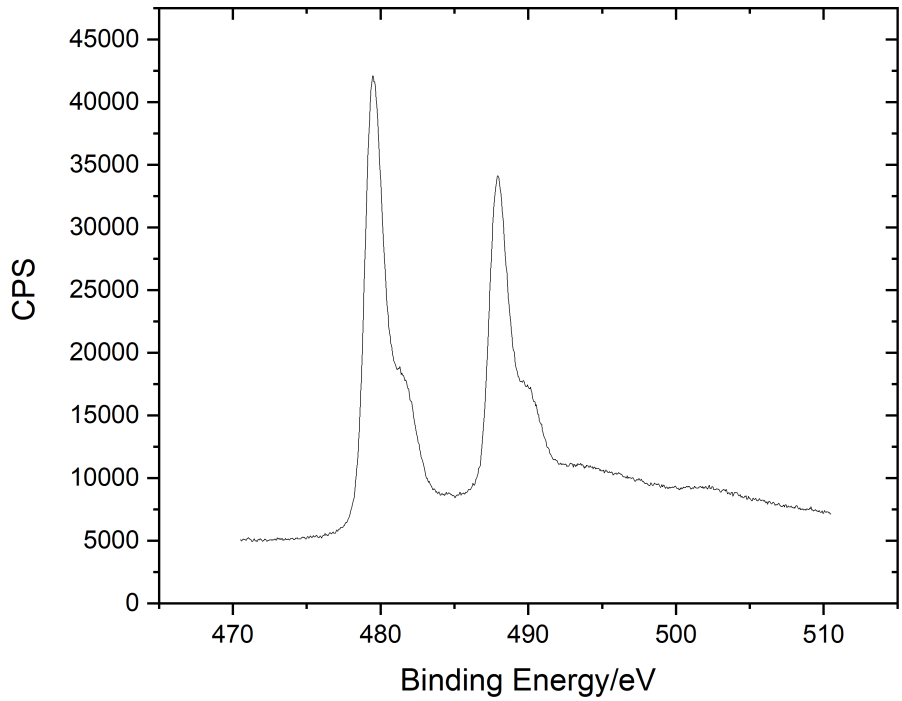

Figure 37: An XPS spectrum showing the two peaks corresponding to tin and tin oxide in a tin terminated NDD sample.

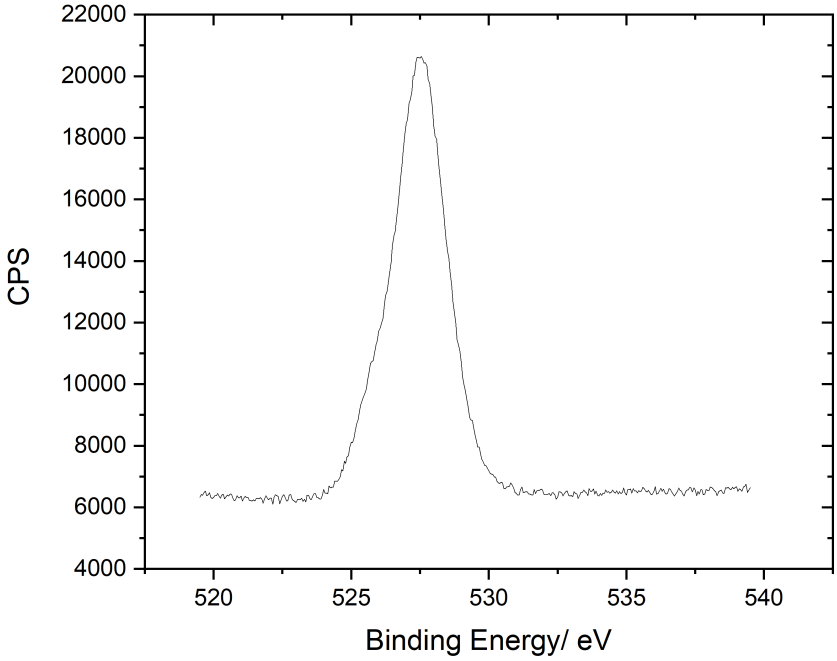

Figure 38: An XPS spectrum showing the peak for the ketone and ether configurations in an SnO terminated NDD sample.

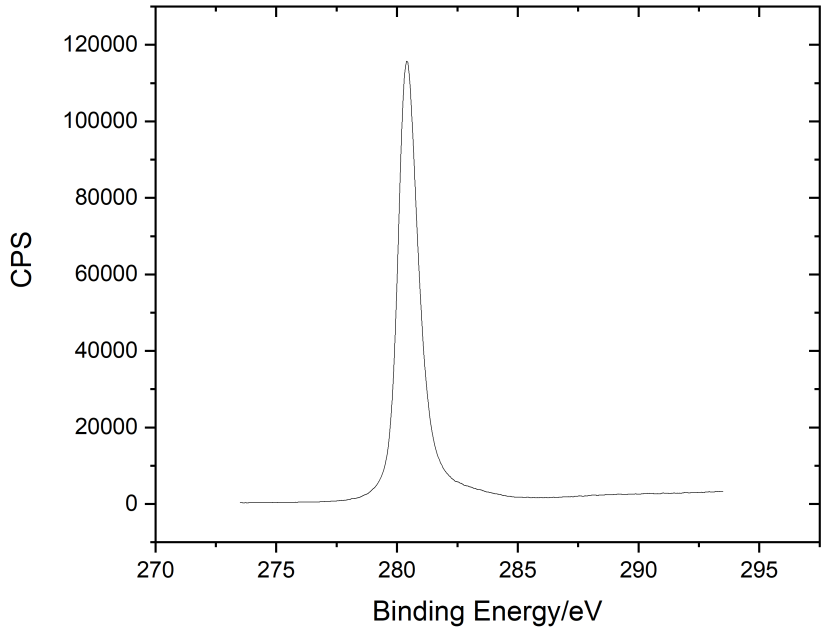

Figure 39: An XPS spectrum showing the peak for C 1s in an SnO terminated NDD sample.

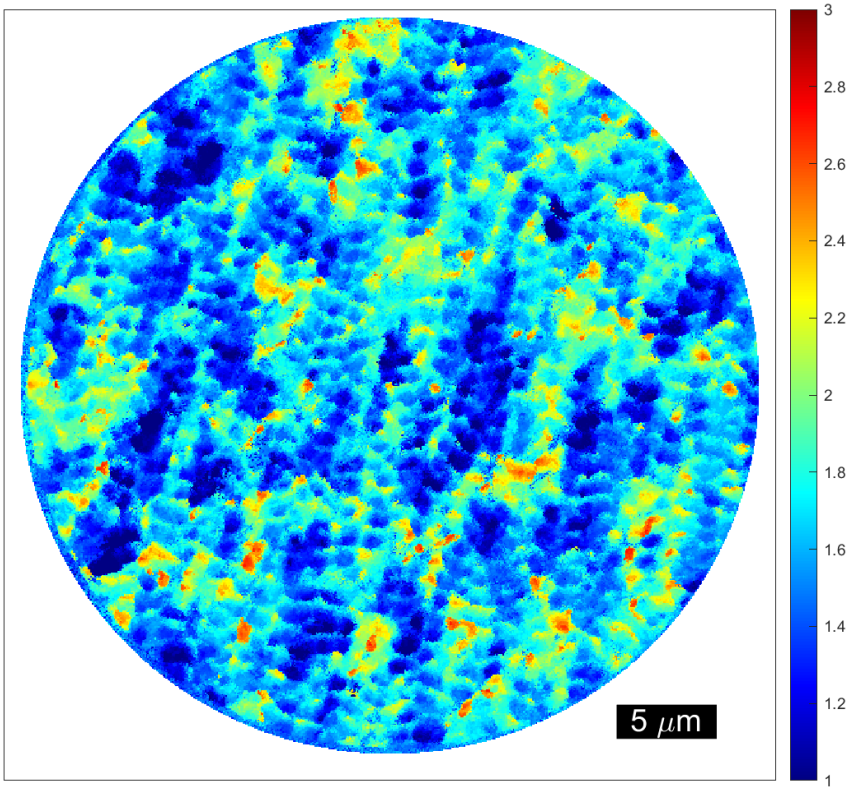

Figure 40: A heat map of the work function of a surface of Phosphorous doped diamond grown in a gas environment containing 0.75 percent CH_4 analysed using a Helium lamp as the photoexcitation source.

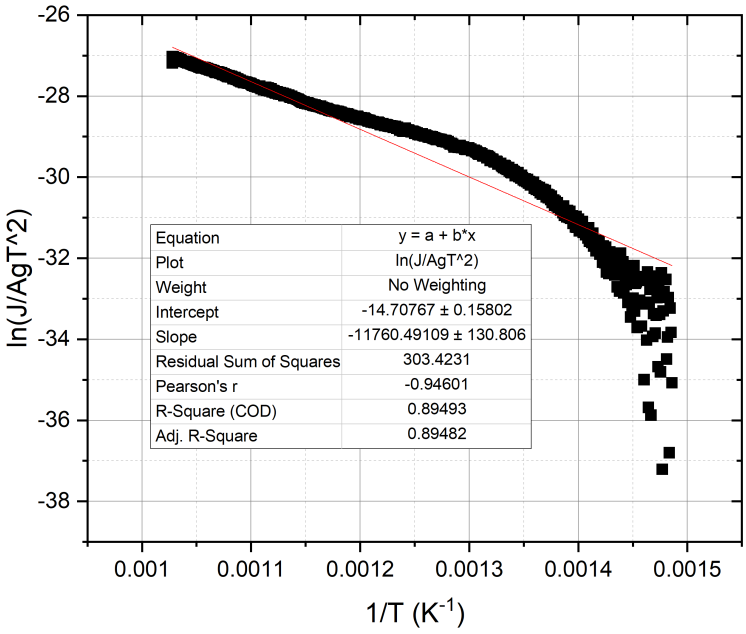

Figure 41: A graph showing the agreement with Richmond behaviour for thermionic emission from an NDD surface.

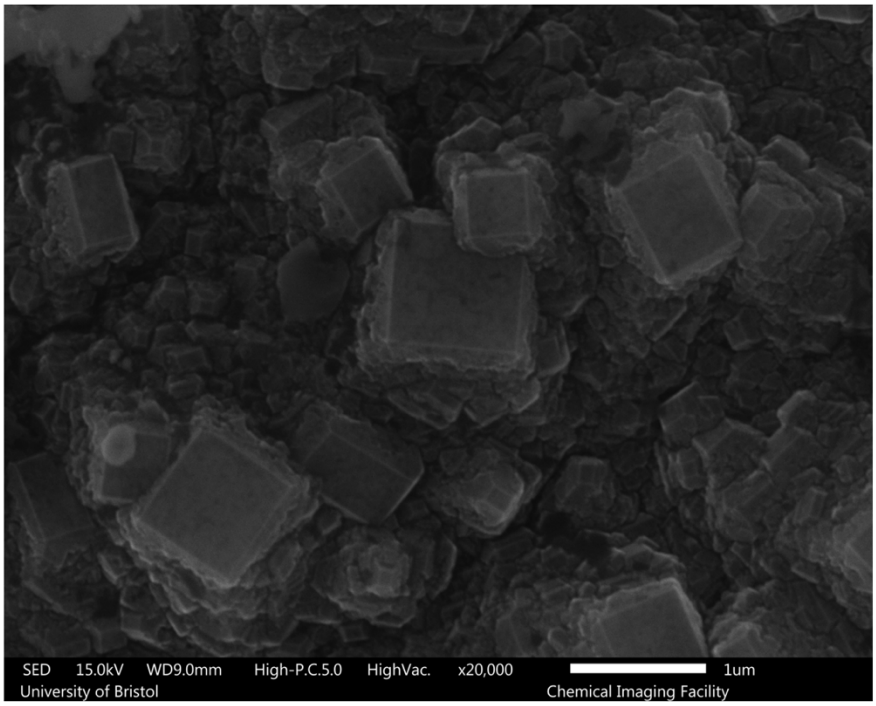

Figure 42: A top down SEM image of the NDD emitter sample at x20,000 magnification.

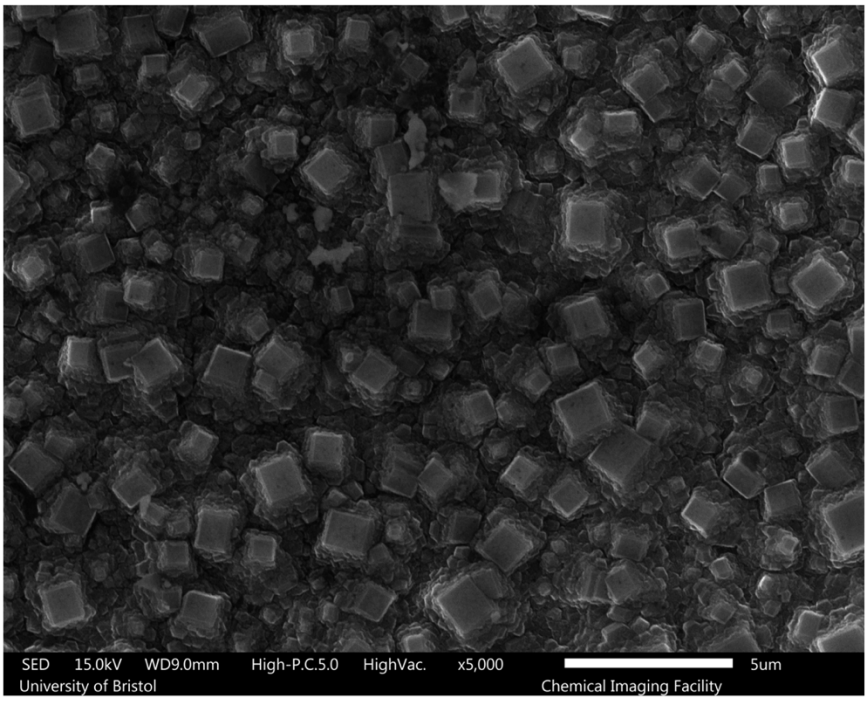

Figure 43: A top down SEM image of the NDD emitter sample at x5000 magnification.

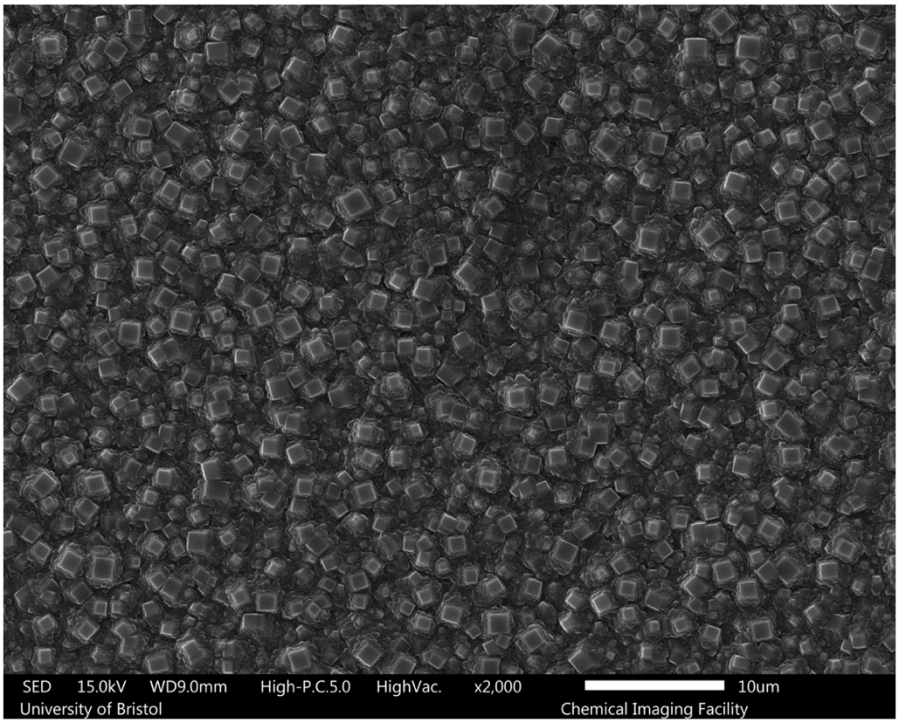

Figure 44: A top down SEM image of the NDD emitter sample at x2000 magnification.

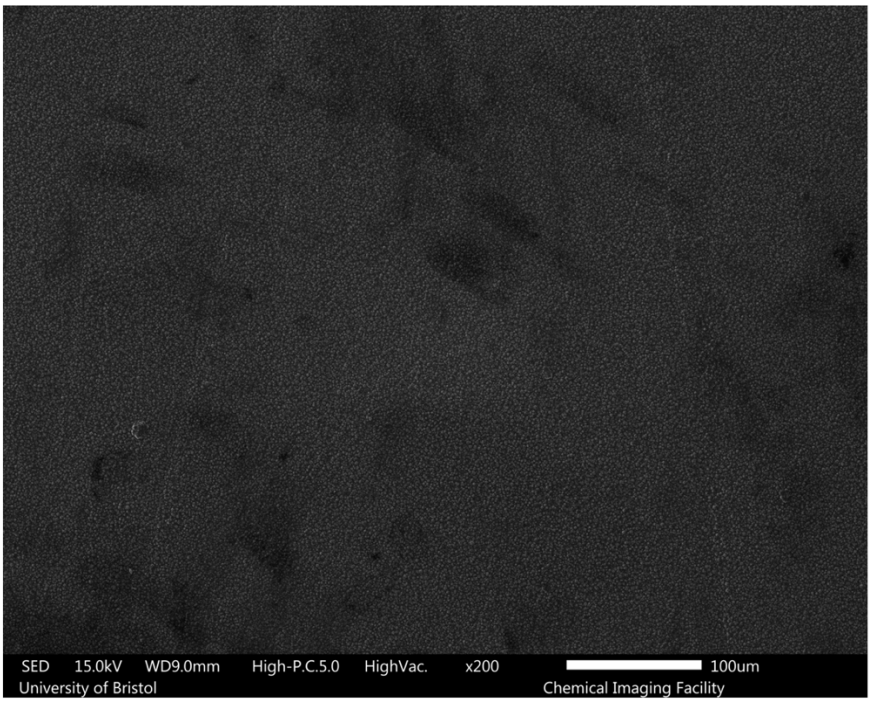

Figure 45: A top down SEM image of the NDD emitter sample at x200 magnification.

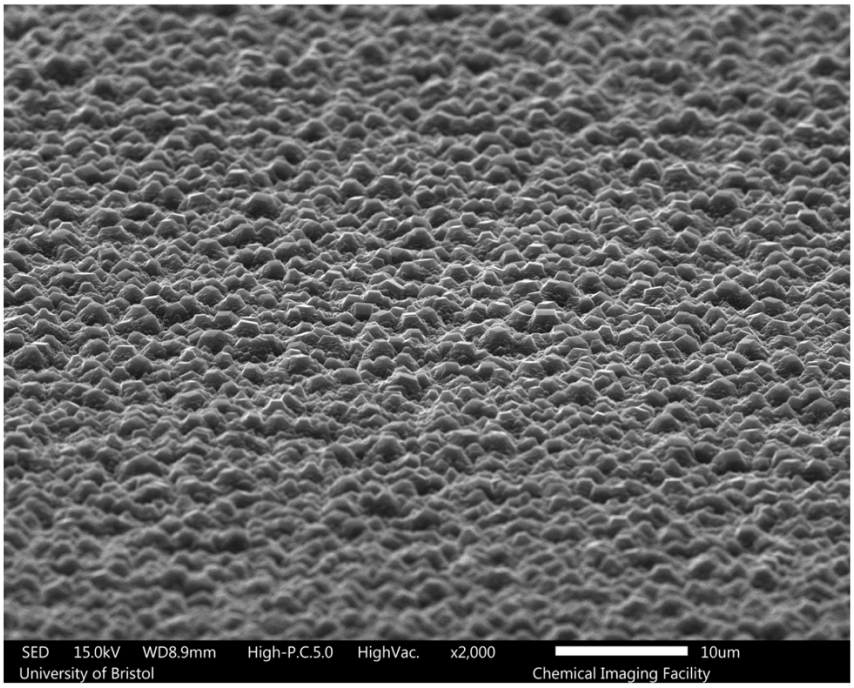

Figure 46: A 70 degree canted SEM image of the NDD emitter sample at x2000 magnification.

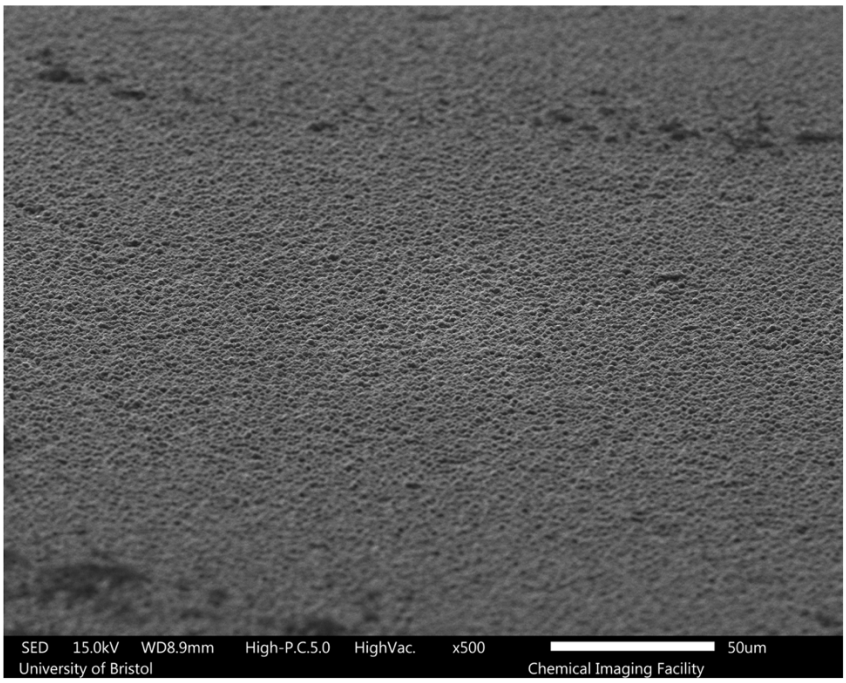

Figure 47: A 70 degree canted SEM image of the NDD emitter sample at x500 magnification.

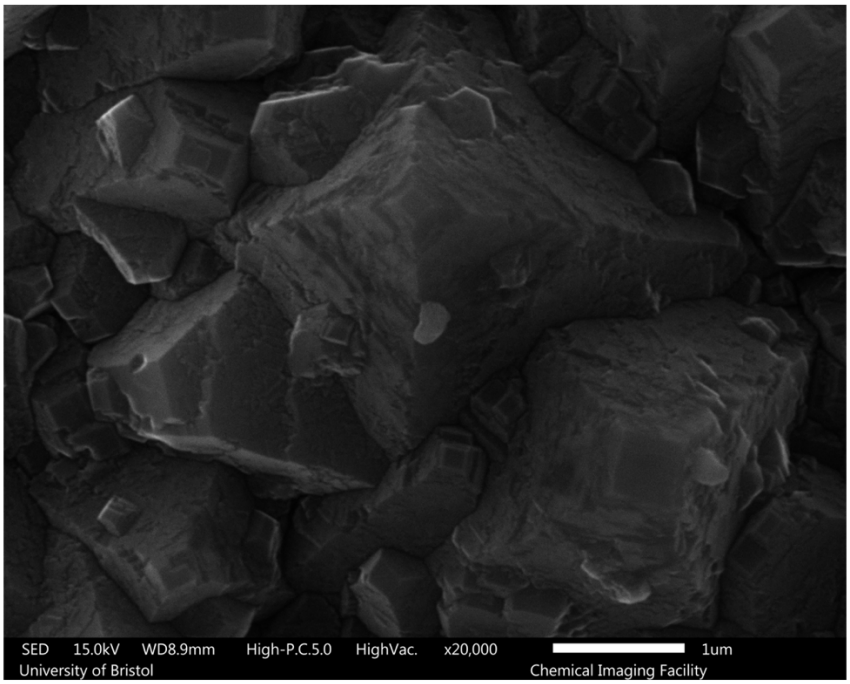

Figure 48: A top down SEM image of the tin monoxide terminated NDD sample at x20,000 magnification.

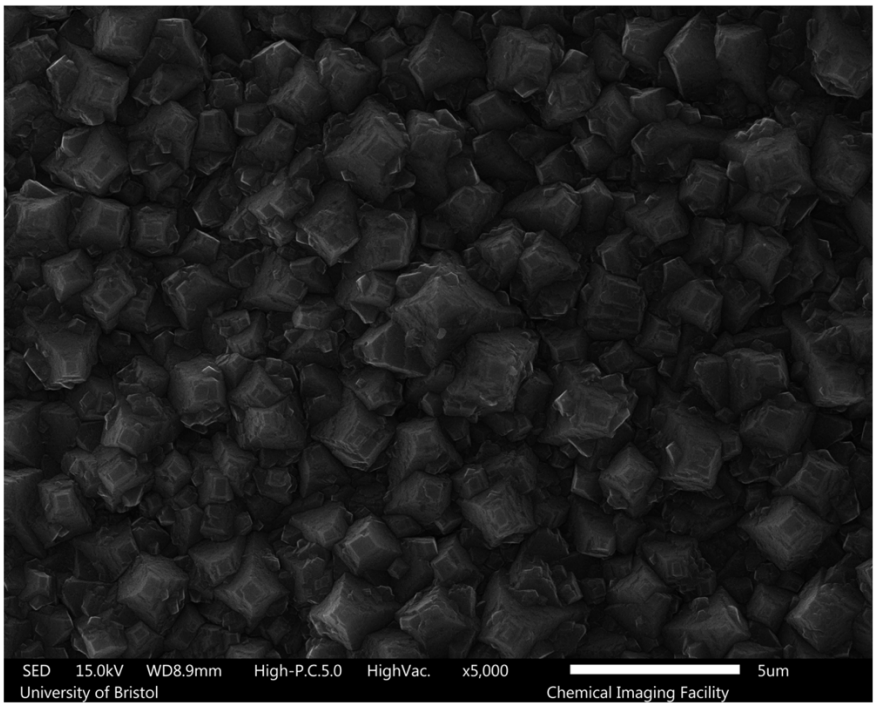

Figure 49: A top down SEM image of the tin monoxide terminated NDD sample at x5000 magnification.

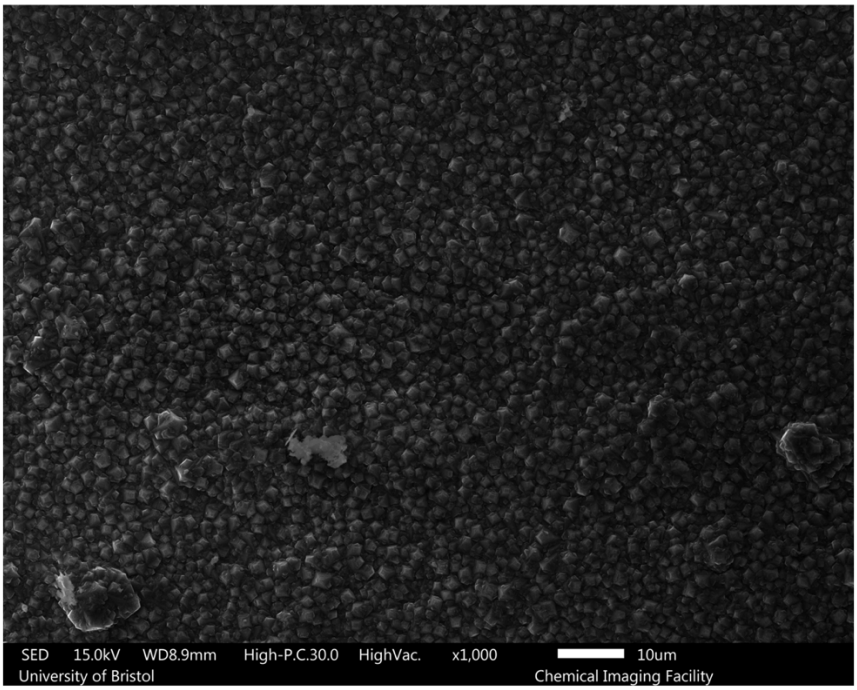

Figure 50: A top down SEM image of the tin monoxide terminated NDD sample at x1000 magnification.

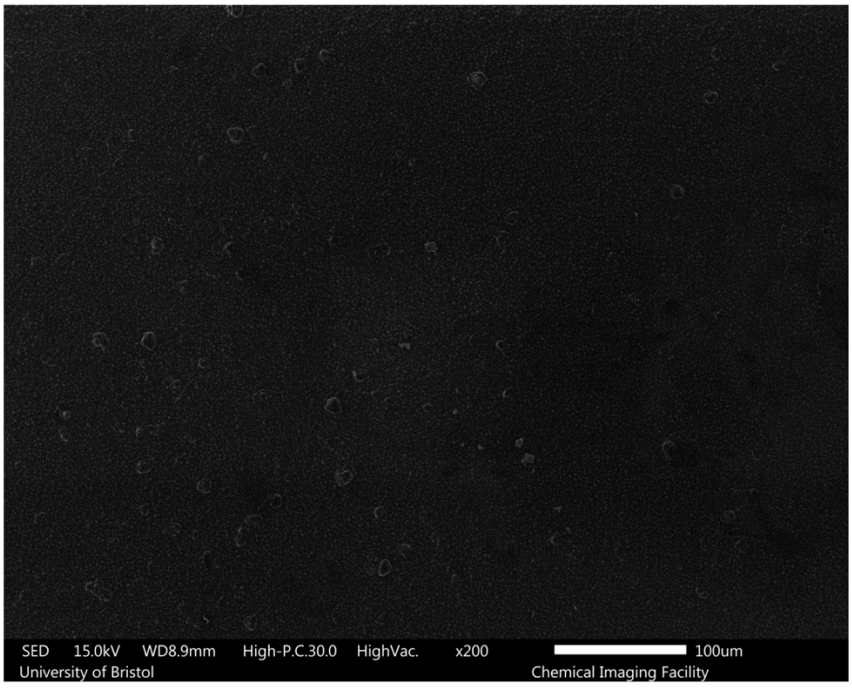

Figure 51: A top down SEM image of the tin monoxide terminated NDD sample at x200 magnification.

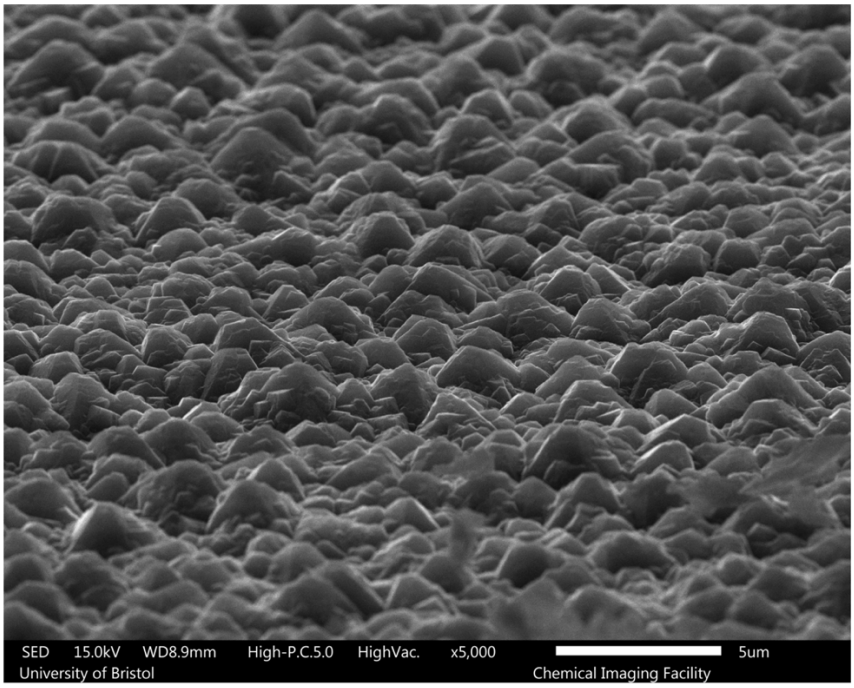

Figure 52: A 70 degree canted SEM image of the tin monoxide terminated NDD sample at x5000 magnification.

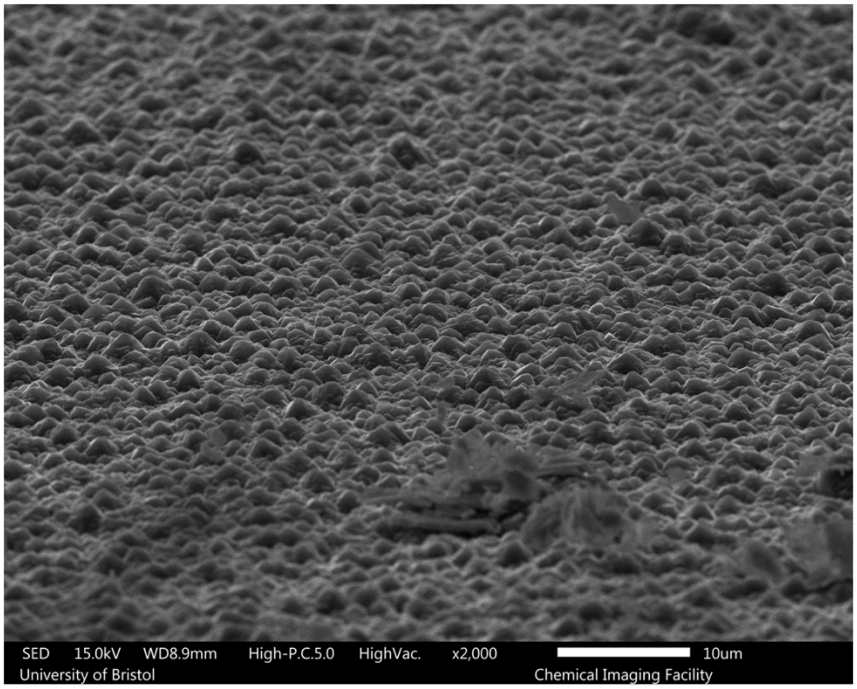

Figure 53: A 70 degree canted SEM image of the tin monoxide terminated NDD sample at x2000 magnification.

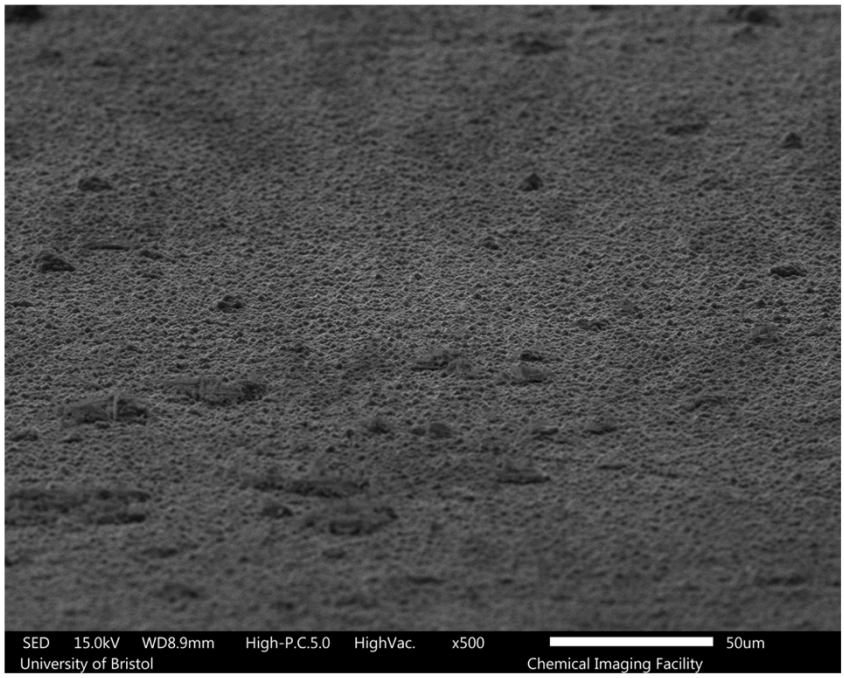

Figure 54: A 70 degree canted SEM image of the tin monoxide terminated NDD sample at x500 magnification.

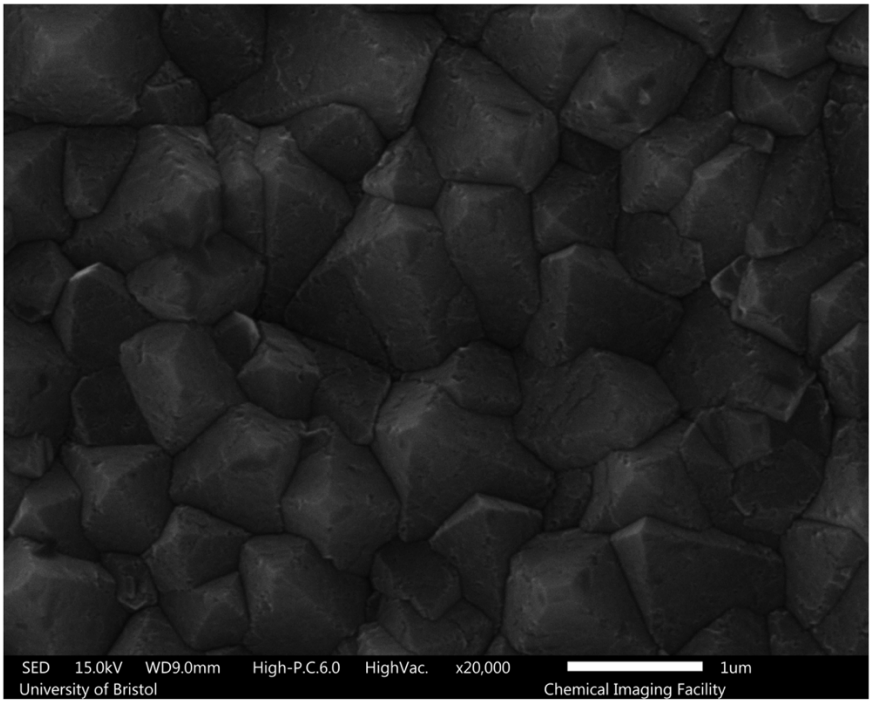

Figure 55: A top down SEM image of the 0.75% CH_4 PDD emitter sample at x20,000 magnification.

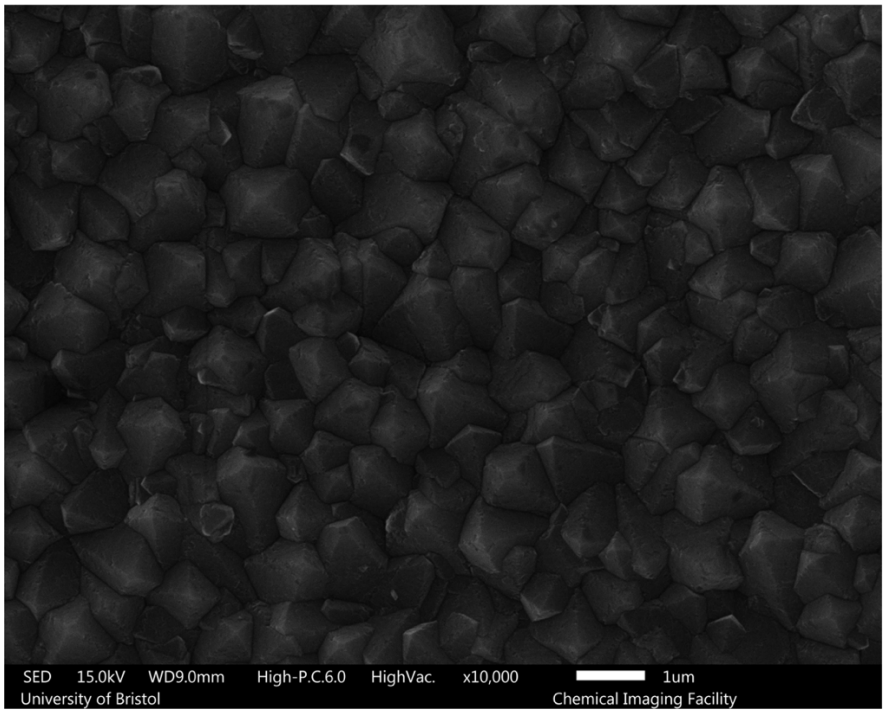

Figure 56: A top down SEM image of the 0.75% CH_4 PDD emitter sample at x10,000 magnification.

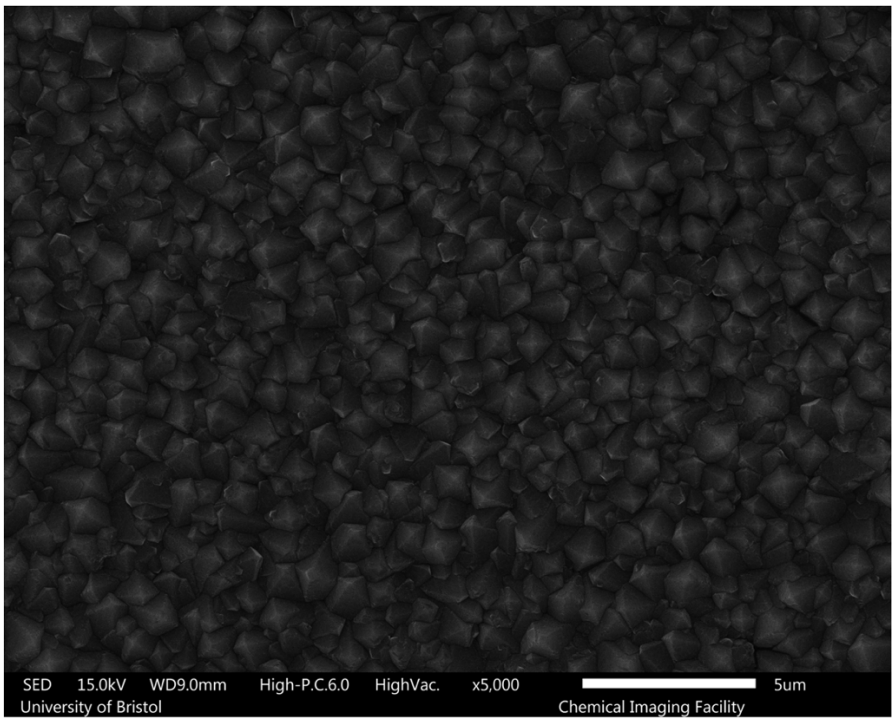

Figure 57: A top down SEM image of the 0.75% CH_4 PDD emitter sample at x5000 magnification.

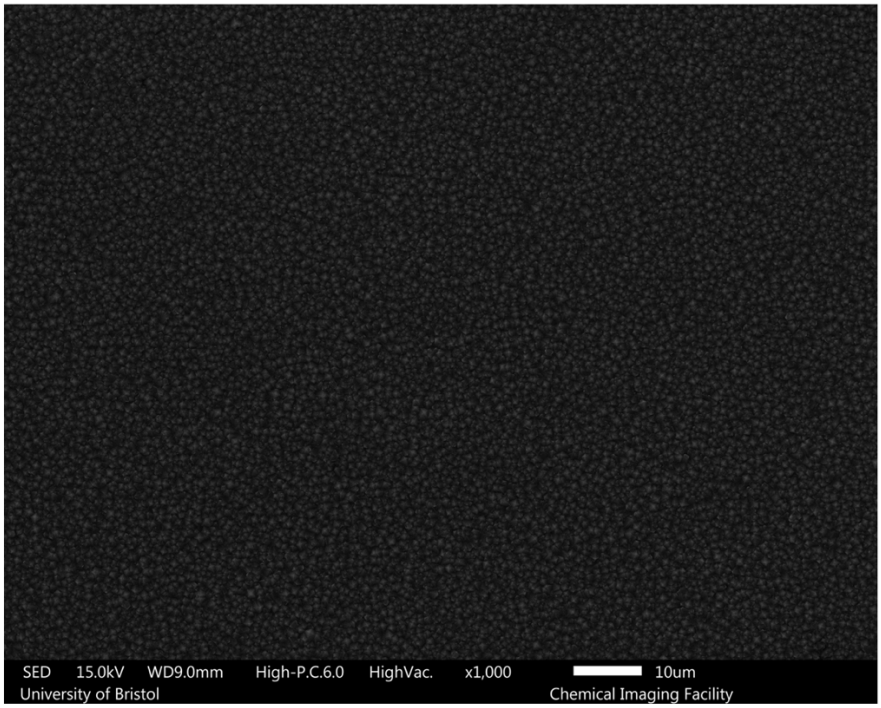

Figure 58: A top down SEM image of the 0.75% CH_4 PDD emitter sample at x1000 magnification.

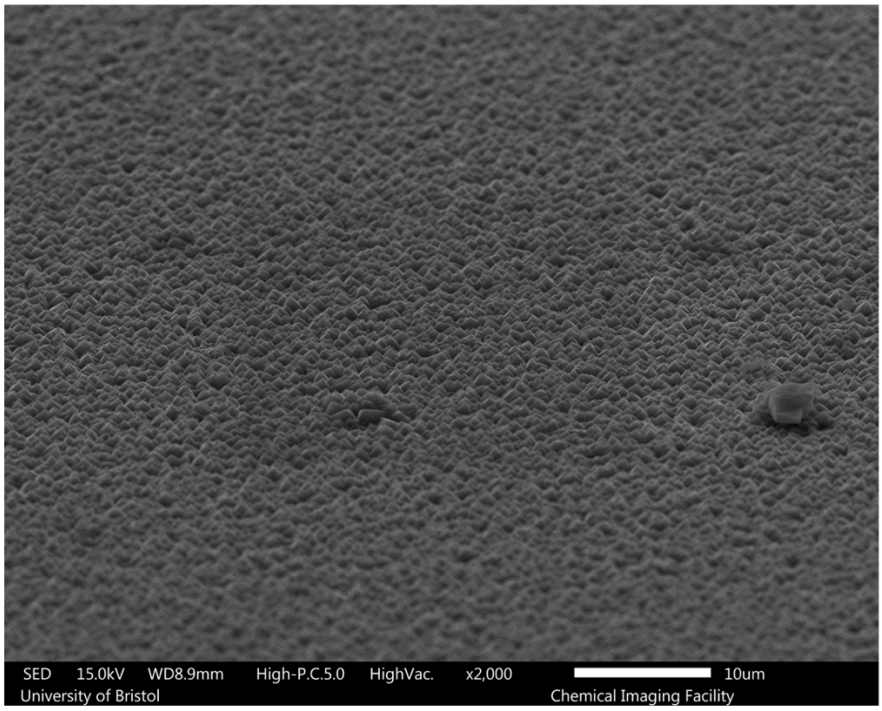

Figure 59: A 70 degree canted SEM image of the 0.75% CH_4 PDD sample at x2000 magnification.

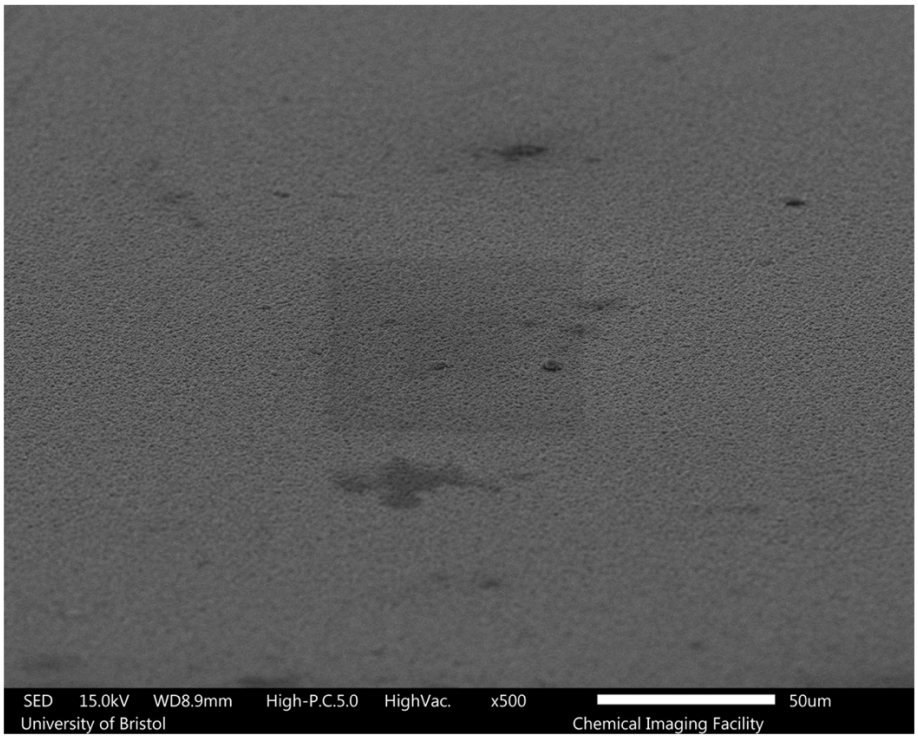

Figure 60: A 70 degree canted SEM image of the 0.75% CH_4 PDD sample at x500 magnification.

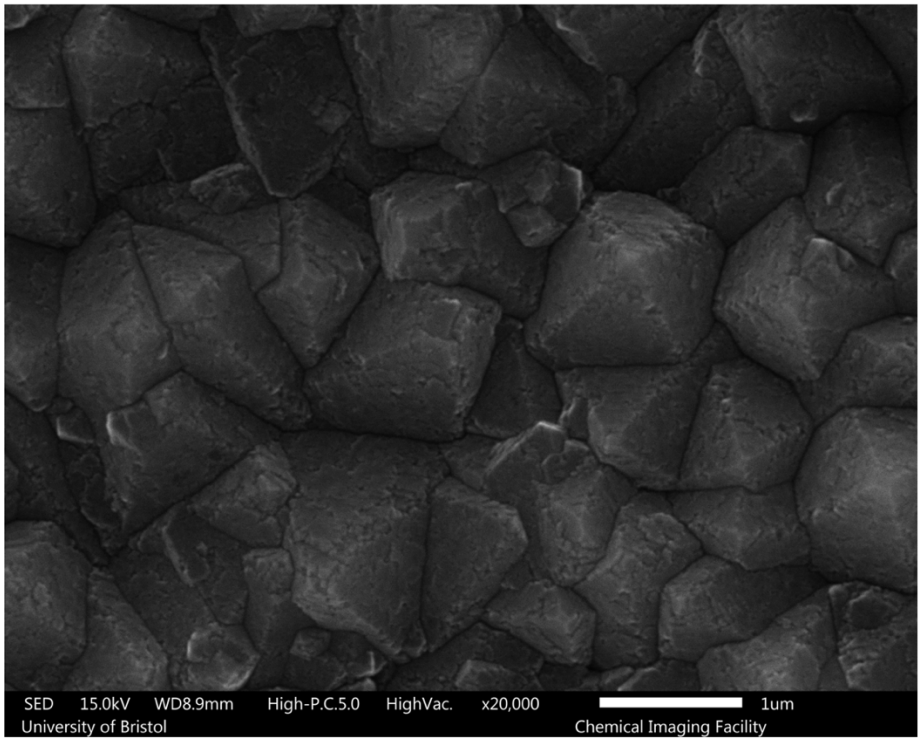

Figure 61: A top down SEM image of the 1.25% CH_4 PDD emitter sample at x20,000 magnification.

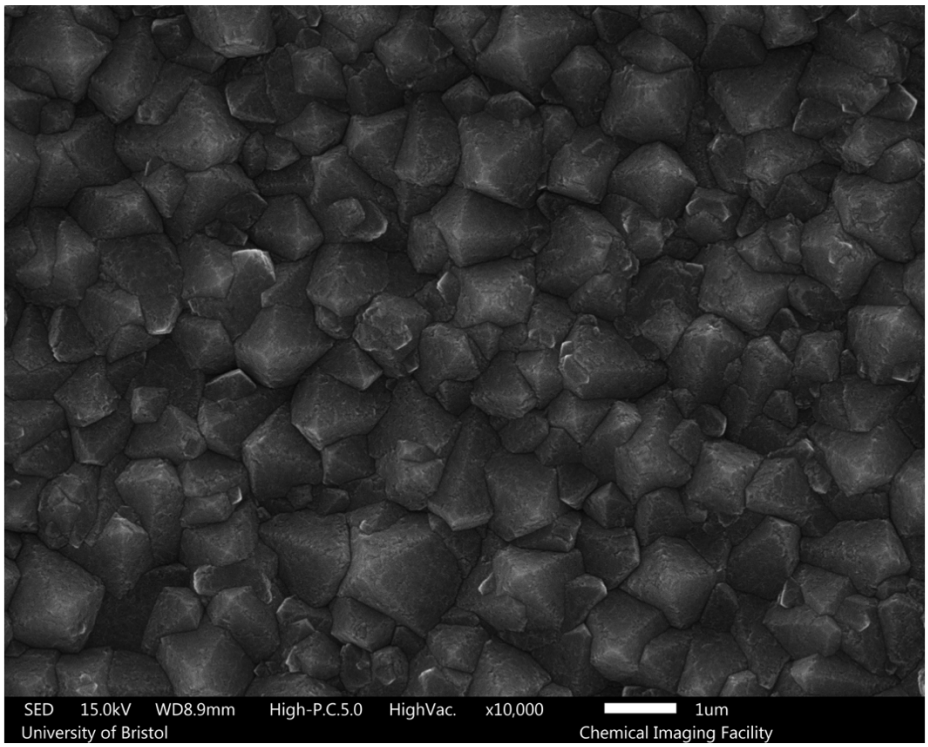

Figure 62: A top down SEM image of the 1.25% CH_4 PDD emitter sample at x10,000 magnification.

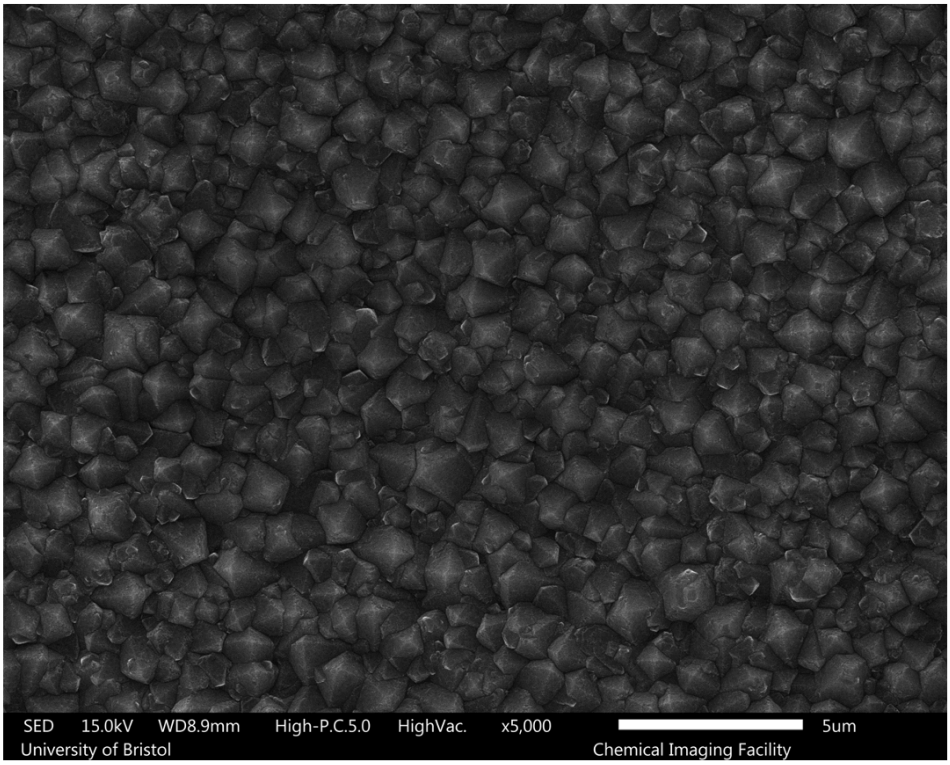

Figure 63: A top down SEM image of the 1.25% CH_4 PDD emitter sample at x5000 magnification.

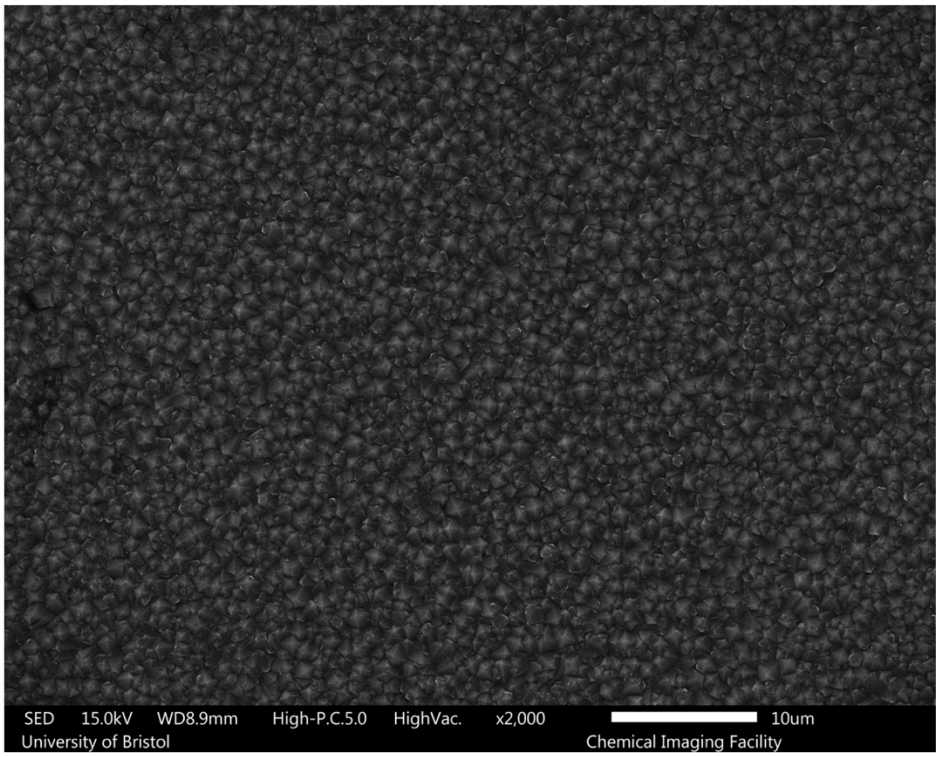

Figure 64: A top down SEM image of the 1.25% CH_4 PDD emitter sample at x2000 magnification.

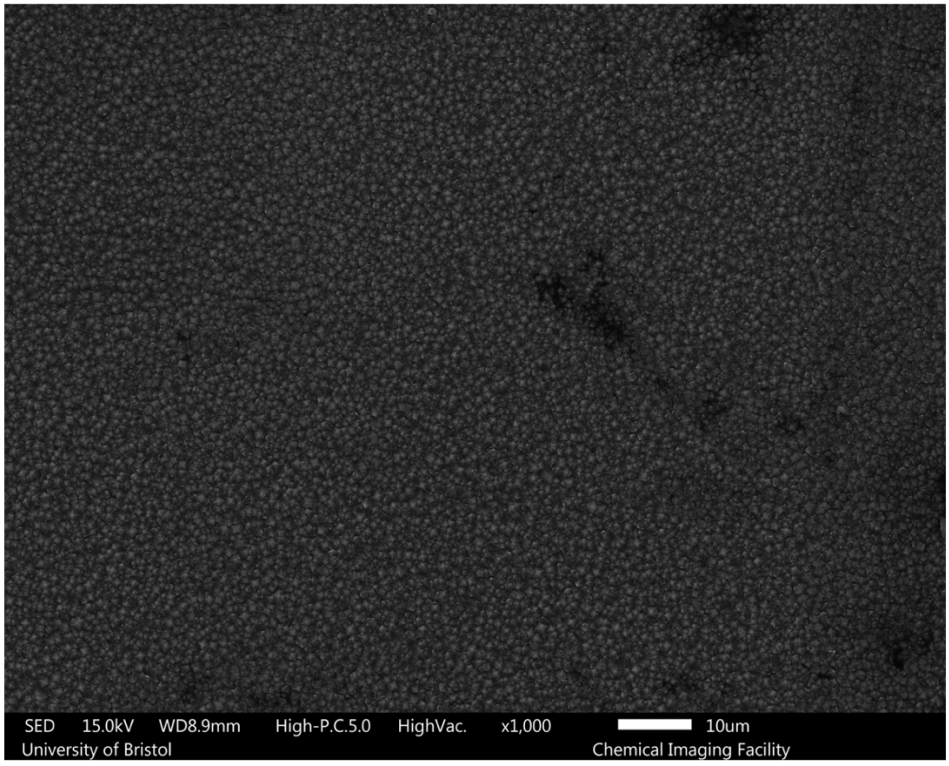

Figure 65: A top down SEM image of the 1.25% CH_4 PDD emitter sample at x1000 magnification.

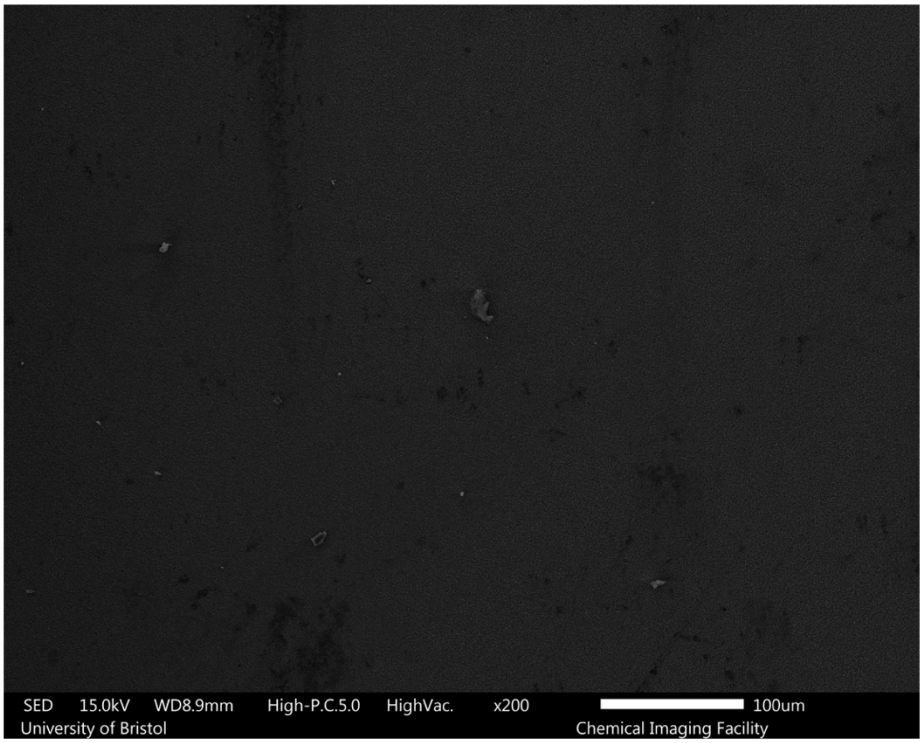

Figure 66: A top down SEM image of the 1.25% CH_4 PDD emitter sample at x200 magnification.

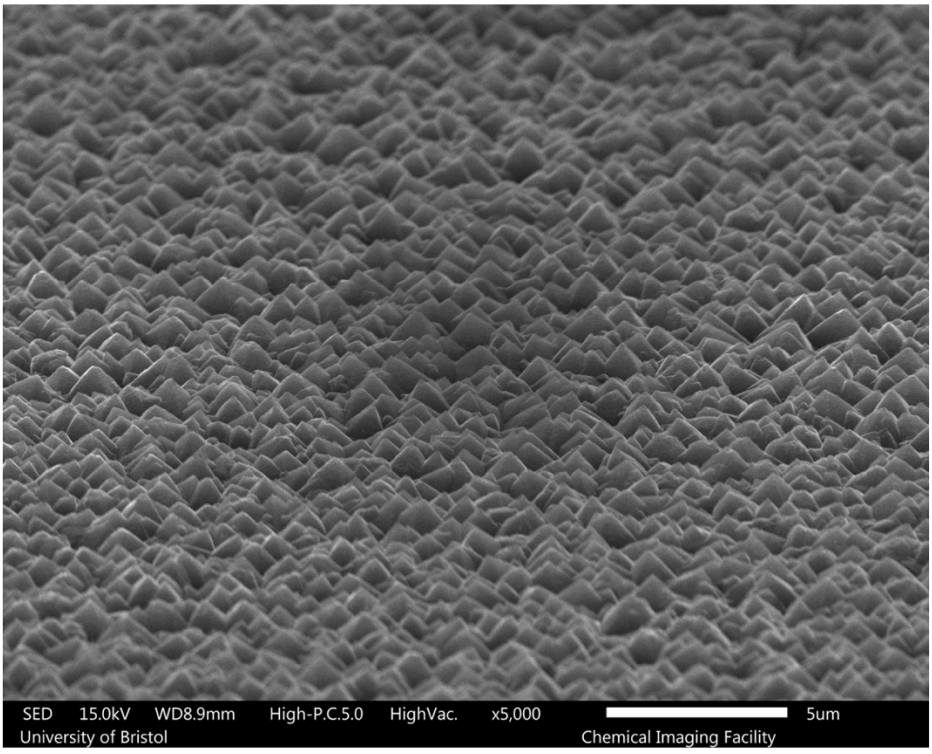

Figure 67: A 70 degree canted SEM image of the 1.25% CH_4 PDD sample at x5000 magnification.

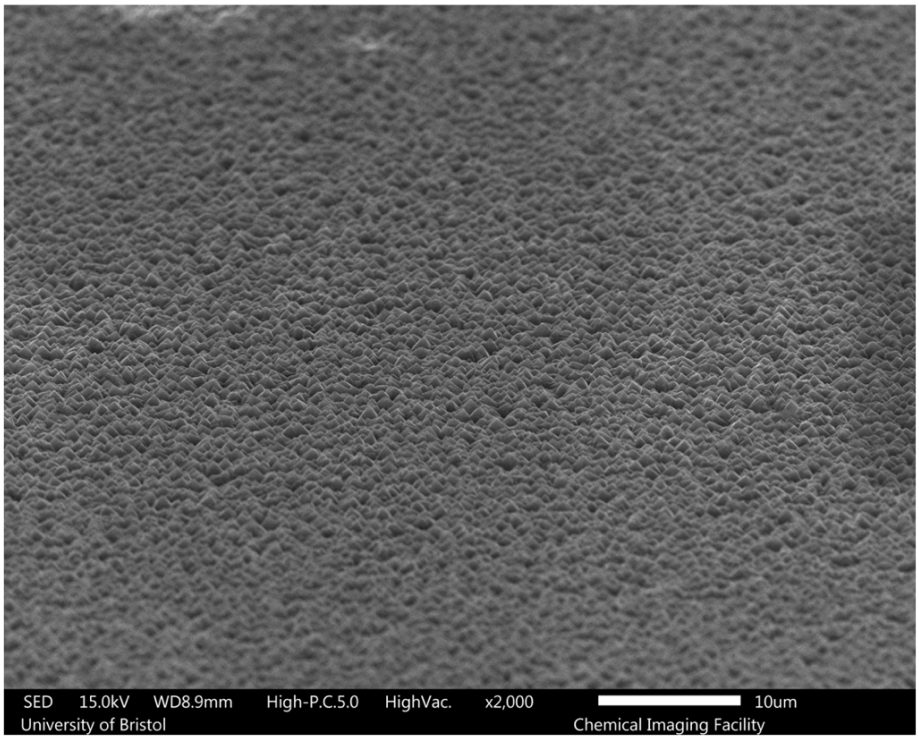

Figure 68: A 70 degree canted SEM image of the 1.25% CH_4 PDD sample at x2000 magnification.